INFRARED INTENSITIES OF WATER AND WATER DIMER

By

BARBARA ANN ZILLES

A DISSERTATION PRESENTED TO THE GRADUATE
COUNCIL OF THE UNIVERSITY OF FLORIDA IN PARTIAL
FULFILLMENT OF THE REQUIREMENTS FOR THE DEGREE OF
DOCTOR OF PHILOSOPHY

UNIVERSITY OF FLORIDA
1980

ACKNOWLEDGMENTS

ii

TABLE OF CONTENTS

iii

LIST OF TABLES

v

LIST OF FIGURES

Abstract of Dissertation Presented to the
Graduate Council of the University of Florida in
Partial Fulfillment of the Requirements for the
Degree of Doctor of Philosophy

INFRARED INTENSITIES OF WATER AND WATER DIMER

By

Barbara Ann Zilles

June 1980

Chairman: Willis B. Person
Major Department: Chemistry

     The atomic polar tensors for water monomer and the linear dimer have

been calculated by the self-consistent field method using the 4-31G basis

set. The atomic polar tensors have been used to obtain infrared absorp-

tion intensities for these two molecules. Atomic polar tensors were also

determined from experimental intensities for water monomer. These

experimental polar tensors were then added to the difference between the

theoretical dimer and monomer polar tensors to obtain scaled polar ten-

sors for the dimer. Intensities from the monomer polar tensors are com-

pared with values determined from gas-phase measurements. Intensities

from both scaled and unscaled 4-31G polar tensors for the dimer are com-

pared with a simulated spectrum, which has been fitted to the experimental

spectrum of water dimer isolated in the nitrogen matrix.

     In addition, the atomic polar tensors for the water monomer and dimer

were analyzed using the charge, charge flux, overlap model. The major

change from monomer to dimer was found in the charge flux tensor on the

hydrogen-bonded hydrogen atom, in the diagonal element along the OH bond. The change in this element was thus shown to be the origin of the characteristic intensity enhancement accompanying hydrogen-bond formation. This result was interpreted in terms of the physical characteristics of the charge flux tensor. The interpretation was consistent with the vibronic charge transfer and dynamic polarization models for the intensity enhancement. Additional conclusions could be made, particularly concerning the effect of the hydrogen-bond on interatomic interactions in the water dimer.

CHAPTER 1

INTRODUCTION

1.1. Perspective

The study of infrared absorption intensities has recently assumed a new prominence in molecular spectroscopy. Experimentally, the capability for obtaining high resolution digital absorbance data--on a routine basis over a wide frequency range--has contributed to this development. Thus, for example, the difficulty of obtaining reliable absorption coefficients for overlapped bands has been considerably reduced. Spectrum-fitting programs are commonly available, which can adjust the intensity parameters (along with the linewidths and band center frequencies) to minimize the difference between the experimental and fitted spectrum. While the number of adjustable parameters in a complex spectrum may be large, the experimental data points are many times more numerous.

Simultaneously, the theoreticians are beginning to make significant advances in the quantum mechanical calculation of infrared intensity parameters. This progress has stimulated the development of new formalisms for interpreting the intensities. These formalisms have led to unprecedented success in understanding molecular intensities and predicting them from chemical and structural information about the molecule [1-17].

The water dimer has been another subject of intense experimental and theoretical interest, during the past twelve years. Morokuma and Pederson performed the first theoretical calculation for this dimer in 1968 [18].

1

Since that time numerous *ab initio* and empirical studies have been carried out. There are two motivations for this interest. First, the water dimer may be regarded as a prototype of liquid water. Direct application of the results for water dimer to the study of liquid water may be severely limited. Nonadditivity of pairwise interactions is generally held to be important [19]. In any case, a thorough understanding of the properties of water dimer must precede that of liquid water.

Secondly, the water dimer is a prominent example of a hydrogen-bonded (H-bonded) complex. These weak complexes have stimulated the imagination of chemists since the 1930's, particularly because of their importance in biological systems [20-21]. The H-bond illustrates the type of interaction found in the more general class of electron donor-acceptor complexes. This interaction can be described as a transfer of electronic charge from an electron-rich portion of the electron donor molecule to the electron-acceptor molecule. In H-bonded complexes the interaction in the electron acceptor is localized in the region of a hydrogen atom. A large number of H-bonded complexes can be formed with the water molecule acting as electron acceptor. The water molecule is also an important electron donor. Thus the water dimer, in which the water molecule acts as both the electron donor and acceptor, plays a unique role in the study of H-bonding.

1.2. Vibrational Properties of H-bonded Complexes

Among the properties of H-bonded complexes that have been studied, the historical importance of vibrational spectroscopy is well-known [22]. Not only can the infrared frequencies and intensities for a particular complex be compared with a wealth of related data for other complexes and for the uncomplexed molecules; but these properties also reveal much about

the bonding characteristics of the molecules, and how they are changed by the H-bond.

The vibration which is most sensitive to the effect of the H-bond is commonly referred to as the AH stretch--where RAH is the electron acceptor and AH is involved in the H-bond. For example, when the electron acceptor is water, AH is the OH bond. However, in this case, the notion of a single H-bonded AH stretch is complicated by the fact that there are two OH bonds in water. In the isolated H_2O molecule, these OH bonds are symmetrically equivalent and couple to give a symmetric and an antisymmetric stretching vibration. Moreover, even though only one of the H atoms forms the H-bond, this coupling is only moderately reduced in the complex. This is because intramolecular forces are much stronger than the H-bond interaction.

Because of this coupling there is more than one absorption band in such complexes whose normal coordinate contains a substantial contribution from the H-bonded OH stretch. Similarly, the normal coordinate for the infrared band most sensitive to the H-bond contains contributions not only from the H-bonded OH stretch, but also from the other, "free," OH stretch, as well as a small contribution from the bend. We therefore refer to this band as the "H-bond band." Furthermore, it should be emphasized that, in theoretical calculations for any complex where water acts as the electron acceptor, a complete normal coordinate analysis is essential for obtaining valid frequencies or intensities.

For all H-bonded complexes, the H-bond band undergoes a shift to lower frequency and a dramatic increase in intensity relative to the isolated electron acceptor molecule. The magnitude of the frequency shift has long been regarded as a measure of the strength of the H-bond [20, chap. 3]. Due to the developments in the field of infrared

intensities mentioned above, however, the intensity enhancement is becoming increasingly recognized as a far more sensitive indicator of the effect of the H-bond [22]. Accordingly, we have undertaken a thorough study of the intensity of this band in the water dimer (as well as that of other bands).

The intensity enhancement is also less readily understood than the frequency shift. The latter results from a weakening of the AH bond upon H-bond formation. Two main factors contribute to this reduction in bond strength. First, the approach of the electron donor molecule on the one side of the H-bonded H atom polarizes the electron density in the AH bond. Some of this density is thus forced to the nonbonding region of the A atom, where it cannot compensate for the AH nuclear repulsion. The plot of electron density versus position along the H-bond, given by Schuster for the water dimer [19, p. 74], is an excellent illustration of this electrostatic polarization effect. Secondly, an equilibrium charge transfer effect occurs, whereby electron density from the electron donor molecule is excited into an antibonding AH orbital.

Neither the electrostatic polarization nor the equilibrium charge transfer effects, however, can begin to account for the overwhelming magnitude of the intensity enhancement. The intensity in the H-bonded complex is generally a factor of 10 or more times that in the isolated molecule, whereas the relative frequency shift is on the order of a few percent for non-ionic binary complexes.

The traditional approach to this problem follows that used to investigate the physical phenomena that contribute to the stabilization energy of H-bonded complexes [23]. Qualitative arguments concerning the origin of the intensity enhancement are basically in agreement [24-27].

So far, however, the large magnitude of this enhancement has not been accounted for on a quantitative basis [23, and references cited therein].

Accordingly, we have approached this problem by applying a quantum mechanical model for the investigation of intensities. This model has previously been applied to various molecules, but not to molecular complexes [4,10]. We have found that such application leads to a unique quantitative formulation for the H-bond intensity enhancement. This formulation is not only consistent with the general trend of ideas on the subject, but also allows certain distinctions to be made which further clarify the concepts involved.

1.3.   Experimental Spectra of Water Dimer

1.3.1.   Matrix Isolation Spectroscopy and Structure of the Water Dimer

Until comparatively recently, the majority of experimental H-bond studies were carried out in solution. In addition to ill-defined medium effects, thermal effects at the temperatures associated with liquids complicate the interpretation of the spectra. Accordingly, the technique of matrix isolation spectroscopy has been employed extensively in the last decade for the study of H-bonded species. This technique involves the rapid condensation, at cryogenic temperatures, of a dilute mixture of the species to be studied in an inert "matrix" gas [28]. The matrix gases used most frequently are nitrogen (N_2) and argon (Ar). Interactions of the matrix with the solute are therefore expected to be minimal.

Several workers have observed the infrared spectra of water isolated in N_2 [29-34] and in Ar [34-40] matrices. We discuss these experimental studies in more detail in the following section. Absorption due to water monomer, dimer and trimer (or higher multimer) generally appears

in these spectra. The relative abundance of the different aggregate species depends on the concentration of water in the gaseous mixture, as well as on other factors which are probably constant for a given set of experiments.

The bands due to each species can in principle be identified by observing spectra at several concentrations and noting the concentration dependence of the band absorbances. The peak absorbances of bands due to monomer are expected to decrease monotonically with concentration, while trimer band absorbances are expected to increase monotonically. The absorbances of dimer bands are expected to show a maximum with respect to concentration. In practice, however, many of the bands are overlapped so that two neighboring bands due to different species can show the same concentration dependence. This difficulty has led to some differences in the bands assigned by various workers to the dimer, as discussed in section 1.3.2.

Tursi and Nixon have obtained a spectrum of water isolated in the N_2 matrix [30,31], in which the dimer bands are quite prominent and well-resolved from the monomer and trimer bands, as compared with spectra reported by other workers. A simulated spectrum, which we have adjusted to give the best fit to this experimental spectrum, is illustrated in Fig. 1-1. The method we have used to calculate the simulated spectrum is discussed in section 3.1. The bands assigned to water monomer, dimer and trimer (or higher multimer) by Tursi and Nixon are indicated in Fig. 1-1. All workers have assigned the monomer bands in the same manner: band I to the antisymmetric stretch, ν_3; band V to the symmetric stretch, ν_1; and band XI to the bend, ν_2.

Tursi and Nixon assigned six absorption bands to the dimer as indicated in Fig. 1-1. With the exception noted below, six bands would
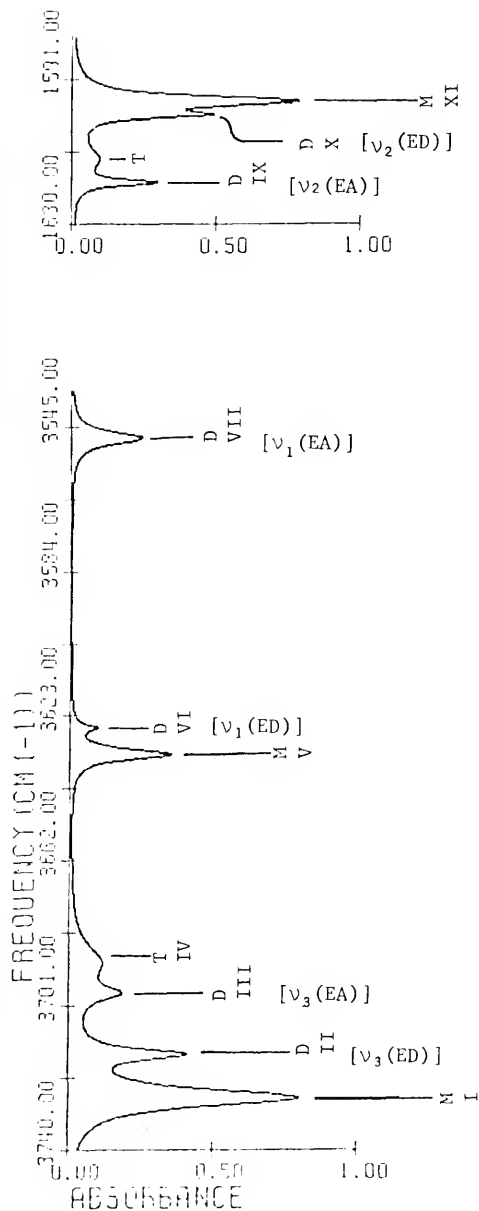
Fig. 1-1. Spectrum fitted to experimental spectrum given by Tursi [31] for water isolated in the N$_2$ matrix. The OH stretching region is from 3540 to 3740 cm^{-1}. The H$_2$O bending region is from 1580 to 1630 cm^{-1}. Bands due to water monomer (M), dimer (D) and trimer or higher multimer (T) are indicated. Dimer band assignments made by Tursi and Nixon [30] in terms of the linear water dimer are also indicated. Roman numerals identify bands for general discussion in the text.

generally be expected for the water dimer, since there are three funda-
mental absorptions for each of the water molecules in the complex. Tursi
and Nixon assigned the six bands in terms of the "linear" structure for
the water dimer illustrated in Fig. 1-2. Their assignments are generally
accepted, and we now discuss how the frequency pattern expected for this
structure is consistent with that in the observed spectrum. In this
discussion we use the simulated spectrum in Fig. 1-1 for reference.

The dimer structure shown in Fig. 1-2 is characterized by the linear
arrangement of the atoms involved in the H-bond: O_3, H_4, and O_5. These
atoms and atom H_6 of the electron acceptor (EA) define a plane of sym-
metry; atoms H_1 and H_2 of the electron donor (ED) are symmetrically
oriented with respect to this plane. Thus the OH stretches in the ED
molecule are symmetrically coupled just as in the monomer. That is, the
antisymmetric and symmetric stretches both have a contribution of equal
magnitude from each individual OH stretch. We further note that neither
H_1 nor H_2 is H-bonded. Accordingly the spectrum of the linear dimer
would be expected to have three bands for the ED molecule shifted
slightly from the monomer bands ν_1, ν_2 and ν_3. Three such bands--bands
II, VI and X--are evident in the spectrum shown in Fig. 1-1. These bands
were assigned by Tursi and Nixon to $\nu_3(ED)$, $\nu_1(ED)$ and $\nu_2(ED)$, respec-
tively.

Figure 1-2 shows that the two OH bonds in the EA molecule are not
symmetrically equivalent. Moreover, the O_5H_4 bond is H-bonded and thus
has a lower stretching force constant than the "free" O_5H_6 bond. The
two stretching vibrations expected for the EA molecule would therefore
contain unequal contributions from these two OH stretches, but would
retain their basic symmetric and antisymmetric character as discussed in
section 1.2. A greater contribution from the H-bonded O_5H_4 stretch would
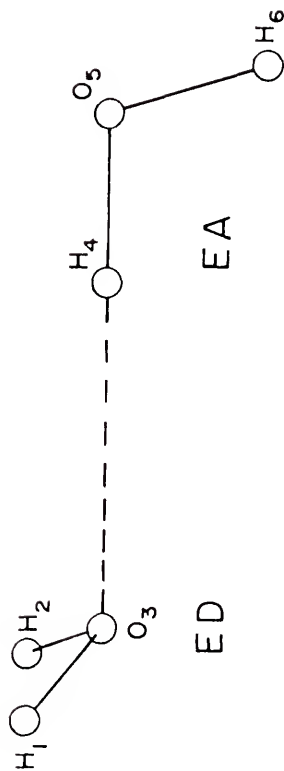
Fig. 1-2. The linear water dimer. The electron donor (ED) and electron acceptor (EA) components are indicated. Atom numbers for the normal coordinate analysis are also indicated.

be expected for the symmetric stretch, $\nu_1(EA)$, which would therefore be shifted to considerably lower frequency from ν_1 of the monomer. Band VII in Fig. 1-1 is consistent with this expectation. This band was assigned to $\nu_1(EA)$ by Tursi and Nixon. The antisymmetric stretch, $\nu_3(EA)$, would be expected to have a greater contribution from the "free" O_5H_6 stretch and a moderate shift to lower frequency from ν_3 of the monomer. Band III exhibits such a shift and was assigned to $\nu_3(EA)$ by Tursi and Nixon.

The bending vibration of the EA molecule in Fig. 1-2 perturbs the linearity of the H-bond. A considerable shift to higher frequency from ν_2 of the monomer would thus be expected for this vibration. Accordingly, band IX in Fig. 1-1 was assigned to $\nu_2(EA)$ by Tursi and Nixon.

Some of the bands in Fig. 1-1 have also been interpreted in terms of the cyclic structure for the water dimer [29,34,36]. This structure has two H-bonds and is characterized by the nonlinear arrangement of the two O atoms and the H atom involved in each H-bond. The structure of the centrosymmetric cyclic dimer is illustrated in Fig. 1-3. This structure is unique in that it has a center of inversion and thus obeys the exclusion rule--three vibrations are active only in the infrared, and three are active only in the Raman spectrum. The three infrared active vibrations are the out-of-phase combinations (ν_1^-, ν_2^- and ν_3^-) of the corresponding monomer vibrations of the two water molecules forming the dimer.

The frequency shifts expected for these vibrations, from ν_1, ν_2 and ν_3 of the monomer, would follow qualitatively the pattern discussed for the vibrations of the EA molecule of the linear dimer. However, the frequency shifts for the cyclic dimer should be smaller because the nonlinear H-bonds are not as strong as linear H-bonds [36,41].
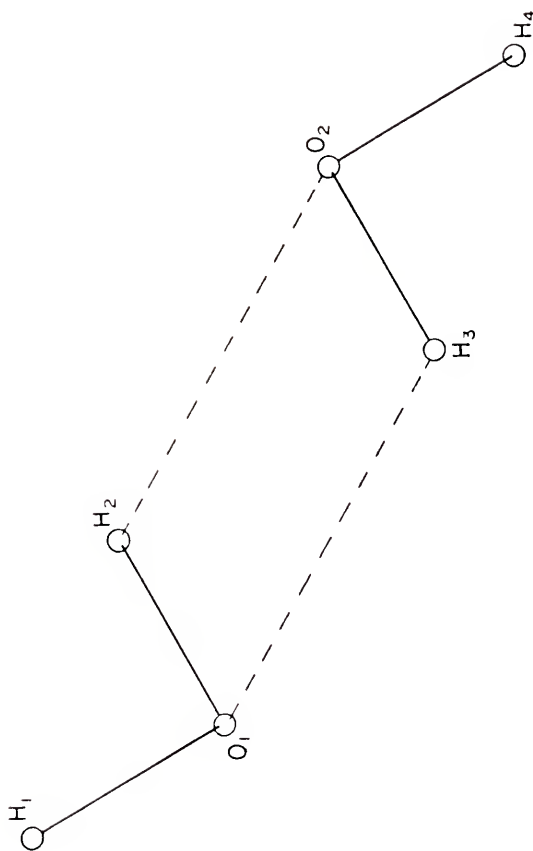
Fig. 1-3. The centrosymmetric cyclic water dimer. The center of inversion is at the midpoint between O_1 and O_2.

1.3.2. Review of Experimental Studies

The first study of matrix isolated water was carried out in the N_2 matrix by Van Thiel, Becker and Pimentel, using a prism monochromator [29]. These authors attributed the dimer bands to the centrosymmetric cyclic structure because only three dimer bands could be observed in their low resolution spectra. Bands II, VI and X in Fig. 1-1 were not resolved from the neighboring monomer bands.

In all the subsequent studies, the experimental spectra of water isolated in the N_2 matrix were basically the same as those obtained by Tursi and Nixon. Three groups of workers [33-35] did not assign certain bands in their spectra in agreement with the assignment made by Tursi and Nixon (the TN assignment). These discrepancies involve bands assigned to dimer and trimer in two regions of the spectrum. One of these regions includes bands III and IV in Fig. 1-1. We recall that band III corresponds to $\nu_3(EA)$ of the linear dimer according to the TN assignment. Now the frequency shift of this vibration from ν_3 of the monomer is due to the H-bond interaction. We therefore refer to this region as the $\nu_3(H-B)$ region.

The other region in which different assignments have been made by various workers includes band VII, which corresponds to $\nu_1(EA)$ according to the TN assignment. We designate this region as the $\nu_1(H-B)$ region. Figure 1-1 shows that in the $\nu_3(H-B)$ region a relatively sharp dimer band is superimposed on a broad trimer band according to the TN assignment. The same situation occurs in the $\nu_1(H-B)$ region. In many of the spectra obtained by various workers a broad shoulder appears on the low frequency side of band VII in Figure 1-1. We refer to that broad absorption as band VIII.

Suppose the TN assignment is correct and that the broad bands are due to trimer while the sharper bands are due to dimer. Then the absorbances of the two broad bands should vary differently with respect to concentration from those of the two sharp bands. However, the concentration dependence of the "true" band absorbances would probably not be observed, because the broad trimer band acts as a baseline for the sharper dimer band. Rather, any increase in the absorbance of the broad trimer band would result in an apparent increase in the absorbance of the dimer band, even though the "true" absorbance of the latter band does not increase. Thus, reliable assignments of these bands cannot be made solely on the basis of their concentration dependence.

Table 1-1 summarizes the discrepancies between the TN assignment and the assignments made by other workers for bands III, IV, VII and VIII. In two of the studies, more than four bands in the OH stretching region were assigned to dimer. Since any given structure for the water dimer can have a maximum of four bands in this region (two bands for each of the component water molecules), alternate interpretations had to be made for the extra bands.

Huong and Cornut obtained spectra of water isolated in both the N_2 and the Ar matrix [34]. As indicated in Table 1-1, these authors attributed bands IV and VII to the dimer. As discussed in section 1.3.1., two stretching vibrations, ν_3^- and ν_1^-, are expected for the centrosymmetric cyclic dimer. Accordingly, Huong and Cornut assigned band IV in the ν_3(H-B) region to ν_3^- and band VII in the ν_1(H-B) region to ν_1^-. They assigned bands II, III, VI and VII to the linear dimer according to the TN assignment. Their overall assignment is therefore not consistent with the relative frequency pattern expected for linear and nonlinear H-bonds (see section 1.3.1.). That is, the assignment attributes larger

Table 1-1. Assignment of bands in the ν_3(H-B) and ν_1(H-B) regions to dimer (D) and trimer (T) by various workers. Bands III, IV and VII are indicated in Fig. 1-1. Band VIII appears on the low frequency side of band VII in many spectra.

	ν_3(H-B) Region		ν_1(H-B) Region		Total Number of Dimer Bands in OH Stretching Region
	III	IV	VII	VIII	
Tursi and Nixon[a]	D	T	D	T	4
Huong and Cornut[b]	D	D	D	D	6
Barletta[c]	D	T	D	D	8[c]
Luck[d]	T	T	D	D	4

[a] Tursi and Nixon [30].

[b] Huong and Cornut [34].

[c] Barletta [33]. Band VIII is resolved into four bands in this work.

[d] Luck [36]. See also Mann, Neikes, Schmidt and Luck [35].

frequency shifts to the bent H-bonds of the cyclic dimer than to the linear H-bond of the structure shown in Fig. 1-2.

Barletta obtained excellent high resolution spectra of water isolated in the N_2 matrix [33]. In these spectra four bands were resolved in the absorption corresponding to band VIII in the ν_1(H-B) region. These four "extra" bands were attributed to the dimer. Of the eight bands thus assigned to the dimer, four were observed to be considerably weaker than the others. The four stronger bands were then assigned to fundamentals of the linear dimer: bands II, III and VII in Fig. 1-1 and one of the four "extra" bands in the ν_1(H-B) region. According to this assignment two vibrations (corresponding to band VII and the "extra" band) have substantially lower frequencies than ν_1 of the monomer. Only one such vibration is expected for the linear dimer as discussed in section 1.3.1. Moreover, band VI in Fig. 1-1 was considered too weak to be a fundamental. This band corresponds to ν_1(ED) according to the TN assignment. It is shown below, however, that on the basis of our calculations for the linear water dimer the intensity of the ν_1(ED) fundamental should indeed be small.

Mann, Neikes, Schmidt and Luck observed the spectra of water isolated in the Ar matrix [35, see also reference 36]. Their spectra were basically the same as those observed for water isolated in the N_2 matrix by the various workers. Table 1-1 shows that these authors assigned both bands in the ν_3(H-B) region to the trimer, while both bands in the ν_1(H-B) region were assigned to the dimer. These authors interpreted the dimer bands in terms of the cyclic structure.

We note that the cyclic dimer can be asymmetric. If one of the two water molecules in the structure shown in Fig. 1-3 is rotated somewhat, the center of symmetry is eliminated. For this structure two weak

stretching bands would be expected, corresponding to the infrared inactive vibrations of the centrosymmetric structure, namely, the in-phase combinations (ν_3^+ and ν_1^+) of the corresponding monomer vibrations of the two water molecules in the dimer. According to these considerations, Mann, Neikes, Schmidt and Luck assigned bands II, VI and VII in Fig. 1-1, as well as band VIII in the ν_1(H-B) region, to the asymmetric cyclic dimer stretching vibrations, ν_3^-, ν_3^+, ν_1^- and ν_1^+, respectively. This assignment is consistent with the relative intensity pattern expected for the out-of-phase and in-phase vibrations. However, the frequency shifts, from the corresponding monomer bands, resulting from this assignment do not seem entirely satisfactory. That is, while frequency shifts of 103 and 97 cm^{-1} are attributed to ν_3^- and ν_1^-, respectively, a relatively small shift of 14 cm^{-1} is attributed to ν_3^-, and a relatively large shift of 171 cm^{-1} is attributed to ν_1^+.

On the other hand, Luck [36] objected to the frequency shift of ν_1(EA), the "H-bond band," resulting from the TN assignment on the basis that it was too small (85 cm^{-1}) for a linear dimer. Several experimental studies were cited, which showed that linear H-bonds were stronger than nonlinear H-bonds. It was pointed out that the water polymer (small crystallites or amorphous clusters of ice) had linear H-bonds, and its H-bond band occurred at 3220 cm^{-1} (in Ar). Luck then stated, "We would expect the absorption of the linear dimers in the region of the H-bond band of large aggregates ('polymer band')" [36, p. 552].

This reasoning does not take into account the importance of cooperative effects in ice, which has a stabilization energy of 11 kcal/mole [42]. In contrast, Clementi has calculated a stabilization energy of

5.6 kcal/mole for the linear water dimer,* using a very large basis set and including correlation effects [43]. Furthermore, we point to the good agreement of the theoretical frequency predicted for the H-bond band of the linear dimer (see Appendix) with that of band VII in Fig. 1-1. The intensity we have calculated is too large. However, evidence will be presented below that this discrepancy is due to an artifact of the calculation rather than to the structure of the model we have chosen.

Tursi and Nixon also observed the spectrum of D_2O and HDO in the N_2 matrix in addition to that of H_2O. They found a one-to-one correspondence between the H_2O bands discussed in section 1.3.1. and those due to D_2O. Corresponding bands were also found for HDO monomer. For the linear HDO dimer, there are two possible isotopes since the EA molecule can be complexed either through the H atom or through the D atom. Tursi and Nixon observed four stretching bands whose frequency pattern was consistent with that expected for a linear HDO dimer with the EA complexed through the D atom. Two additional bands expected for the other isotope were not observed, nor were any dimer bands in the HDO bending region observed.

Tursi and Nixon used the nine frequencies they observed for H_2O, D_2O and HDO monomers to obtain a force field for water monomer. Similarly, they obtained a force field for the linear water dimer using twelve frequencies for $(H_2O)_2$ and $(D_2O)_2$, and the four frequencies for $(HDO)_2$. We have used these two force fields in our intensity calculations, and they are discussed further below.

_____

* Experimental studies give estimates of 5.2 kcal/mole [44] and 3.0 kcal/mole [45]. But the theoretical value is the most reliable and probably close to the true value.

Recently, the infrared spectrum of the various isotopes of water isolated in the N_2 matrix was again studied by Fredin, Nelander and Ribbegard [32]. They made assignments for all the isotopic dimer bands in terms of the linear structure, in agreement with Tursi and Nixon. Moreover, they found that increasing the intensity of the irradiating beam and/or decreasing the temperature of the sample led to the appearance of the bands for linear $(HDO)_2$ not observed by Tursi and Nixon--the dimer bands in the HDO bending region and those corresponding to the EA complexed through the H atom. Thus, all the bands for $(D_2O)_2$ and $(HDO)_2$ have been observed at those frequencies which are expected for the linear structure shown in Fig. 1-2. The consistency of these results with those for $(H_2O)_2$ strongly confirms the assignments given in section 1.3.1.

As mentioned above, Huong and Cornut [34] and Mann, Neikes, Schmidt and Luck [35] have obtained spectra of water isolated in the Ar matrix which are basically the same as those in the N_2 matrix. Several workers have obtained a totally different type of spectrum for water in the Ar matrix [37-40]. These workers have assigned the majority of bands in the spectrum to vibration-rotation transitions of the monomer. The relative absorbances of these bands show a complicated time and temperature dependence. This behavior has been interpreted in terms of conversion from ortho to para spin states of the hydrogen nuclei [37-39]. According to this interpretation, the most recent results for the time and temperature dependence of the various bands indicate the following [39]. Unexpectedly rapid spin conversion occurs during the deposition process-- to an ortho/para ratio characteristic of a temperature roughly halfway between room temperature and the temperature of the matrix. Thereafter, the conversion process continues at a slower rate in matrices with

relatively high water concentrations. But in dilute matrices no conver-
sion occurs after deposition.

This interpretation is rather elaborate, and it should be pointed out
that other explanations may exist for the profuse spectrum of water in the
Ar matrix. Matrices giving rise to this type of spectrum have been
deposited at lower temperatures (4-10°K) than those giving rise to the
simple spectrum (16-20°K). At higher temperatures, the matrix is likely
to be annealed during deposition so that the orientation of the Ar
crystallites in the matrix is more uniform. It is possible that the
importance of nonequilibrium effects in the lower temperature matrix
results in a larger number of interactive sites, each having a different
energy and thus giving rise to different frequency shifts for the vibra-
tions. In addition, the possibility of N_2 impurity in the Ar matrix
cannot be ignored. Mixed aggregates of H_2O and N_2 molecules could
account for some of the bands in the profuse spectrum.*

Within the context of attributing most of the bands to monomer
vibration-rotation transitions, Ayers and Pullin have assigned five bands
in the profuse spectrum of water in Ar to the linear water dimer [40].
In the frequency region corresponding to that expected for the $\nu_3(ED)$
vibration, no band could be attributed to the dimer, all bands in this
region having been assigned to the monomer. The "absence" of this band
is somewhat disturbing since our calculations predict the intensity of
$\nu_3(ED)$ to be second only to that of the H-bond band, $\nu_1(EA)$. Possibly
one of the "rotating monomer" bands could be attributed to this vibration.

---

* In this regard, a number of bands have been induced in the spectrum of
hydrogen halides (HX) in the Ar matrix by doping with N_2 impurity. These
bands have been attributed to various aggregates of the HX and N_2 mole-
cules in the Ar matrix [46].

1.4. Theoretical Calculation of Vibrational
Properties of the Water Dimer

1.4.1. Frequencies

Matrix isolated spectra of the water dimer have provided new data
that are important for the study of H-bonding. Theoretical calculations
are an additional source of such data. Moreover, the development of
theoretical methods is now approaching a level, where they can be used as
a reliable guide for interpretation of the experimental spectra.

Curtiss and Pople have performed a set of quantum mechanical calcu-
lations with the 4-31G basis set in order to obtain force constants for
water monomer and the linear dimer [47]. The vibrational frequencies for
monomer and dimer were then calculated from each force field. These
frequencies agree reasonably well with the experimental ones observed by
TN, but they are all 10% too large. It is typical for Hartree-Fock
calculations to overestimate frequencies by approximately this amount
[19, p. 33].

The absolute differences between the calculated and experimental
frequencies (about 360 cm^{-1} in the stretching region and 160 cm^{-1} in the
bending region) might seem too large for the calculations to be of any
use for the experimentalist. However, the factors in the calculation
that lead to overestimation of the force constants, and thus of the
frequencies, should be nearly constant for the monomer and dimer. One
method of comparing calculation with experiment, which minimizes the
effect of constant errors in the calculation, is to examine the calculated
and observed frequency *shifts* from monomer to dimer.

An alternate approach makes use of the fact that the physical
phenomena responsible for the frequency shifts (for example, changes in

bond strengths) appear directly as changes in the force constants. Thus, in this approach one is concerned with the change in each force constant, $\Delta f(th.)$, which is obtained from the theoretically calculated monomer and dimer force constants, according to

$$\Delta f(th.) = f(th., \; dimer) - f(th., \; monomer).$$

A set of scaled dimer force constants can then be calculated using the experimental monomer force constant:

$$f(scaled, \; dimer) = f(exptl., \; monomer) + \Delta f(th.).$$

This set of scaled dimer force constants is then used in a standard normal coordinate calculation to obtain dimer frequencies which can be compared directly with experiment.

In this scaling procedure, errors in the theoretically calculated monomer and dimer force constants compensate more effectively than they do in the comparison of frequency shifts. This is because, in the normal coordinate calculation of the frequencies the dimer force constants are weighted differently, by the geometrical parameters and the masses, from the monomer force constants. The force constant errors are thus also weighted differently in the calculated frequencies.

This scaling procedure has been applied to the theoretical force constants calculated by Curtiss and Pople (see Appendix). It has also been applied to a set of force fields calculated by the CNDO method for the linear water dimer. The resulting frequencies predicted for the water dimer agree quite will with the experimental frequencies.

1.4.2. Intensities

Little work has been done in the area of theoretical intensity calculations for the water dimer. In the work that has been done, only the intensity of the H-bonded OH stretch has been calculated, and normal modes have not been taken into account [48, and references cited therein]. Because theoretical intensities can provide valuable assistance in the interpretation of experimental spectra, we have calculated a complete set of intensities for the normal modes of the linear water dimer.

As discussed in section 2.4., the intensities are proportional to the square of the derivative of the molecular dipole moment with respect to the normal coordinates. These dipole derivatives, like the force constants, reflect the chemical bonding characteristics of the molecule. One of the goals of infrared intensity theory is to study how the dipole derivatives change from one molecule to another and interpret these changes in terms of the types of atoms and bonds present. Dipole deriva- tives can also be expressed in terms of other forms of the vibrational coordinates which are more useful for interpretation than the normal coordinates.

The space-fixed cartesian representation for the dipole derivatives has proven particularly advantageous for understanding the chemical factors that determine the intensities [1-10]. These dipole derivatives are composed of a set of atomic polar tensors (APT's), one for each atom in the molecule [1]. Studies have indicated that the values of the APT elements for a given atom tend to be relatively independent of which molecule the atom is in [4,7]. Remarkable success has been achieved in predicting intensities for one molecule by transferring APT's from other chemically related molecules, and then transforming these APT's to

dipole derivatives with respect to the normal coordinates of the first molecule [5]. These results suggest that the APT's are fundamental indicators of the chemical properties of atoms in molecules.

Accordingly, we have calculated APT's for the water monomer and dimer using quantum mechanical methods in order to predict intensities for these two molecules. As for the force constants, we expect that the errors in the quantum mechanical calculation of the APT's are nearly the same for the dimer complex as for the monomer. To the extent that this is true, we might expect that the *changes* in the APT's from monomer to dimer are well-represented by the calculation. With this idea in mind, we have applied a scaling procedure, analogous to that described above for the force constants, to obtain APT's for atoms in the dimer from the known APT's for those atoms in the monomer.

First, the change in the APT of atom A from monomer to dimer, $\underline{\Delta P}^A$(th.), was obtained from the theoretical calculation by,

$$(1) \qquad \underline{\Delta P}^A(\text{th.}) = \underline{P}^A(\text{th., dimer}) - \underline{P}^A(\text{th., monmer}) \quad .$$

Then the experimental APT for atom A in the monomer was used to obtain the scaled dimer APT:

$$(2) \quad \underline{P}^A(\text{scaled, dimer}) = \underline{P}^A(\text{exptl., monomer}) + \underline{\Delta P}^A(\text{th.}).$$

The APT's from both the *ab initio* quantum mechanical calculation, $\underline{P}^A$(th., dimer), and from the scaling procedure, $\underline{P}^A$(scaled, dimer), were used to obtain intensities for the absorption bands of the water dimer. These theoretical dimer APT's thus provided an independent source of data, which we have used for comparison with experiment. The comparison will be discussed in detail in chapter 3.

The APT's also contain more information than do the intensities for a relatively large, unsymmetrical molecule like the water dimer. That is, the intensities can be obtained from the APT's, but the APT's can only be calculated theoretically. Both the APT's and the intensities reflect the redistribution of charge that takes place as the molecule vibrates. In the APT's, this vibrational redistribution of charge is resolved into contributions from each atom.

As mentioned previously, in the study of H-bonded complexes our chief interest lies in the changes that take place relative to the uncomplexed molecule. We have thus compared the theoretical APT's which we have calculated for each atom in the dimer with the corresponding APT in the monomer. We have found that changes in the APT's from monomer to dimer are restricted to a few critical elements. Moreover, the *major* changes are restricted to those dimer atoms that are involved in the H-bond. We have also used the quantum mechanical definition of the dipole moment to resolve each APT into charge, charge flux, and overlap contributions. Again, we have found that changes from monomer to dimer are restricted to a few critical elements. These results are presented and discussed in chapter 4.

CHAPTER 2

DESCRIPTION OF CALCULATIONS

2.1. Outline

The essence of our method lies in the quantum mechanical calculations
and in the scaling procedure used for the dimer polar tensors, given in
Eqs. 1 and 2. However, we wish to predict the intensities for the
normal modes of vibration of the molecule, and thus the calculation of
intensities from polar tensors (APT's) is intimately bound up with the
normal coordinate analysis. The forms of the normal coordinates depend
on the force field and on the geometry and atomic masses of the molecule.

Our purpose in this chapter is to include enough details about our
calculations so that the reader can reproduce our results or obtain
analogous results, using a different force field or theoretical APT's
from a different basis set. In order to do this, we must refer in some
detail to the equations involved in the normal coordinate analysis; thus,
in section 2.2 we set down these equations. In section 2.3 we give the
equations relating the intensities and the APT's. Then in section 2.4
we describe how we have applied these equations and give all the data
we have used, except for the theoretical APT's. In section 2.5 we
describe the numerical and quantum mechanical methods we have used in
calculating the theoretical APT's. Finally, in section 2.6, we give our
procedure for calculating the scaled APT's and intensities for the dimer.

25

2.2.   Normal Coordinate Analysis

As mentioned previously, there are several ways of representing the vibrational coordinates of the molecule. The normal coordinates, Q_i, are characterized by the fact that each fundamental absorption band depends on a single Q_i within the harmonic oscillator approximation. Moreover, in the normal coordinate representation, both the kinetic and potential vibrational energy of the molecule are a sum of independent contributions. Each of these contributions also depends on a single Q_i. We have used the Wilson FG matrix method to obtain the normal coordinates. The most important equations in this method are presented here. Detailed discussion of these equations can be found elsewhere [49].

The internal valence coordinates, R_i, provide a useful representation for the force constants. For an N-atomic molecule, the (3N-6)-dimensional column vector of internal coordinates, $\underline{R}$, is related to that of normal coordinates, $\underline{Q}$, by the matrix equation:

$$(3) \qquad\qquad \underline{R} = \underline{L}\underline{Q}.$$

The normal coordinate transformation matrix, $\underline{L}$, is determined by solving the eigenvalue problem,

$$(4) \qquad\qquad \underline{G}\underline{F}\underline{L} = \underline{L}\underline{\Lambda}.$$

The eigenvalues of this equation form the elements of the diagonal matrix of frequency parameters, $\underline{\Lambda}$, while the eigenvectors are given by the corresponding columns of the $\underline{L}$ matrix. The solution depends on the inverse kinetic energy matrix, $\underline{G}$, and the potential energy matrix, $\underline{F}$. The latter is composed of the force constants, given by

$$(5) \qquad F_{ij} = \frac{\partial^2 V}{\partial R_i \partial R_j} \quad ,$$

where V is the vibrational potential energy of the molecule.

As discussed in the previous chapter, the space-fixed cartesian coordinates constitute the most useful representation for the intensities. The 3N-dimensional vector of these coordinates, $\underline{X}$, is related to the vector, $\underline{R}$, by

$$(6) \qquad \underline{R} = \underline{B}\,\underline{X} \quad .$$

The $[(3N - 6) \times 3N]$-dimensional $\underline{B}$ matrix is related to the $\underline{G}$ matrix in Eq. 4, according to

$$(7) \qquad \underline{G} = \underline{B}\,\underline{M}^{-1}\underline{B}^{\dagger} \quad ,$$

where $\underline{B}^{\dagger}$ indicates the transpose of $\underline{B}$. The diagonal matrix of inverse masses, $\underline{M}^{-1}$, is given by

$$(8) \qquad (M^{-1})_{ii} = \frac{1}{m_1} \quad , \quad i = 1,2,3$$

$$\frac{1}{m_2} \quad , \quad i = 4,5,6$$

$$\vdots$$

$$\frac{1}{m_N} \quad , \quad i = 3N-2,\ 3N-1,\ 3N \quad ,$$

for the N atoms of the molecule.

A third type of vibrational coordinates is used to simplify the eigenvalue problem of Eq. 4. In the symmetry coordinate representation, the $\underline{G}$ and $\underline{F}$ matrices factor into different symmetry blocks. The symmetry coordinate vector, $\underline{S}$, is related to $\underline{R}$ by

(9a) $$\underline{S} = \underline{U}\underline{R}$$

(9b) $$\underline{S} = \underline{B}\underline{X} \quad .$$

The symmetrized $\underline{B}$ matrix, $\underline{\mathcal{B}}$, is given by

(10) $$\underline{\mathcal{B}} = \underline{U}\underline{B}$$

The symmetrized $\underline{F}$ matrix, $\underline{\mathcal{F}}$, is then defined as

(11a) $$F_{ij} = \frac{\partial^2 E}{\partial S_i \partial S_j}$$

(11b) $$\mathcal{F} = \underline{U}\underline{F}\underline{U}^\dagger \quad ,$$

where $\underline{U}$ is an orthogonal transformation, that is $\underline{U}^\dagger = \underline{U}^{-1}$. Similarly, the symmetrized $\underline{G}$ matrix, $\underline{\mathcal{G}}$, is given by

(12a) $$\underline{\mathcal{G}} = \underline{\mathcal{B}}\underline{M}^{-1}\underline{\mathcal{B}}^\dagger$$

(12b) $$\underline{\mathcal{G}} = \underline{U}\underline{G}\underline{U}^\dagger \quad .$$

Finally, we define the symmetrized $\underline{L}$ matrix:

(13a) $$\underline{S} = \underline{\mathcal{L}}\underline{Q}$$

(13b) $$\underline{\mathcal{L}} = \underline{U}\underline{L} \quad .$$

It can be seen from Eqs. 11b, 12b and 13b that Eq. 4 is equivalent to

(14) $$\underline{\mathcal{G}}\underline{\mathcal{F}}\underline{\mathcal{L}} = \underline{\mathcal{L}}\underline{\Lambda} \quad .$$

Each of the matrices in this equation is block diagonal. Thus, neither the symmetry nor the normal coordinates in a given block can mix with those in the other blocks. There is one block for each of the

irreducible representations of the vibrations in the symmetry group to which the molecule belongs.

The units we have used for the various matrices can be discussed on the basis that there are two types of symmetry coordinates, S_i. Those involving bond stretches (r-type) have units of length. For those involving angle deformations (θ-type) we have used units of radians (rad). There are, then, three types of force constants, depending on whether S_i and S_j in Eq. 11a are both r-type, both θ-type, or one of each. The resulting force constants all have similar magnitudes, if the energy in that equation is given in units of millidyne $\overset{\circ}{A}$ (md $\overset{\circ}{A}$, which is 10^{-11} erg) and the length in $\overset{\circ}{A}$. The units of the force constant, F_{ij}, in the three cases for S_i and S_j cited above, are then md $(\overset{\circ}{A})^{-1}$, md $\overset{\circ}{A}$ rad^{-2}, or md rad^{-1}, respectively. When S_k is r-type, the $\underline{k}$th row of $\underline{B}$ is unitless, whereas it has units of rad $(\overset{\circ}{A})^{-1}$ when S_k is θ-type. For the masses we have used atomic mass units (u). Thus, the $\underline{k}$th row of $\underline{L}$ has units of $u^{-\frac{1}{2}}$ when S_k is r-type and units of rad $(\overset{\circ}{A})^{-1} u^{-\frac{1}{2}}$, when S_k is θ-type.

The $\underline{G}$ matrix in Eq. 14 is completely determined by the $\underline{B}$ and $\underline{M}^{-1}$ matrices, according to Eq. 12a. Thus, the solution to Eq. 14 depends on the geometry, masses and force constants of the molecule. The eigenvector matrix, $\underline{L}$, describes the forms of the normal coordinates. Hence, $\underline{L}$ enters into the calculation of the intensities.

2.3 Intensity Relations

There are a number of ways of expressing infrared intensities. Overend [50] has given the relation between the integrated molar absorption coefficient of the $\underline{i}$th band, A_i, and the derivative of the dipole moment vector, $\vec{p}$, with respect to the $\underline{i}$th normal coordinate, Q_i:

$$A_i = \frac{N_A \pi}{3c^2} \left| \frac{\partial \vec{p}}{\partial Q_i} \right|^2$$

Here, N_A is Avogadro's number, and c is the speed of light in cm sec^{-1}. This equation gives A_i in cm mole^{-1} when $\partial\vec{p}/\partial Q_i$ is in esu g$^{-\frac{1}{2}}$. However, for the latter we have used the atomic units electron (e) u$^{-\frac{1}{2}}$. Thus, we have used the equation

$$(15) \qquad A_i = \frac{\pi}{3c^2} \left(N_A q_e\right)^2 \left| \frac{\partial \vec{p}}{\partial Q_i} \right|^2$$

where q_e gives the electronic charge ($q_e = 4.803 \times 10^{-10}$ esu), and A_i is still in cm mole^{-1}. This equation assumes that the vibrational frequency of each band is large enough so that all of the molecules are in the ground vibrational state at the temperature of the measurement. It also involves the assumptions of mechanical and electrical harmonicity, that is, the dipole moment is expanded as a linear function of the Q_i, and the harmonic oscillator wavefunctions are used for the vibrational Schrodinger equation.

The remaining equations in this section have been treated previously [1-3,6]. Eq. 15 may be expressed in terms of the $\underline{P}_Q$ matrices defined by Person and Newton [1],

$$(16) \qquad A_i = \frac{\pi}{3c^2} \left(N_A q_e\right)^2 (\underline{P}_Q^{+}\underline{P}_Q)_{ii} \quad , \quad i = 1, \ldots, 3N-6,$$

where

$$(P_Q)_{jk} = \frac{\partial p_j}{\partial Q_k} \ , \qquad\qquad \begin{array}{l} j = x, y, z \\ k = i, \ldots, 3N-6 \end{array}$$

is the matrix of dipole derivatives with respect to the normal

coordinates. The matrix of dipole derivatives with respect to the 3N space-fixed cartesian coordinates, $\underline{P}_X$ is related to the $\underline{P}_Q$ matrix by

$$(17) \qquad \underline{P}_Q = \underline{P}_X \underline{AL} \quad .$$

The $\underline{AL}$ product matrix gives the transformation from the vector of normal coordinates, Q, to the vector of space-fixed coordinates, $\underline{X}$:

$$(18) \qquad \underline{X} = \underline{ALQ}$$

$$= \underline{ALQ} \quad .$$

The $\underline{A}$ and $\underline{A}$ matrices are related by

$$\underline{A} = \underline{AU}\dagger$$

and are given by [3]

$$(19) \qquad \underline{A} = \underline{M}^{-1}\underline{B}\dagger\underline{G}^{-1}$$

$$\underline{A} = \underline{M}^{-1}\underline{B}\dagger\underline{G}^{-1} \quad .$$

The $\underline{AL}$ product matrix has units of $u^{-\frac{1}{2}}$, and $\underline{P}_X$ has units of e.

The $\underline{P}_X$ matrix is comprised of N juxtaposed APT's for each of the atoms of the molecule. If k^A represents the cartesian coordinates of atom A, the APT on atom A, P^A, is given by

$$(20) \qquad (P^A)_{jk} = \frac{\partial p_j}{\partial k^A} \quad , \qquad\qquad j,k^A = x,y,z.$$

Then the $\underline{P}_X$ matrix has the form

$$(21) \qquad \underline{P}_X = (\underline{P}^1 \; \underline{P}^2 \; \text{---} \; \underline{P}^N) \quad .$$

From Eqs. 17 and 21 we can see that it is necessary to specify the $\underline{A}$ and $\underline{l}$ matrices, in addition to the APT's, in order to determine the $\underline{P}_Q$

matrix and therefore the intensities. From Eqs. 19, 12a and 8, we see that the $\underline{A}$ matrix is determined by the $\underline{B}$ matrix and the masses of the molecule.

In order to obtain intensity predictions for the fundamental vibrations of water and water dimer, we have transformed the theoretically calculated APT's to the $\underline{P}_Q$ matrix, according to Eqs. 17 and 21. We shall also need the inverse transformation from the $\underline{P}_Q$ to the $\underline{P}_X$ matrix. This is because we wish to use the experimental APT's for the water monomer in our scaling procedure (see Eq. 2), and these must be obtained from the experimental intensities. The desired inverse transformation is given by

$$(22) \qquad \underline{P}_X = \underline{P}_Q \underline{L}^{-1} \underline{B} + \underline{D} \quad .$$

In this equation, the $\underline{D}$ matrix is the permanent dipole moment rotation matrix resulting from the transformation from the molecule-fixed normal coordinate representation to the space-fixed cartesian coordinate representation.

Like the $\underline{P}_X$ matrix, the $\underline{D}$ matrix is comprised of N juxtaposed tensors. It has the form of Eq. 21 with $\underline{p}^A$ replaced everywhere by $\underline{D}^A$. The rotational tensor, $\underline{D}^A$, for atom A is given by

$$(23) \qquad \underline{D}^A = \underline{((\vec{p}^0))} \underline{I}^{-1} \underline{((\vec{r}_A^{\,0}))} \underline{m}_A \quad .$$

Each of the factors in Eq. 23 is a second order tensor of rank 3. All three elements of the diagonal tensor, $\underline{m}_A$, are equal to the mass of atom A; $\vec{p}^0$ is the permanent dipole moment vector of the molecule; and $\vec{r}_A^{\,0}$ is the equilibrium position vector of atom A with respect to the center of mass. The notation, $\underline{((\vec{v}))}$ [represented by $\underline{((\vec{p}^0))}$ in Eq. 23, for example], indicates the tensor formed from the vector, $\vec{v}$, according to [6]

$$(24) \qquad \underline{((\vec{v}))} = \begin{pmatrix} 0 & v_z & -v_y \\ -v_z & 0 & v_x \\ v_y & -v_x & 0 \end{pmatrix} \quad .$$

In Eq. 23, $\underline{I}^{-1}$ is the inverse of the moment of inertia tensor, $\underline{I}$, which is given by

$$(25) \qquad \underline{I} = \sum_A m_A \underline{((\vec{r}_A{}^0))}^{\dagger} \underline{((\vec{r}_A{}^0))} \quad .$$

Thus, in order to determine the $\underline{D}$ matrix, we must know the masses and position vectors of the atoms with respect to the center of mass of the molecule, $\vec{r}_A{}^0$, and the permanent dipole moment, $\vec{p}^0$. We have used e $\overset{\circ}{A}$ for the units of the dipole moment, u for the masses, and $\overset{\circ}{A}$ for the position vectors in Eqs. 23 and 25. The rotational tensor, $\underline{D}^A$, therefore has units of e.

2.4. Application to Intensities for Water and Water Dimer

We may now apply these equations to the intensity calculations for water monomer and dimer. For the monomer we are interested in evaluating the theoretical APT's by comparing the resulting intensities with the experimental gas-phase intensities and with those from other calculations. Thus, we have used the $\underline{A}$ matrix and the experimental gas-phase $\underline{L}$ matrix in Eqs. 16 and 17 to calculate the intensities from these APT's. The $\underline{A}$ matrix was determined from the monomer $\underline{B}$ matrix and the atomic masses, according to Eq. 19. The $\underline{L}$ matrix was obtained by solving Eq. 14, using the experimental values of the force constants for the gas-phase monomer [51]. As mentioned above, the $\underline{G}$ matrix in Eqs. 14 and 19 is determined from the $\underline{B}$ matrix and the masses by Eq. 12a. Since we are

also interested in the observed intensities for the monomer in the N_2 matrix,* we have calculated a set of intensities using the $\underline{L}$ matrix derived from the force constants reported for the monomer in the matrix [30].

For the matrix-isolated dimer, we have calculated a set of intensities using the corresponding $\underline{A}$ and $\underline{L}$ matrices with the APT's obtained directly from the theoretical calculations for the dimer. The $\underline{L}$ matrix was derived from the force constants reported for the dimer in the N_2 matrix [30], as well as the $\underline{B}$ matrix and masses, using Eq. 14. An additional set of intensities was calculated from the scaled APT's using the same $\underline{A}$ and $\underline{L}$ matrices. In order to investigate the effect of changing the $\underline{L}$ matrix on the predicted intensities, we have also obtained an $\underline{L}$ matrix using force constants derived from the theoretical calculations of Curtiss and Pople [47]. Intensities were then obtained using this $\underline{L}$ matrix and the scaled dimer APT's. To obtain the latter we have used the experimental APT's for the monomer along with the monomer and dimer APT's calculated theoretically, according to Eqs. 1 and 2.

The experimental monomer APT's were calculated from the experimental intensities by first obtaining the $\underline{P}_Q$ matrix elements according to Eq. 16, and then by using this $\underline{P}_Q$ matrix with the monomer $\underline{B}$, $\underline{L}$ and $\underline{D}$ matrices in Eq. 22. Experimental intensities are not available for the monomer in the matrix, so we have assumed they are about equal to those in the gas-phase. To be consistent, we have used the monomer $\underline{L}$ matrix derived from the gas-phase force constants to calculate the experimental monomer APT's.

---

* Here we refer to the inert solid environment discussed in section 1.3. The word "matrix," in this sense, should not be confused with the mathematical term. The meaning of the word should be clear, from the context in which it is used, in all cases.

From the above discussion, it is clear what data must be specified in order for the reader to reproduce our results from the water monomer and dimer APT's. For the monomer these include the $\underline{B}$ matrix, the masses, and the experimental force constants, both for the gas-phase and for the monomer in the N_2 matrix. For the dimer we must give the $\underline{B}$ matrix, the masses, and the experimental force constants for the dimer in the matrix, as well as those derived from the theoretical calculation. We must also specify the data from which the experimental monomer APT's were obtained. For completeness we give both the data and the resulting APT's. We also give the position vectors from which the two $\underline{B}$ matrices were obtained, and the $\underline{L}$ matrix derived from each set of force constants we have used.

For the masses we have used $m_O = 16.0$ and $m_H = 1.008$ u throughout. The $\underline{B}$ matrix defines the relationship between the space-fixed cartesian and symmetry coordinates of the molecule, according to Eq. 9b. It is obvious that a given $\underline{B}$ matrix applies to a particular ordered sequence for both sets of coordinates. For the cartesian coordinates it is sufficient to give the order of the atoms; the atomic x, y and z coordinates are ordered consecutively.

In practice the $\underline{B}$ matrix is obtained first, thus defining the internal coordinates according to Eq. 6. Then, in order for the symmetry coordinates to have the properties described in the previous section, they are obtained as the normalized results of the symmetry projection operators on the internal coordinates. This determines the $\underline{U}$ matrix according to Eq. 9a, and the $\underline{B}$ matrix is then calculated from Eq. 10.

The coordinate system, atom numbering, and bond lengths and angles for H_2O are shown in Fig. 2-1. As indicated, the origin is centered on the O atom. The equilibrium position vectors were determined from the experimental structural parameters, $r_{OH} = 0.9572$ Å and $\theta = 104.52°$ [52].
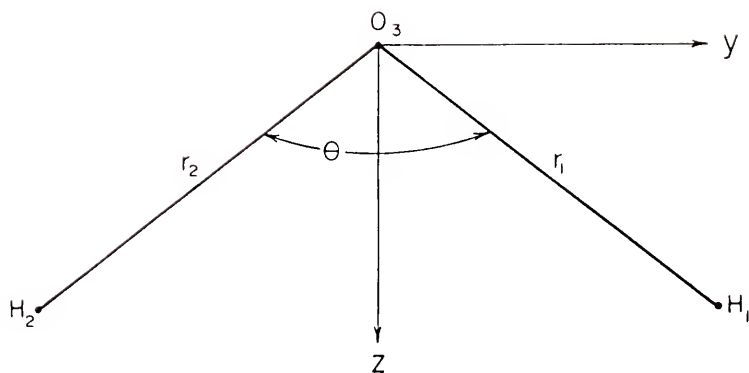
Fig. 2-1. Molecular coordinate system of water monomer.
Atom numbers, bond lengths and angle are indicated.

These vectors are given in Table 2-1. The definiton of internal

coordinates, which was used in calculating the $\underline{B}$ matrix, is given on the

left side of Table 2-2. The H_2O molecule has C_{2v} symmetry. The reducible

representation spanned by the internal coordinates is given by

$$\Gamma_R = 2a_1 + b_2 \quad .$$

The corresponding symmetry coordinates are given on the right side of

Table 2-2, and the resulting $\underline{\underline{B}}$ matrix in Table 2-3.

The coordinate system for the linear water dimer is shown in

Fig. 2-2. The origin is on the O atom of the electron donor molecule

(atom 3). The atom numbering is given in Fig. 1-2. The equilibrium

position vectors we have used are given in Table 2-4. Large basis set

calculations for the water dimer have indicated that the bond distances

and angles of the two component water molecules do not differ appreciably

from their values in the monomer [53,54]. Accordingly, we have used the

experimental values of r_{OH} and θ given above for each of the water mole-

cules in the dimer. We have taken the intermolecular geometry from the

minimum energy structure calculated for the dimer by Hankins, Moscowitz

and Stillinger near the Hartree-Fock limit [53]. For the dimer structure

illustrated in Fig. 2-2 and discussed in section 1.3.1, the intermolecu-

lar geometrical parameters which determine the position vectors are the

O-O distance and the angle ϕ, which the C_2 axis of the electron donor

makes with the negative y axis as shown in the figure. The theoretical

values for these parameters are $R_{O-O} = 3.00 \overset{\circ}{A}$ and $\phi = 40°$ [53].

The internal coordinates of water dimer are defined on the left side

of Table 2-5 in terms of the bond lengths and angles in Fig. 2-2. Note

that we have only included the six intramolecular vibrational coordinates

and not the six additional intermolecular coordinates. This is because

Table 2-1. Equilibrium position vectors for water monomer. Coordinate system and atom numbering are given in Fig. 2-1. Units are Å.

Atom No.:	1	2	3
x^0	0.0	0.0	0.0
y^0	0.756950	-0.756950	0.0
$z^{0,\ a}$	0.585882	0.585882	0.0

[a] The prime indicates that values are not with respect to the center of mass.

Table 2-2. Definition of internal and symmetry coordinates for water monomer. Bond lengths and angles are indicated in Fig. 2-1.

Internal Coordinates	Symmetry Coordinates	Symmetry	Units
$R_1 = \Delta r_1$	$S_1 = (R_1 + R_2)/\sqrt{2}$	a_1	Å
$R_2 = \Delta r_2$	$S_2 = R_3$	a_1	rad
$R_3 = \Delta\theta$	$S_3 = (R_1 - R_2)/\sqrt{2}$	b_2	Å

Table 2-3. The $\underline{B}$ matrix for water monomer. Row 2 has units of rad $\overset{\circ}{A}^{-1}$. All other rows are unitless.

Symmetry Coordinate	Cartesian Coordinate		
	x_1	y_1	z_1
S_1	0.0	0.559178	0.432805
S_2	0.0	0.639448	-0.826156
S_3	0.0	0.559178	0.432805
	x_2	y_2	z_2
S_1	0.0	-0.559178	0.432805
S_2	0.0	-0.639448	-0.826156
S_3	0.0	0.559178	-0.432805
	x_3	y_3	z_3
S_1	0.0	0.0	-0.865611
S_2	0.0	0.0	1.652312
S_3	0.0	-1.118355	0.0
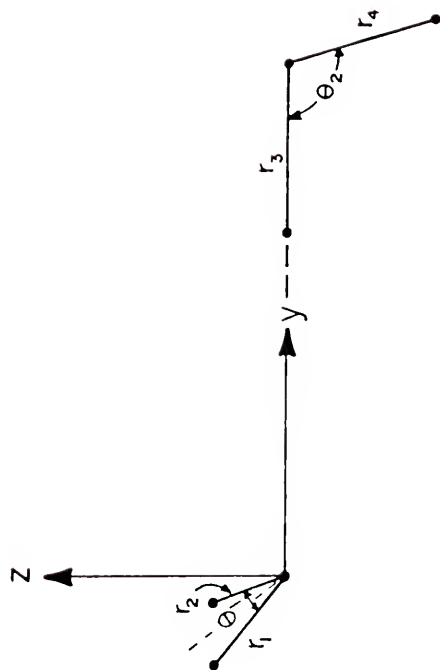
Fig. 2-2. Molecular coordinate system of the linear water dimer. Bond lengths and angles are indicated.

Table 2-4. Equilibrium position vectors for the linear water dimer. Coordinate system is given in Fig. 2-2 and atom numbering in in Fig. 1-2. Units are Å.

Atom No.:	1	2	3	4	5	6
x^0	0.756950	-0.756950	0.0	0.0	0.0	0.0
y^0	-0.448812	-0.448812	0.0	2.042800	3.0	3.239987
z^0	0.376598	0.376598	0.0	0.0	0.0	-0.926627

Table 2-5. Definition of internal and symmetry coordinates for the linear water dimer. Bond lengths and angles are indicated in Fig. 2-2.

Internal Coordinates	Symmetry Coordinates	Symmetry	Units
$R_1 = \Delta r_1$	$S_1 = R_4$	A'	Å
$R_2 = \Delta r_2$	$S_2 = (R_1 + R_2)/\sqrt{2}$	A'	Å
$R_3 = \Delta r_3$	$S_3 = R_3$	A'	Å
$R_4 = \Delta r_4$	$S_4 = R_6$	A'	rad
$R_5 = \Delta\theta_1$	$S_5 = R_5$	A'	rad
$R_6 = \Delta\theta_2$	$S_6 = (R_1 - R_2)/\sqrt{2}$	A''	Å

with one possible exception [40, and references cited therein], the six low-frequency intermolecular absorptions of the water dimer have not yet been observed. Thus, there are no reliable frequencies from which to determine the force constants, and no experimental spectrum in the literature with which to compare the intermolecular intensities. The dimer molecule in Fig. 2-2 has C_s symmetry, and the reducible representation of the six internal coordinates is given by

$$\Gamma_R = 5a' + a'' \quad .$$

The corresponding symmetry coordinates are given on the right side of Table 2-5. The $\underline{B}$ matrix obtained from these data appears in Table 2-6.

To calculate the $\underline{B}$ matrices in Tables 2-3 and 2-6, and to solve the eigenvalue problem of Eq. 14, we used the normal coordinate programs WMAT and CHARLY [55]. The operation of these programs has been discussed in detail elsewhere [56]. Program WMAT calculates the $\underline{B}$ and $\underline{G}$ matrices and outputs a transformation of the $\underline{G}$ matrix which facilitates the diagonalization of the $\underline{GF}$ product. The input to WMAT includes the masses and equilibrium position vectors of the atoms, the definition of the internal coordinates, and the $\underline{U}$ matrix. We note that the $\underline{B}$ matrix must represent a transformation to a true molecule-fixed coordinate system--that is, it must be invariant to rigid translations and rotations of the whole molecule. Program WMAT insures this by using the "little $\underline{s}$ vector" technique [49] to calculate the $\underline{B}$ matrix in Eq. 6 and then transforming according to Eq. 10. The input to program CHARLY includes the output from WMAT and the force constant matrix, $\underline{F}$. The output from CHARLY includes the frequencies (determined from the $\underline{\Lambda}$ matrix) and the eigenvector matrix, $\underline{L}$.

In order to obtain the experimental gas-phase $\underline{L}$ matrix for H_2O, we used the $\underline{F}$ matrix given by Cook, De Lucia and Helminger [51]. It was obtained

Table 2-6. The $\underline{B}$ matrix for water dimer. Rows 4 and 5 have units of rad Å^{-1}. All other rows are unitless.

Symmetry Coordinate	Cartesian Coordinate								
	x_1	y_1	z_1	x_2	y_2	z_2	x_3	y_3	z_3
S_1	0.0	0.0	0.0	0.0	0.0	0.0	0.0	0.0	0.0
S_2	0.559178	-0.331548	0.278202	-0.559178	-0.331548	0.278202	0.0	0.663096	-0.556404
S_3	0.0	0.0	0.0	0.0	0.0	0.0	0.0	0.0	0.0
S_4	0.0	0.0	0.0	0.0	0.0	0.0	0.0	0.0	0.0
S_5	0.639448	0.632872	-0.531043	-0.639448	0.632872	-0.531043	0.0	-1.265744	1.062085
S_6	0.559178	-0.331548	0.278202	0.559178	0.331548	-0.278202	-1.118355	0.0	0.0

Symmetry Coordinate	Cartesian Coordinate								
	x_4	y_4	z_4	x_5	y_5	z_5	x_6	y_6	z_6
S_1	0.0	0.0	0.0	0.0	-0.250717	0.968060	0.0	0.250717	-0.968060
S_2	0.0	0.0	0.0	0.0	0.0	0.0	0.0	0.0	0.0
S_3	0.0	-1.0	0.0	0.0	1.0	0.0	0.0	0.0	0.0
S_4	0.0	0.0	1.044713	0.0	-1.011346	-1.306641	0.0	1.011346	0.261923
S_5	0.0	0.0	0.0	0.0	0.0	0.0	0.0	0.0	0.0
S_6	0.0	0.0	0.0	0.0	0.0	0.0	0.0	0.0	0.0

by fitting the observed infrared frequencies, as well as the quartic distortion coefficients from microwave data, for H_2O and its deuterated and tritiated isotopes. This $\underline{F}$ matrix is given in Table 2-7 along with the resulting $\underline{L}$ matrix elements.

The experimental $\underline{F}$ matrix for water monomer in the N_2 matrix was taken from Tursi and Nixon [30]. It was obtained from a fit to the frequencies of H_2O and its deuterated isotopes in the matrix. The $\underline{F}$ and $\underline{L}$ matrices are given in Table 2-7. It can be seen that the stretch-bend interaction force constant, F_{12}, has a different sign for H_2O monomer in the N_2 matrix from that for H_2O in the gas-phase. The effect of this change on the intensities is discussed in the following chapter.

The experimental $\underline{F}$ matrix for water dimer in the N_2 matrix was also obtained from Tursi and Nixon [30], and was derived in the same manner as that for H_2O. It is given in Table 2-9 in terms of the symmetry coordinates of Table 2-5, together with the corresponding $\underline{L}$ matrix. Intermolecular coupling force constants were not included in the analysis of Tursi and Nixon. The $\underline{F}$ and $\underline{L}$ matrix elements for the electron donor (ED) molecule (see Fig. 1-2) appear in the upper part of Table 2-9, and those for the electron acceptor (EA) molecule in the lower part.

The "theoretical" force constants we have used for the water dimer were derived from those calculated with the 4-31G basis set by Curtiss and Pople [47], using the scaling procedure described in section 1.4.1. The details of the derivation are given in the Appendix, as well as the comparison of the resulting frequencies with experiment. The agreement is quite satisfactory. This $\underline{F}$ matrix and the corresponding $\underline{L}$ matrix are given in Table 2-10. We note that intermolecular coupling force constants were included by Curtiss and Pople, and the $\underline{F}$ and $\underline{L}$ matrix elements for these interactions are given in the middle part of the table.

Table 2-7. Experimental F and L matrices for water monomer in the gas-phase. The F matrix is from Cook, DeLucia and Helminger [51].

F_{11}	7.653 md $\overset{\circ}{A}^{-1}$	L_{11}	1.013 $u^{-\frac{1}{2}}$
F_{12}	0.5124 md rad^{-1}	L_{12}	-0.1117 $u^{-\frac{1}{2}}$
F_{22}	0.6398 md $\overset{\circ}{A}$ rad^{-2}	L_{21}	0.0800 rad $\overset{\circ}{A}^{-1}$ $u^{-\frac{1}{2}}$
F_{33}	7.838 md $\overset{\circ}{A}^{-1}$	L_{22}	1.526 rad $\overset{\circ}{A}^{-1}$ $u^{-\frac{1}{2}}$
		L_{33}	1.034 $u^{-\frac{1}{2}}$

Table 2-8. Experimental F and L matrices for water monomer in the N_2 matrix. The F matrix is from Tursi and Nixon [30].

F_{11}	7.335 md $\overset{\circ}{A}^{-1}$	L_{11}	1.012 $u^{-\frac{1}{2}}$
F_{12}	-0.4223 md rad^{-1}	L_{12}	0.1229 $u^{-\frac{1}{2}}$
F_{22}	0.6945 md $\overset{\circ}{A}$ rad^{-2}	L_{21}	-0.2710 rad A^{-1} $u^{-\frac{1}{2}}$
F_{33}	7.697 md $\overset{\circ}{A}^{-1}$	L_{22}	1.504 rad A^{-1} $u^{-\frac{1}{2}}$
		L_{33}	1.034 $u^{-\frac{1}{2}}$

Table 2-9. Experimental $\underline{F}$ and $\underline{L}$ matrices for the linear water dimer in the N_2 matrix. The $\underline{F}$ matrix is from Tursi and Nixon [30].

Electron Donor			
F_{22}	7.3205 md $\overset{\circ}{A}^{-1}$	L_{22}	1.012 $u^{-\frac{1}{2}}$
F_{25}	-0.4088 md rad^{-1}	L_{25}	0.1198 $u^{-\frac{1}{2}}$
F_{55}	0.6927 md $\overset{\circ}{A}$ rad^{-2}	L_{52}	-0.2664 rad $\overset{\circ}{A}^{-1} u^{-\frac{1}{2}}$
F_{66}	7.6545 md $\overset{\circ}{A}^{-1}$	L_{55}	1.505 rad $\overset{\circ}{A}^{-1} u^{-\frac{1}{2}}$
		L_{66}	1.034 $u^{-\frac{1}{2}}$

Electron Acceptor			
F_{11}	7.498 md $\overset{\circ}{A}^{-1}$	L_{11}	0.9492 $u^{-\frac{1}{2}}$
F_{13}	-0.2200 md $\overset{\circ}{A}^{-1}$	L_{13}	0.3794 $u^{-\frac{1}{2}}$
F_{14}	-0.3350 md rad^{-1}	L_{14}	0.0979 $u^{-\frac{1}{2}}$
F_{33}	7.036 md $\overset{\circ}{A}^{-1}$	L_{31}	-0.4026 $u^{-\frac{1}{2}}$
F_{34}	-0.3350 md rad^{-1}	L_{33}	0.9387 $u^{-\frac{1}{2}}$
F_{44}	0.7211 md $\overset{\circ}{A}$ rad^{-2}	L_{34}	0.1057 $u^{-\frac{1}{2}}$
		L_{41}	-0.1082 rad $\overset{\circ}{A}^{-1} u^{-\frac{1}{2}}$
		L_{43}	-0.2824 rad $\overset{\circ}{A}^{-1} u^{-\frac{1}{2}}$
		L_{44}	1.498 rad $\overset{\circ}{A}^{-1} u^{-\frac{1}{2}}$

Table 2-10. Scaled 4-31G F and L matrices for the linear water dimer
in the N_2 matrix. The F matrix was obtained by scaling
the 4-31G F matrix of Curtiss and Pople [47], as
described in the Appendix.

Electron Donor			
F_{22}	7.428 md Å^{-1}	L_{22}	-1.018 u$^{-\frac{1}{2}}$
F_{55}	0.6963 md Å rad^{-2}	L_{55}	1.524 rad Å^{-1} u$^{-\frac{1}{2}}$
F_{66}	7.804 md Å^{-1}	L_{66}	1.034 u$^{-\frac{1}{2}}$

Intermolecular			
F_{12}	-0.0170 md A^{-1}	L_{12}	-0.0088 u$^{-\frac{1}{2}}$
F_{23}	-0.0070 md A^{-1}	L_{21}	-0.0287 u$^{-\frac{1}{2}}$
F_{45}	0.0027 md A rad^{-2}	L_{23}	0.0418 u$^{-\frac{1}{2}}$
		L_{32}	0.0504 u$^{-\frac{1}{2}}$
		L_{45}	0.1137 rad A^{-1} u$^{-\frac{1}{2}}$
		L_{54}	0.1137 rad A^{-1}u$^{-\frac{1}{2}}$

Electron Acceptor			
F_{11}	7.616 md A^{-1}	L_{11}	0.9338 u$^{-\frac{1}{2}}$
F_{13}	-0.182 md A^{-1}	L_{13}	0.4270 u$^{-\frac{1}{2}}$
F_{33}	7.126 md A^{-1}	L_{31}	-0.4399 u$^{-\frac{1}{2}}$
F_{44}	0.7330 md A rad^{-2}	L_{33}	0.9265 u$^{-\frac{1}{2}}$
		L_{44}	1.524 rad A^{-1} u$^{-\frac{1}{2}}$

However, stretch-bend coupling force constants were neglected by Curtiss and Pople for both the ED and EA molecules, while they were included by Tursi and Nixon. The effect on the intensities of neglecting these interactions is discussed in the following chapter. In calculating the $\underline{L}$ matrix of Table 2-10 from Eq. 14, the cross-terms in the $\underline{G}$ matrix corresponding to the stretch-bend interactions were constrained to zero. If this had not been done, the interaction terms in the $\underline{GF}$ product matrix would not be zero but would depend on the values of the stretch and bend diagonal force constants. This somewhat arbitrary procedure was also adopted by Curtiss and Pople. Due to the neglect of the stretch-bend interactions by Curtiss and Pople, there are fewer $\underline{F}$ and $\underline{L}$ matrix elements listed in Table 2-10 for the ED and EA molecules of the dimer. These values are given in the upper and lower parts of the table, respectively.

We now give the data used to obtain the experimental APT's, $\underline{P}^A$, for the monomer. The experimental dipole derivatives with respect to dimensionless normal coordinates, $\partial p_i / \partial q_j$, have been given by Clough, Beers, Klein and Rothman for water monomer in the gas-phase [57, see also reference 58]. Although the total integrated intensities give only the magnitudes of the dipole derivatives (see Eq. 15), these authors chose the signs so that the observed vibration-rotation effects on intensities were reproduced in the fundamental bands of H_2O. These sign choices agree with those obtained by a number of *ab initio* calculations (see section 3.2).

The $\partial p_i / \partial q_j$ values given by these authors were converted to $\partial p_i / \partial Q_j$ to give the elements of the $\underline{P}_Q$ matrix, using the equation [59]

$$q_j = 2\pi(c\omega_j/h)^{\frac{1}{2}}Q_j \quad ,$$

where h is Planck's constant in erg sec, ω_j is the jth harmonic frequency in cm^{-1}, and c is the speed of light in cm sec^{-1}. We used the harmonic frequencies, ω_1 = 3832.2, ω_2 = 1648.5, and ω_3 = 3942.5 cm^{-1}, given by Benedict, Gailar and Plyler [52], in the conversion.

Each component of the dipole moment vector belongs to a different irreducible representation of the C_{2v} symmetry group. Hence there are only three non-zero elements in the $\underline{P}_Q$ matrix for H_2O: $\partial p_z/\partial Q_1$, $\partial p_z/\partial Q_2$ and $\partial p_y/\partial Q_3$, according to the axis system shown in Fig. 2-1. The values of these elements derived from the data of Clough, Beers, Klein and Rothman are 0.0479, -0.2344 and 0.2139 e $u^{-\frac{1}{2}}$, respectively.

This $\underline{P}_Q$ matrix was used with the $\underline{L}$ matrix in Table 2-7 and the $\underline{B}$ matrix in Table 2-3 to calculate $\underline{P}_Q\underline{L}^{-1}\underline{B}$, which was then added to the $\underline{D}$ matrix to obtain $\underline{P}_X$ according to Eq. 22. The $\underline{P}_Q\underline{L}^{-1}\underline{B}$ matrix is composed of three juxtaposed tensors (the "vibrational tensors"): one for each of the atoms in the H_2O molecule. These tensors are given in the upper part of Table 2-11 for H_1 and O_3 of Fig. 2-1. For all the tensors given in this table, the corresponding H_2 tensor is the same as that for H_1, except that the off-diagonal elements of the H_2 tensor have the opposite sign from that for the H_1 tensor (according to the transformation shown in Eq. 30 below).

The rotational tensors, $\underline{D}^A$, were calculated from Eq. 23 using the effective dipole moment for the ground vibrational state, p_z^0 = 0.3861 e $\overset{\circ}{A}$, taken from Clough, Beers, Klein and Rothman [57]. Since $p_x^0 = p_y^0 = 0$, the last row of $\underline{((\vec{p}^0))}$ is zero (see Eq. 24). Hence, only the x and y components of the diagonal inverse moment of inertia tensor, $\underline{I}^{-1}$, were used in Eq. 23. These values were calculated using the equilibrium position vectors with respect to the center of mass, $\vec{r}_A^0$, in Eq. 25. The values of the x and y coordinates, x_A^0 and y_A^0, with respect to the

center of mass are the same as those given in Table 2-1 with respect to an origin on the O atom as shown in Fig. 2-1. Because the center of mass is displaced in the positive z direction away from the O atom, the values, $z_{O_3}{}^0 = -0.0655689$ Å, $z_{H_1}{}^0 = z_{H_2}{}^0 = 0.520313$ Å, were used in Eq. 25 rather than the $z_A{}^0$' of Table 2-1. The resulting principal moments of inertia are $I_{xx} = 1.76993$ Å^2 u and $I_{yy} = 0.614651$ Å^2 u, while the corresponding elements of $\underline{I}^{-1}$ are just the reciprocals of these values.

The $\underline{D}^A$ tensors obtained using Eq. 23 and the parameters given above are shown in the middle part of Table 2-11. The total APT's, $\underline{P}^A$, were obtained as the sum of the vibrational and rotational tensors and are given in the lower part of the table. These experimental APT's for the monomer were used in Eqs. 1 and 2 together with the monomer and dimer APT's calculated theoretically to obtain scaled APT's for the dimer. In the remainder of this chapter we describe the methods we have used for obtaining the theoretical APT's and the scaled APT's for the dimer.

2.5. Calculation of Theoretical Polar Tensors

The theoretical APT's for water monomer and dimer were calculated numerically from the theoretical values of the dipole moments for the equilibrium configuration and for a set of displaced configurations for each molecule. The calculated dipole moments were fitted to a linear function of the cartesian displacement coordinates, Δj^A. This treatment is consistent with the assumption of electrical harmonicity used to derive Eq. 15 and the linear relation between normal coordinates and the space-fixed cartesian coordinates given by Eq. 18. Thus,

Table 2.11. Experimental atomic polar tensors for water monomer in the gas phase (P^A). Vibrational and rotational tensors are also given. Units are e, where 1e = 1.602×10^{-19} coulombs. Coordinate system is given in Fig. 2-1.

Atom	H_1			O_3		
$\underline{P}_Q \underline{L}^{-1} \underline{B}$	0.0	0.0	0.0	0.0	0.0	0.0
	0.0	0.1156	0.0895	0.0	-0.2312	0.0
	0.0	-0.0624	0.1489	0.0	0.0	-0.2978
$\underline{D}^A$	0.3295	0.0	0.0	0.6591	0.0	0.0
	0.0	0.1144	-0.1665	0.0	-0.2289	0.0
	0.0	0.0	0.0	0.0	0.0	0.0
$\underline{P}^A$	0.3295	0.0	0.0	0.6591	0.0	0.0
	0.0	0.2301	-0.0770	0.0	-0.4601	0.0
	0.0	-0.0624	0.1489	0.0	0.0	-0.2978

$$(27) \qquad p_i \simeq p_i^{\ 0} + \sum_A \sum_j \left(\frac{\partial p_i}{\partial j^A}\right)_0 \Delta j^A \qquad i, j^A = x, y, z$$

$$A = 1, \ldots, N$$

$$\simeq p_i^{\ 0} + \sum_A \sum_j (P^A)_{ij} \Delta j^A \qquad ,$$

where $(P^A)_{ij}$ is an element of the APT on atom A (see Eq. 20). Here p_i is is the $\underline{i}$th component of the total dipole moment of the molecule for the displaced configuration, and $p_i^{\ 0}$ is the value of that component for the equilibrium configuration.

The displaced configurations we have used involve the displacement of a single atom, A, along the x, y or z direction of the molecular axis system. Thus, for each displaced configuration, only one of the terms in the double summation of Eq. 27 is non-zero. We have used, in general, two configurations for each atom and each direction--one involving a displacement in the positive x direction, for example, and one involving a displacement of the same magnitude in the negative x direction. The dipole moment components for the equilibrium and the two displaced configurations--$p_i^{\ 0}$, $p_i(+\Delta j^A)$, and $p_i(-\Delta j^A)$--were used to determine the first, second or third column of the APT on atom A when j^A was x, y or z, respectively. Thus, Eq. 27 leads to

$$(28) \qquad (P^A)_{ij} = \left[\frac{p_i(+\Delta j^A) - p_i^{\ 0}}{2|\Delta j^A|}\right] + \left[\frac{p_i^{\ 0} - p_i(-\Delta j^A)}{2|\Delta j^A|}\right] \qquad ,$$

$$i, j^A = x, y, z$$

The condition that the two terms in brackets should be nearly equal was used to check the calculations.

To determine the APT on one of the atoms in each of the molecules H_2O and $(H_2O)_2$, we have used the relation [1],

$$(29) \qquad \sum_{A} \underline{p}^{A} = 0 \quad .$$

We have also used the fact that the two H atoms in the monomer and in the electron donor molecule of the dimer are symmetrically equivalent. Thus, in both cases, we have obtained $\underline{p}^{H_2}$ from $\underline{p}^{H_1}$ using the transformation [2]

$$(30) \qquad \underline{p}^{H_2} = \underline{\underline{T}}\,\underline{p}^{H_1}\underline{\underline{T}}^{\dagger}$$

where $\underline{\underline{T}}$ is the matrix for reflection across the xz symmetry plane for H_2O ($T_{11} = T_{33} = 1$, $T_{22} = -1$, $T_{ij} = 0$, $i \neq j$); and the yz symmetry plane for $(H_2O)_2$ ($T_{11} = -1$, $T_{22} = T_{33} = 1$, $T_{ij} = 0$, $i \neq j$).

The equilibrium configurations about which the displacements were made for H_2O and $(H_2O)_2$ are given by the position vectors in Tables 2-1 and 2-4, respectively. As noted previously, the H_2O configuration was derived from experimental measurements, while that of $(H_2O)_2$ was derived from the extended basis set calculation by Hankins, Moscowitz and Stillinger [53]. More recently, Dyke, Mack and Muenter have obtained structural parameters for water dimer produced by expanding the vapor through a supersonic nozzle jet [60]. They used electric resonance spectroscopy to determine microwave transition frequencies, and their results indicated an equilibrium structure similar to that given in Table 2-4 (with $R_{O-O} = 3.00$ Å), except that $R_{O-O} = 2.98(\pm 0.01)$ Å and $\phi = 58(\pm 6)°$. Although the experimental value of ϕ appears to differ significantly from the value of $40°$ which we have used, the wavefunction for the water dimer is not expected to be very sensitive to this parameter. A basis set similar to that used by Hankins, Moscowitz and Stillinger has been used by Popkie, Kistenmacher and Clementi [61] to calculate the binding energy of the dimer as a function of ϕ, with all other structural parameters held constant at the same values as those

consistent with Table 2-4. For values of ϕ = 15°, 30°, 45°, and 60°, binding energies of -4.49, -4.58, -4.58, and -4.39 kcal/mole, respectively, were obtained. Thus, the calculated binding energy of the dimer is not very sensitive to this parameter, and the calculated APT's would be expected to be relatively independent of the value of ϕ chosen for the equilibrium configuration.

We used two different quantum mechanical methods [62] to calculate the dipole moments for each set of geometrical configurations: the *ab initio* self-consistent field (SCF) method using a 4-31G basis set and the approximate SCF method of complete neglect of differential overlap (CNDO).

The SCF method involves iteratively solving a set of simultaneous linear equations, the Roothaan equations, that arise from the Schrodinger equation when the $\underline{i}$th molecular orbital, ψ_i, is expanded as a linear combination of basis set orbitals, ϕ_{μ_A}, on each atom, that is,

$$(31) \qquad \psi_i = \sum_A \sum_{\mu_A} c_{\mu_A i} \phi_{\mu_A} \quad .$$

The Roothaan equations are solved for the $c_{\mu_A i}$, whose coefficients are integrals involving the basis set orbitals, ϕ_{μ_A}.

In the *ab initio* SCF method, the integrals are evaluated analytically from the functional form of the basis set. In the CNDO method many of these integrals are neglected, and combinations of others are parameterized--that is, adjusted to fit *ab initio* SCF results for orbital energies and eigenvectors of small molecules. Both the *ab initio* SCF method and the approximations in the CNDO method have been described in reference 62.

The CNDO/2 parameterization of the integrals was used in this work, and this has been given in detail also in reference 62.

The CNDO calculations were performed using QCPE program CNINDO [63]. Essentially, the only input to this program is composed of the atomic position vectors for each geometrical configuration. The 4-31G calculations were carried out using version 5 of the IBMOL program by Clementi and Mehl [64]. This program is designed to accept "contracted" (fixed linear combinations of) Gaussian functions as basis set orbitals. The input to the program includes the exponents for the "primitive" (uncontracted) Gaussian functions, the contraction coefficients, and the coefficients for the symmetrized orbitals, as well as the geometrical configuration data.

The symmetrized orbitals we used were the same as the contracted orbitals, except for those involving 1s orbitals on H_1 and H_2 of both H_2O and $(H_2O)_2$ (see Figs. 1-2 and 2-1). For these orbitals, the symmetrized functions, χ_{1s}^+ and χ_{1s}^-, were constructed, where

$$\chi_{1s}^+ = \frac{1}{N^+}[\phi_{1s}(H_1) + \phi_{1s}(H_2)]$$

for A_1 symmetry of H_2O and A' symmetry of $(H_2O)_2$; and

$$\chi_{1s}^- = \frac{1}{N^-}[\phi_{1s}(H_1) - \phi_{1s}(H_2)]$$

for B_2 symmetry of H_2O and A'' symmetry of $(H_2O)_2$. N^+ and N^- are the corresponding normalization factors.

For the Gaussian exponents and contraction coefficients we have used those given by Ditchfield, Hehre and Pople [65]. Their 4-31G contraction is the result of a systematic sequence of studies aimed at finding a computationally efficient basis set while maintaining an optimal degree

of accuracy and flexibility. The basis set consists of a single con-
tracted Gaussian orbital (CGO) for the core orbitals and two CGO's for
each valence orbital--an "inner" CGO, having relatively large exponents,
and an "outer" CGO with smaller exponents. The core CGO's consist of
four primitive Gaussians, the inner CGO's of three primitive Gaussians,
and the outer or diffuse CGO's of one Gaussian, each. We have used the
optimized exponents and coefficients given in Tables I and II of
reference 65, modified by the scaling parameters for the H_2O molecule
recommended in Table III, according to Eq. 7 of that reference.

The output from the IBMOL program included the total energy and the
eigenvectors--that is, the coefficients $c_{\mu_A i}$ in Eq. 31. The input to
IBMOL and the eigenvector output were used in program POPULAN [66] to
calculate the dipole moments and the Mulliken population analysis for
each configuration.

The analytic form for the expectation value of the dipole moment is
related to the Mulliken gross atomic charge [67] on each of the atoms.
We have made use of this relation to analyze further the intensity
changes upon going from water monomer to dimer. Moreover, the dipole
moments calculated by the CNINDO program involve an approximation, in
addition to those used in calculating the eigenvectors, that is best
indicated by considering the expectation value of the dipole moment $\langle \vec{p} \rangle$
in terms of the Mulliken gross atomic charges. For closed shell mole-
cules, such as water and water dimer, $\langle \vec{p} \rangle$ is given in terms of the
molecular orbitals, ψ_i, by

$$(32) \qquad \langle \vec{p} \rangle = \sum_{A=1}^{N} Z_A \vec{R}_A - 2 \sum_{i=1}^{n} \int \psi_i(1) \vec{r}_1 \psi_i(1) d\tau_1 \qquad .$$

In this equation, n is the number of orbitals (half the number of elec-
trons), $\vec{R}_A$ is the position vector of nucleus A and $\vec{r}_1$ that of electron 1.
Z_A is the charge of nucleus A. Using Eq. 31 for the molecular orbital
and the definition of the density matrix element, $D_{\mu_A \nu_B}$, which is

$$D_{\mu_A \nu_B} = 2 \sum_{i=1}^{n} c_{\mu_A i} c_{\nu_B i} \quad,$$

Eq. 32 becomes

$$(33) \qquad <\vec{p}> = \sum_A [Z_A \vec{R}_A - \sum_B \sum_{\mu_A} \sum_{\nu_B} D_{\mu_A \nu_B} <\mu_A|\vec{r}_1|\nu_B>] \quad.$$

Here we have used the bracket notation for integrals:

$$<\mu_A|\vec{r}_1|\nu_B> = \int \phi_{\mu_A}(1)\vec{r}_1 \phi_{\nu_B}(1)d\tau_1 \quad.$$

The electronic position vector may be expressed as

$$(34) \qquad \qquad \vec{r}_1 = \vec{R}_A + \vec{r}_A \quad,$$

where $\vec{r}_A$ is the position vector of electron 1 with respect to nucleus A.
Substituting Eq. 34 into Eq. 33 and noting that $\vec{R}_A$ comes out of the
integral and summations in the second term of Eq. 33, we have

$$(35) \qquad <\vec{p}> = \sum_A (\vec{R}_A[Z_A - \sum_B \sum_{\mu_A} \sum_{\nu_B} D_{\mu_A \nu_B} S_{\mu_A \nu_B}]$$

$$- \sum_B \sum_{\mu_A} \sum_{\nu_B} D_{\mu_A \nu_B} <\mu_A|\vec{r}_A|\nu_B>) \quad,$$

where $S_{\mu_A \nu_B}$ is the overlap integral:

$$S_{\mu_A \nu_B} = \langle \mu_A | \nu_B \rangle \quad .$$

The Mulliken gross atomic population on atom A, N(A), is defined as [67]

(36) $$N(A) = \sum_B \sum_{\mu_A} \sum_{\nu_B} D_{\mu_A \nu_B} S_{\mu_A \nu_B} \quad .$$

The gross atomic charge on atom A, Q_A, is [67]

(37) $$Q_A = Z_A - N(A) \quad .$$

Substituting Eqs. 36 and 37 into Eq. 35 gives

(38) $$\langle \vec{p} \rangle = \sum_A [Q_A \vec{R}_A - \sum_B \sum_{\mu_A} \sum_{\nu_B} D_{\mu_A \nu_B} \langle \mu_A | \vec{r}_A | \nu_B \rangle] \quad .$$

In the CNINDO program the dipole moments are approximated by neglecting terms for which B $\neq$ A in the second term of Eq. 38. The only remaining non-zero terms are those in which μ_A = $2s_A$ and ν_A = $2p_A$. Thus, this is the "sp polarization" term defined by Pople and Segal [68]. The gross atomic charges are also approximated in the CNINDO program, in that $S_{\mu_A \nu_B}$ in Eq. 36 is replaced by $\delta_{\mu_A \nu_B}$, where δ is the Kronecker delta.

The dipole moments for the appropriate configurations from programs CNINDO and POPULAN were used in Eq. 28 to calculate the theoretical APT elements.

2.6 Scaled Polar Tensors and Intensities

The theoretically calculated APT's for the water monomer were subtracted from those of the dimer in order to obtain the scaled APT's

for water dimer, according to Eqs. 1 and 2. We note that the orientation of the H_2O monomer molecule with respect to the principal axis system in Fig. 2-1 differs from the orientation of each of the component H_2O molecules of the dimer with respect to the molecular coordinate system of the dimer in Fig. 2-2. The values of the APT's in a given coordinate system depend on the molecular orientation with respect to that coordinate system. Thus, since we have calculated the monomer APT's in the coordinate system of Fig. 2-1 and the dimer APT's in the coordinate system of Fig. 2-2, we have transformed the APT's for atom A in the monomer and dimer to a rotated axis system, before subtracting them. The axes of this rotated coordinate system have the same orientation with respect to the H_2O molecule which contains atom A in the monomer as in the dimer.

In general, a transformed APT, $(\underline{p}^A)'$, in a rotated axis system is related to that in the original axis system, $\underline{p}^A$, by [3]

$$(39) \qquad\qquad (\underline{p}^A)' = \underline{R}\,\underline{p}^A\underline{R}\dagger \qquad .$$

The transformation matrix, $\underline{R}$, has elements, R_{ij}, which are the cosines between the $\underline{i}$th rotated axis and the $\underline{j}$th original axis, i,j = x,y,z. The transformation matrix is orthogonal, that is, $\underline{R}^{-1} = \underline{R}\dagger$. For the water monomer and dimer we have used two different rotated axis systems, one for the H atoms and one for the O atoms.

The "bond system" is particularly useful for considering APT's for H atoms. The bond system for H_1 of the monomer is illustrated in Fig. 2-3 and can be uniquely defined for each H atom, H_i, as follows. The positive y axis is directed along the OH bond containing H_i from O to H_i. The z axis is perpendicular to this y axis and lies in the plane of the H_2O moiety which contains H_i. The positive z axis is directed between the two OH bonds of that H_2O moiety, as shown in Fig. 2-3. The
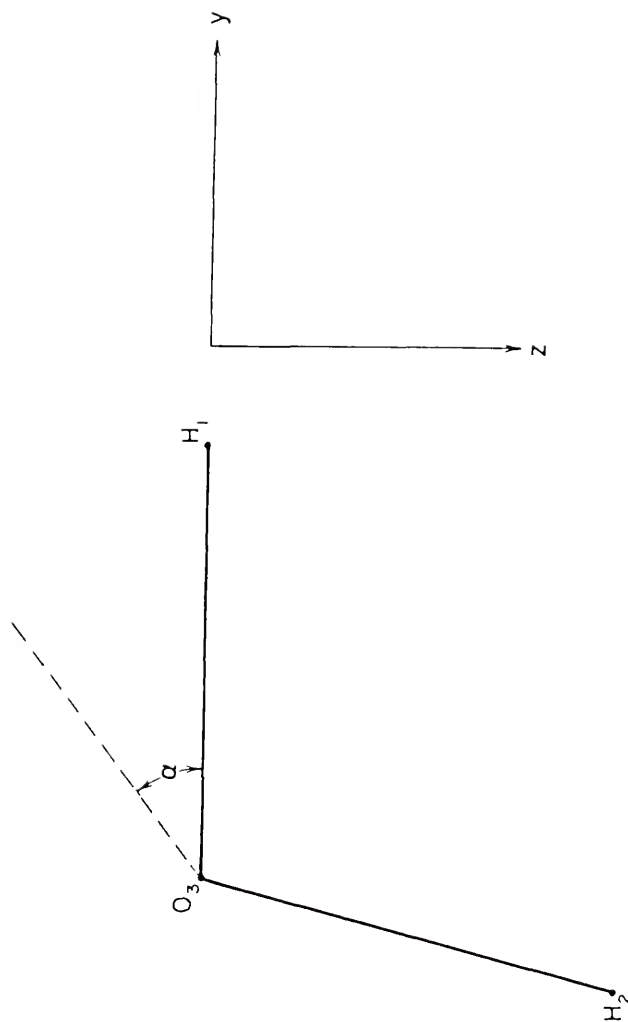
Fig. 2-3. Bond coordinate system for atom H_1 of the water monomer. The x axis is determined by the right-hand rule.

x axis is perpendicular to the plane of the H_2O moiety which contains H_i, and the positive x direction is determined by the right-hand rule. For both the monomer and dimer, the APT for H_1 in the bond system of H_1 is identical by symmetry with the APT for H_2 in the bond system of H_2. Thus, for the water monomer there is only one distinct APT for the H atom in the bond system.

The theoretically calculated APT's for the monomer and dimer H atoms in the *bond system* were used in Eq. 1. Similarly, the experimental APT for the monomer H atom in the *bond system* was used in Eq. 2. The theoretical and experimental APT's for the monomer H atom in the bond system were calculated as $(\underline{P}^A)'$ in Eq. 39, where $\underline{P}^A$ was the APT for H_1 in the molecular coordinate system of the monomer shown in Fig. 2-1, and $\underline{R}$ was the transformation matrix *from* that coordinate system *to* the bond system of H_1 (see Fig. 2-3). This transformation matrix is given in Table 2-12. Table 2-13 shows the experimental APT for the monomer H atom in the bond system, obtained by transforming the APT for H_1 given in Table 2-11. The theoretical APT's for H_i (i = 1,4,6) of the dimer in the bond system were also obtained as $(\underline{P}^A)'$ in Eq. 39. where $\underline{P}^A$ was the theoretical APT for H_i in the molecular coordinate system of the dimer in Fig. 2-2, and $\underline{R}$ was the transformation matrix *from* that coordinate system *to* the bond system of H_i. These transformation matrices are given in Table 2-14 for i = 1,4,6.

For the O atoms a unique bond system cannot be defined since each O atom belongs to more than one bond. Accordingly, we transformed the theoretical APT's for the two dimer O atoms, O_i, to a rotated axis system whose orientation, with respect to the H_2O moiety which contains O_i, is the same as the orientation illustrated in Fig. 2-1 for the monomer molecule and axes. This rotated axis system is called the "molecular

Table 2-12. Transformation matrix, R^{H_1}, from the molecular coordinate system of the monomer, shown in Fig. 2-1, to the bond system of the monomer H_1 atom, shown in Fig. 2-3.

R^{H_1}		
1	0	0
0	$\cos(37.74°)$	$\cos(52.26°)$
0	$\cos(142.26°)$	$\cos(37.74°)$

Table 2-13. Experimental polar tensor for the monomer H atom in the bond system. Units are e, where $1e = 1.602 \times 10^{-19}$ coulombs.

P^{H_1} (exptl.,monomer)		
0.3295	0.0	0.0
0.0	0.1322	-0.0641
0.0	-0.0495	0.2468

system of the monomer" (MSM) for the dimer O atoms and is illustrated in Fig. 2-4 for O_5.

The transformed theoretical APT's for the dimer O atoms were calculated as $(\underline{p}^A)'$ in Eq. 39, where $\underline{p}^A$ was the APT for O_i in the molecular coordinate system of the dimer shown in Fig. 2-2, and $\underline{R}$ was the transformation *from* that system *to* the MSM of O_i, $i = 3,5$. These transformation matrices are given in Table 2-15 for O_3 and O_5 of the dimer. The theoretical APT for the monomer O atom in the coordinate system of Fig. 2-1 was subtracted from each of these transformed APT's for the dimer O atoms, according to Eq. 1. The resulting changes in the theoretical APT's from monomer to dimer, $(\underline{\Delta p}^O)'$, in the MSM were then added to the experimental APT for the monomer O atom given in Table 2-11, according to Eq. 2.

The resulting scaled APT's for the dimer O atoms were thus expressed in the MSM. The same procedure was used for the theoretical monomer and dimer APT's for the H atoms in the bond system and the experimental bond system APT given in Table 2-13 for the monomer H atom. The scaled APT's for the dimer O and H atoms, in their corresponding rotated axis systems were then transformed back to the molecular coordinate system of the dimer shown in Fig. 2-2. The inverse of the transformation given in Eq. 39 was used, namely

$$(40) \qquad \underline{p}^A = \underline{R}^\dagger (\underline{p}^A)' \, \underline{R} \qquad ,$$

where $(\underline{p}^A)'$ represents the scaled APT for the dimer in the rotated axis system; $\underline{p}^A$, the scaled APT in the molecular system of the dimer; and $\underline{R}$ the appropriate transformation matrix given in Tables 2-14 and 2-15 for each atom. The scaled APT for H_2 in the molecular system of the dimer was obtained from that for H_1, according to Eq. 30. All of the scaled
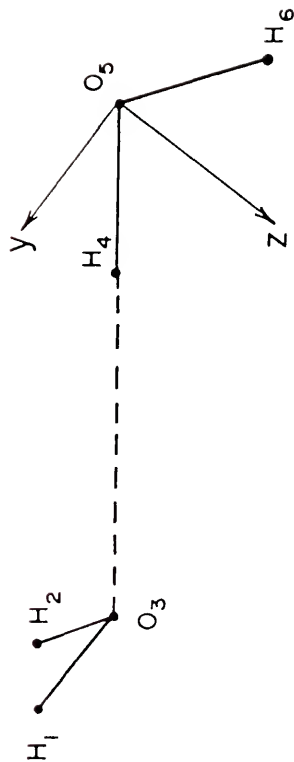
Fig. 2-4. Molecular coordinate system of the monomer for O_5 of the water dimer. The x axis is determined by the right-hand rule.

Table 2-14. Transformation matrix, R^{H_i}, from the molecular coordinate system of the dimer, shown in Fig. 2-2, to the bond system of dimer H_i atoms, $i = 1,4,6$.

R^{H_1}	0	$\cos(130°)$	$\cos(140°)$
	$\cos(37.74°)$	$\cos(117.96°)$	$\cos(66.83°)$
	$\cos(127.74°)$	$\cos(127.29°)$	$\cos(59.45°)$
R^{H_4}	1	0	0
	0	-1	0
	0	0	-1
R^{H_6}	-1	0	
	0	$\cos(75.48°)$	$\cos(165.48°)$
	0	$\cos(165.48°)$	$\cos(104.52°)$

Table 2-15. Transformation matrices from the molecular coordinate system of the dimer to the MSM of dimer O_i atoms, $i = 3,5$ (see text and Fig. 2-4).

R^{O_3}	0	$\cos(50°)$	$\cos(40°)$
	-1	0	0
	0	$\cos(140°)$	$\cos(50°)$
R^{O_5}	1	0	0
	0	$\cos(142.26°)$	$\cos(52.26°)$
	0	$\cos(127.74°)$	$\cos(142.26°)$

APT's for the dimer in that system were then juxtaposed to form the $\underline{P}_X$ matrix, according to Eq. 21.

This scaled dimer $\underline{P}_X$ matrix was multiplied by the $\underline{AL}$ product matrix according to Eq. 17 to obtain the $\underline{P}_Q$ matrix. This $\underline{P}_Q$ matrix was then used to obtain the intensities, according to Eq. 17. Similarly, the (unscaled) theoretical APT's for the dimer, as well as those for the monomer, were juxtaposed to form the corresponding $\underline{P}_X$ matrices, which were then used to obtain the intensities. These theoretical APT's are presented and discussed in chapter 4 and the resulting intensities in chapter 3.

CHAPTER 3

COMPARISON OF THEORETICAL INTENSITIES WITH EXPERIMENT

3.1 Simulation of Experimental and Theoretical Spectra

In this chapter we compare the intensities calculated from the theoretical APT's with experimental spectra for water monomer and dimer in the N_2 matrix. Experimental values have not been determined for the intensities of either species in the matrix. However, as mentioned in section 1.3.2, Tursi has given a spectrum of water isolated in N_2, in which the monomer and dimer bands were quite well resolved [31]. We have simulated this experimental spectrum using a sum of Lorentzian linefunctions. That is, the absorbance y_i for each frequency point x_i was calculated as

$$(41) \qquad y_i(x_i) = \frac{1}{\pi} \sum_j \frac{S_j \Delta_j}{(x_i - \omega_j)^2 + \Delta j^2} \quad , \qquad j = 1,11,$$

where the sum was taken over the three monomer bands, six dimer bands, and two trimer bands in Tursi's spectrum. In Eq. 41, S_j represents the integrated absorbance of each band; Δ_j, the half bandwidth at half maximum; and ω_j, the frequency of the band center.

The absorbance values $y_i(x_i)$ depend primarily on the Δ_j and S_j parameters of those bands with peak frequencies in the neighborhood of x_i. We have adjusted all three parameters of each band so that the simulated spectrum could be superimposed on the experimental spectrum. The final "fitted" parameters are given in Table 3-1. The "fitted experimental"

67

Table 3-1. Lorentzian parameters for fitted experimental spectrum.

Species[a]	S,[b] inch cm^{-1}	ω,[c] cm^{-1}	Δ,[d] cm^{-1}
M	13.8	3725.7	2.8
D	3.99	3713.9	1.8
D	1.88	3697.5	2.1
T	3,46	3689.2	5.6
M	3.71	3633.2	1.7
D	0.47	3626.1	1.0
D	3.08	3547.8	2.0
D	1.73	1618.6	1.0
T	1.79	1612.3	3.7
D	2.20	1600.3	1.0
M	7.85	1596.7	1.7

[a] Monomer (M), dimer (D), or trimer (T).

[b] Integrated band absorbance.

[c] Frequency of band center.
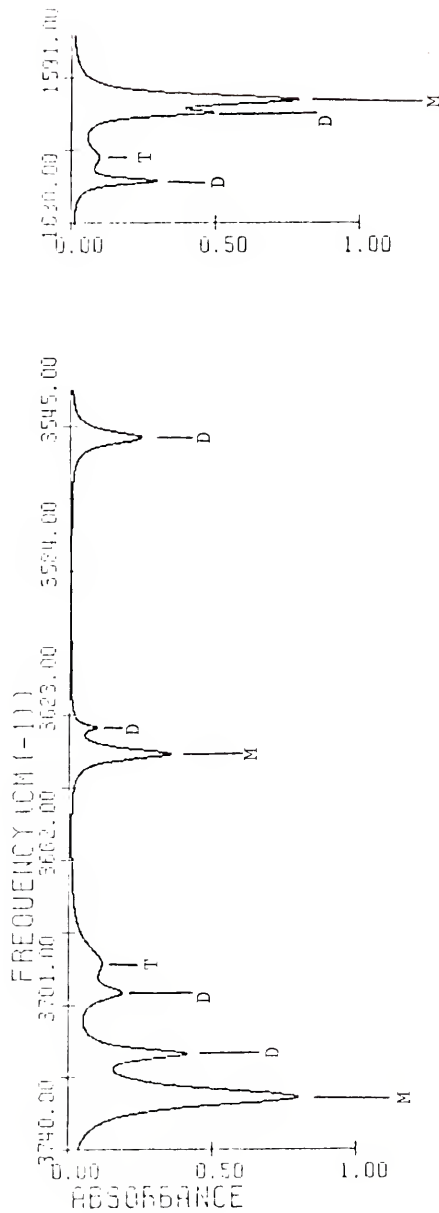
[d] Half bandwidth at half maximum.

Fig. 3-1. Spectrum fitted to experimental spectrum given by Tursi [31] for water isolated in the N_2 matrix. Bands due to water monomer (M), dimer (D) and trimer or higher multimer [2](T) are indicated.

spectrum calculated from these parameters according to Eq. 41 is shown in Fig. 3-1.

As described in chapter 2, we have calculated quantum mechanical absorption coefficients, A_j, for each band of water monomer and dimer. We have used these calculated absorption coefficients to obtain theoretical spectra according to Eq. 41 for comparison with experiment. For the experimental matrix spectrum, the amount of each absorbing species in the path of the irradiating beam has not been determined, and the absolute absorbance has not been given. Thus, we have calculated relative theoretical spectra on the same scale as that used for the spectrum in Fig. 3-1. This was done using relative integrated absorbances, $S_j(r)$ with respect to a fitted band, band r. One band for each species was chosen as the fitted band. The relative integrated absorbances for the remaining bands were calculated using the fitted absorbance S_r from Table 3-1, according to

$$(42) \qquad S_j(r) = \frac{S_r A_j}{A_r} \quad ,$$

where A_j and A_r are the calculated absorption coefficients for the jth and rth bands.

For purposes of comparison with the theoretical spectra, Eq. 41 was used to calculate separate fitted experimental spectra for water monomer and for the dimer, summing over the corresponding three and six bands, respectively. In calculating the theoretical spectra, the fitted Δ_j and ω_j parameters in Table 3-1 were used for all the bands.

3.2 Water Monomer Intensities

The infrared intensities from the 4-31G polar tensors are compared
with those obtained from several other *ab initio* calculations in the
upper part of Table 3-2. The latter intensities were taken from works by
Pulay [69]; Smith, Jorgensen and Öhrn [70]; and Krohn and Kern [71].
Pulay presented dipole moment functions for two different basis sets--
"Pulay I" and "Pulay II." The experimental $\underline{L}$ matrix in Table 2-7 was
used to obtain the intensities from our 4-31G calculation. We used the
same $\underline{L}$ matrix to calculate the intensities from the two dipole moment
functions given by Pulay and also from that given by Smith, Jorgensen
and Öhrn. We report the intensities given by Krohn and Kern directly.
They included the effects of electrical anharmonicity on the dipole
moment function, using terms up to fourth order in the normal coordinates.
They also used an experimental normal coordinate transformation, which
included the effects of mechanical anharmonicity through cubic and
quartic force constants.

The experimental intensities measured in the gas-phase by several
workers are given in the lower part of Table 3-2. The spread in the
measured values indicates that at least some of the discrepancy between
experimental and calculated values may be attributed to uncertainties in
the former. The experimental values from Clough, Beers, Klein and
Rothman (underlined) are the most recent and probably the most reliable.
These intensities correspond to the $\underline{P}_Q$ matrix elements which we used to
obtain the experimental APT's, as discussed in section 2.4. The signs
reported for those $\underline{P}_Q$ matrix elements agree with the signs predicted by
nearly all the *ab initio* calculations represented in the upper part of
Table 3-2. The only discrepancy is in the sign calculated from the

smaller basis set used by Pulay, Pulay I, for the $\partial P_z/\delta Q_1$ element. That calculation predicted a negative sign for this element while the others predicted a positive sign, in agreement with the experimental sign choice.

The calculated intensities in Table 3-2 are ordered according to the quality of the basis set, as evidenced by the calculated energy minimum, E_0. There appears to be an overall tendency for the calculated intensities of each band to increase as the basis set is improved. The upper limits of the calculated intensities are in excess of the best experimental values, particularly for intensities A_1 and A_2. This may be attributed in part to the error in the Hartree-Fock approximation. It can be seen that the 4-31G intensities agree with the experimental values within a factor of 2.3. This level of agreement has been found for a number of other 4-31G calculated intensities [4,72,73]. Hence, we expect that the intensities for the water dimer can also be predicted from 4-31G calculations within a factor of 2.5 or better.

Before discussing the dimer intensities, however, it is useful to compare the experimental intensities of the monomer isolated in the N_2 matrix with those from the gas-phase spectrum. Thus we have calculated a spectrum using the experimental gas-phase intensities of H_2O by the method of section 3.1. Relative absorbances were obtained by using the experimental A_i (underlined values) from Table 3-2 in Eq. 42. For reasons given below, ν_3 was chosen as the fitted band (that is, r = 3 in Eq. 42). The resulting spectrum (B) is compared with the fitted experimental spectrum of water monomer in the N_2 matrix (A) in Fig. 3-2. These spectra indicate that the gas-phase intensities are quite different from those in the matrix. Relative to A_3, the gas-phase value of A_1 is too small, while that of A_2 is too large.

Table 3-2. Theoretical and experimental intensities for gas-phase H_2O. Units are km/mole (E_0 in Hartrees).

Theoretical Calculations	A_1	A_2	A_3	E_0
Pulay I[a]	1.91	66.6	6.03	−75.867
4-31G[b]	1.07	90.1	19.7	−75.909
Pulay II[a]	8.77	93.5	34.3	−76.035
Smith, *et al.*[c]	13.6	108.5	65.3	−76.041
Krohn and Kern[d]	15.4	99.0	64.7	−76.051
Experimental Measurements	2.24[e]	53.6[e]	44.6[e]	−76.431[f]
	2.51[g]	55.4[h]	59.8[i]	
	2.26[j]	54−81[k]	46.6[j]	
		49.2[l]	40−59[m]	
		59.3[n]	42.3[o]	
		103.4[p]		
		71−89[q]		

[a] Pulay [69].

[b] Present work.

[c] Smith, Jorgensen and Öhrn [70].

[d] Krohn and Kern [71].

[e] Clough, Beers, Klein and Rothman [57].

[f] Quoted by J. Smith [74, p. 31].

[g] Toth [75].

[h] Goldstein [76].

[i] Maclay [77].

[j] Flaud and Camy-Peyret [78].

[k] Ludwig, Ferriso and Abeyta [79].

[l] Goldman and Oppenheim [80].

[m] Jaffe and Benedict [81].

[n] Ben Aryeh [82].

[o] Hirshfeld, Jaffe and Ross [83].

[p] Krakow and Healy [84].

[q] Von Rosenberg, Pratt and Bray [85].

One possible source of this discrepancy is a change in the mechanical effects on the H_2O molecule upon going from the gas-phase to the N_2 matrix. According to the theory of infrared intensities, mechanical effects influence the intensities through the $\underline{L}$ matrix while electrical effects are reflected in the APT's. We have thus attempted to obtain an indication of the mechanical effects on the H_2O intensities as follows.
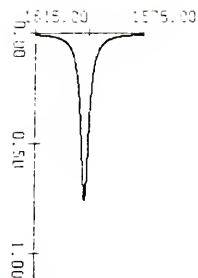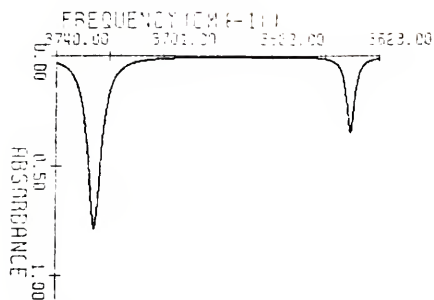
Intensities were calculated from $\underline{L}(N_2)$ and $\underline{P}^A(g)$. The $\underline{P}^A(g)$ represent the experimental APT's determined from the gas-phase data as described in section 2.4 (see Table 2-11), while $\underline{L}(N_2)$ denotes the $\underline{L}$ matrix determined from the force field given by Tursi and Nixon [30] for H_2O in the N_2 matrix (see Table 2-8). These intensities are compared in Table 3-3 with intensities calculated from $\underline{L}(g)$ and $\underline{P}^A(g)$--where $\underline{L}(g)$ is the $\underline{L}$ matrix determined from the force field given by Cook, DeLucia and Helminger [51] for H_2O in the gas-phase (see Table 2-7). Since the $\underline{P}^A(g)$ were determined using $\underline{L}(g)$, the latter intensities are just the experimental gas-phase intensities.

Table 3-3. Intensities calculated for H_2O from experimental gas-phase polar tensors using two different $\underline{L}$ matrices. Units are km/mole.

	A_1	A_2	A_3
$\underline{L}(N_2)$	9.80	46.0	44.6
$\underline{L}(g)$	2.24	53.6	44.6

Table 3-3 shows that the intensities obtained using $\underline{L}(N_2)$ show a substantial increase in A_1 and a decrease in A_2 relative to the gas-phase intensities. As pointed out in section 2.4, the major difference between

Fig. 3-2.   Comparison of fitted experimental spectrum of H_2O in the N_2 matrix (A) with spectra calculated using experimental gas-phase APT's. Spectrum (B) was obtained using $\underline{L}(g)$ and represents the experimental gas-phase intensities. Spectrum (C) was calculated using $\underline{L}(N_2)$. All frequencies and band widths have been fitted to the experimental spectrum of H_2O in the N_2 matrix. For the calculated spectra (B and C), the intensity of ν_3 also has been fitted. Band assignments are indicated at the bottom of the spectrum (C).
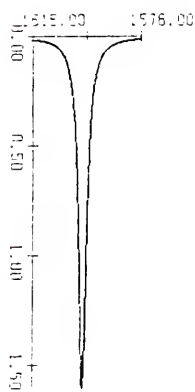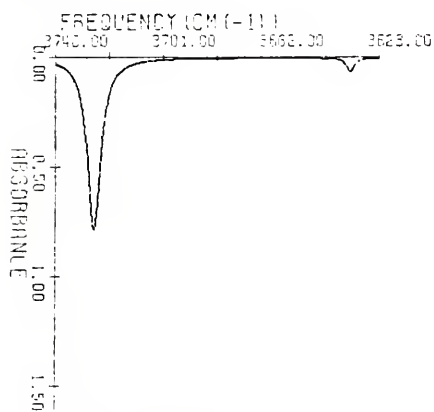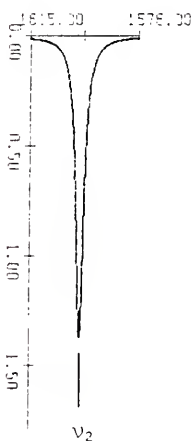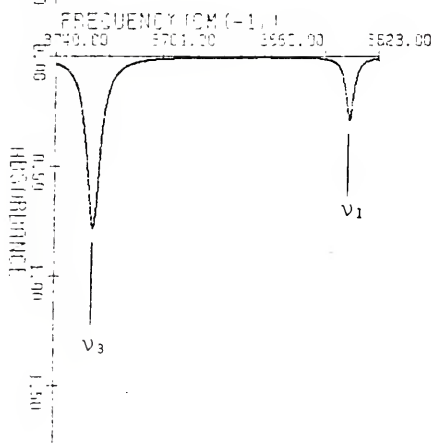
the force fields corresponding to $\underline{L}(N_2)$ and $\underline{L}(g)$, is that the values of the stretch-bend interaction force constant, F_{12}, have opposite signs (compare Tables 2-7 and 2-8). This discrepancy probably accounts for much of the difference between the two sets of intensities in Table 3-3. We note that the same value of A_3 was obtained using both force fields. This is because ν_3 is the only vibration in the B_2 symmetry group, and thus the corresponding $\underline{L}$ matrix element (L_{33}) is independent of the force constants.

We have calculated a spectrum from the intensities obtained using $\underline{L}(N_2)$ by the method of section 3.1. This spectrum (C) is compared with that calculated from the gas-phase intensities (B) and with the fitted experimental spectrum of H_2O in the N_2 matrix (A) in Fig. 3-2. For the calculated spectra (B and C), ν_3 was chosen as the fitted band because A_3 does not depend on the force field. Figure 3-2 indicates that the intensities calculated using $\underline{L}(N_2)$ give substantially better agreement with the experimental intensities in the N_2 matrix than do the gas-phase intensities. This result suggests that the mechanical changes in the H_2O molecule on going from the gas-phase to the N_2 matrix environment (if well-represented by the $\underline{L}$ matrices in Tables 2-7 and 2-8), may account for much of the discrepancy between the H_2O intensities in the two environments.

3.3. Water Dimer Intensities

In this section we present and discuss the theoretical intensity calculations for the water dimer. The dimer bands and intensities are designated by the same notation used in section 1.3.1. That is, the vibrations corresponding to the electron donor water molecule of the dimer complex are labeled (ED) and those corresponding to the electron

acceptor are labeled (EA). Analogous numbering to that for the monomer is used--that is, ν_3 refers to the antisymmetric stretch, ν_1 to the symmetric stretch, and ν_2 to the bend.

We begin by comparing the intensities calculated from the theoretical APT's for the dimer with corresponding intensities for the monomer. In all cases we used the experimental $\underline{L}$ matrices for water monomer and dimer isolated in the N_2 matrix (determined from the force fields given by Tursi and Nixon [30]) to obtain intensities from the APT's. Table 3-4 shows the intensities obtained from the *ab initio* APT's calculated for water monomer and dimer using the 4-31G basis set.

Table 3-4. Intensities calculated from *ab initio* 4-31G APT's for water monomer and dimer. Units are km/mole.

	A_3(ED)	A_3(EA)	A_1(ED)	A_1(EA)	A_2(EA)	A_2(ED)
Monomer	19.7	19.7	10.1	10.1	81.2	81.2
Dimer	44.4	43.5	26.4	165.6	86.0	87.6

According to the calculation, the intensities of the four dimer stretching vibrations are strongly enhanced relative to the corresponding monomer intensities, while the bending intensities remain nearly the same. A dramatic increase by a factor of nearly 17 is predicted for ν_1(EA), while the other three stretching intensities are predicted to increase by factors ranging from 2.2 to 2.6.

Table 3-3 shows that the *ab initio* APT's from the 4-31G calculation for the monomer, underestimate the stretching intensities by a factor of 2 and overestimate the intensity of the bend by a factor of 2. It might be expected that the same errors would be found in the APT's calculated

for the dimer using the 4-31G basis set. In this event some improvement
in the predicted dimer intensities could be obtained by scaling these
theoretical APT's according to the procedure described in section 1.4.2.

We have thus used the theoretical monomer and dimer APT's, as well
as the experimental APT's for the monomer, in Eqs. 1 and 2 of that
section, to calculate scaled dimer APT's. The intensities obtained from
the scaled dimer APT's are compared in Table 3-5 with those obtained
from the experimental APT's for the monomer. Both sets of intensities
were calculated using the corresponding matrix isolated $\underline{L}$ matrix.

Table 3-5. Intensities calculated from scaled dimer 4-31G APT's and
experimental monomer polar tensors. Units are km/mole.

	$[A_3(ED)]$	$[A_3(EA)]$	$[A_1(ED)]$	$[A_1(EA)]$	$[A_2(EA)]$	$[A_2(ED)]$
Monomer	44.6	44.6	9.80	9.80	46.0	46.0
Dimer	79.2	74.6	26.0	182.2	49.9	50.9

Again, the intensities of the bending vibrations are predicted to be
about the same for the monomer and dimer. The predicted intensity of
$\nu_1(EA)$ is enhanced by a factor of nearly 19, while those of the other
three stretching vibrations are 1.7 to 2.7 times greater than in the
monomer.

Calculated spectra were obtained as described in section 3.1 using
the intensities, A_i, shown in Tables 3-4 and 3-5. These spectra are
compared in Fig. 3-3 with the fitted experimental dimer spectrum. For
the calculated spectra, $\nu_2(EA)$ was chosen as the fitted band, since the
intensities of the bending modes are expected to be least affected by
H-bond formation [56, see also Tables 3-4 and 3-5]. The other bend

Fig. 3-3. Comparison of fitted experimental spectrum of water dimer isolated in the N_2 matrix (A) with spectra calculated using unscaled (B) and scaled (C) 4-31G polar tensors. For the calculated spectra (B and C), the intensity of ν_2 (EA) has been fitted to the experimental spectrum of water dimer in the N_2 matrix. All frequencies and band-widths have also been fitted. Band assignments are indicated at the bottom of spectrum (C).
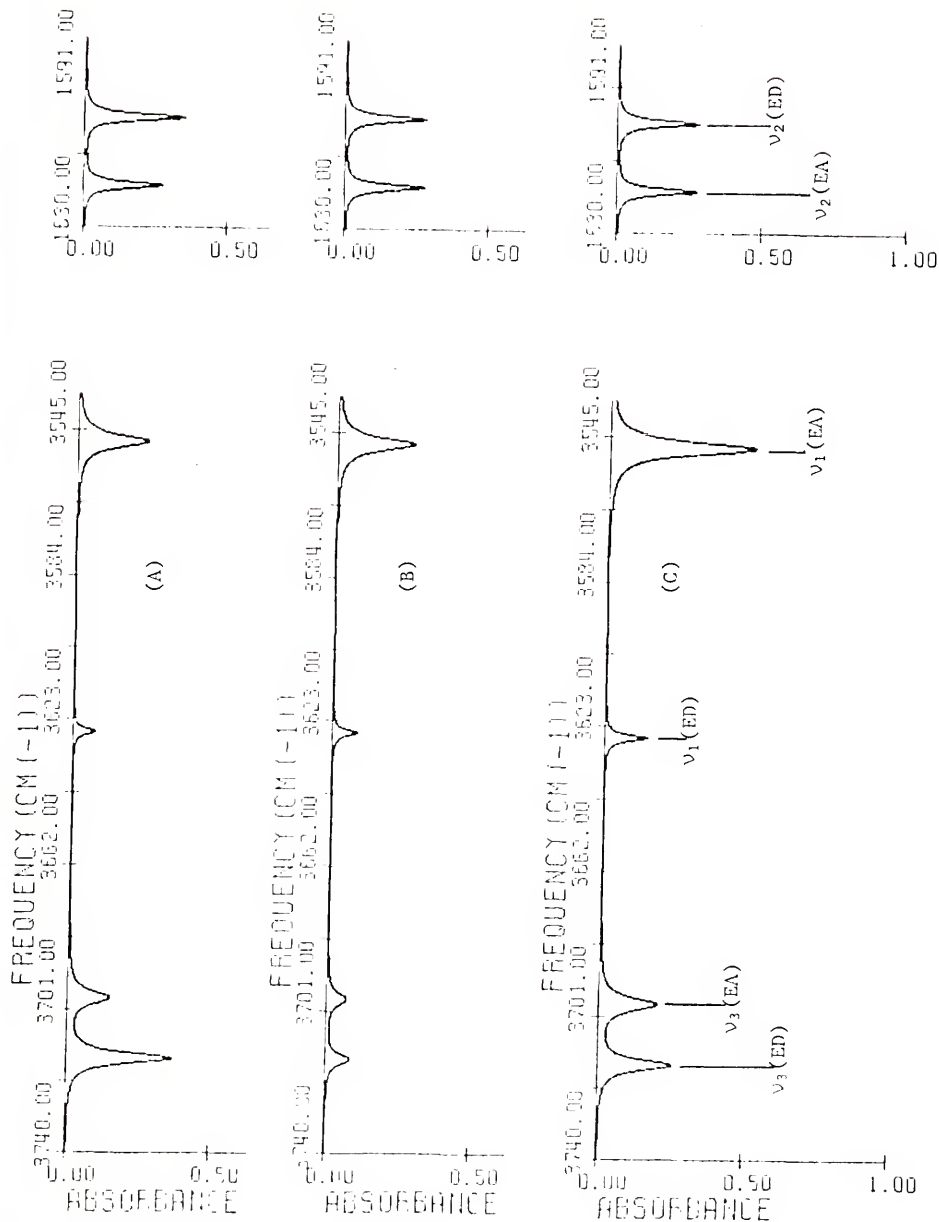
ν_2(ED) strongly overlaps with the corresponding monomer band in the experimental spectrum (see Fig. 3-1). The value of the absorbance used to fit this band is therefore less certain.

Figure 3-3 shows that in the spectrum calculated using the *ab initio* APT's (B), the intensities of the antisymmetric stretches are much smaller than those in the fitted experimental spectrum (A). For the spectrum obtained using scaled APT's (C), the overall agreement is better except for ν_1(EA), whose intensity is predicted to be approximately twice that in the fitted experimental spectrum. The normal coordinate for ν_1(EA), contains the largest contribution from the H-bonded OH stretch. This vibration therefore corresponds to the "H-bond band" whose intensity was discussed in section 1.2.

This overestimation of the H-bond band intensity is probably related to the fact that the dimer stabilization energy calculated with the 4-31G basis set is too large--8.2 kcal/mole [47], as compared to the most accurate value of 5.6 kcal/mole [43]. In general, small basis set molecular orbital calculations have been found to predict this extra stabilization, and this phenomenon has been investigated for a number of H-bonded complexes [86-90; 19, pp. 63-65].

The overestimation of the stabilization energy (and presumably of the H-bond band intensity) is a consequence of the small basis set which inadequately represents the orbitals on each molecule of the complex. In the molecular orbital method, the total energy of the complex is optimized. The additional basis functions on one molecule are then allowed to compensate for the limited number of basis functions on the other molecule, in order to achieve optimization. Thus, intermolecular orbital mixing occurs to a greater extent in small basis set calculations

than in those using large basis sets, and "basis set superposition error" results.

An additional measure of the H-bond strength is given by the inter-molecular separation, the O-O distance in the case of water dimer. A stronger H-bond interaction results in a shorter O-O distance. The minimum energy configuration calculated with the 4-31G basis set for the water dimer occurs for an O-O distance of 2.83 $\overset{\circ}{A}$ [47]. This compares with the experimental [60] and most accurate theoretical [43] value of 2.98 $\overset{\circ}{A}$.

Because both the H-bond band intensity and the O-O distance are correlated with the dimer stabilization energy, and the latter is affected by basis set superposition error in the calculations, we decided to investigate the dimer intensities as a function of O-O distance.

Accordingly we have calculated an entire set of scaled APT's for the water dimer at each of three different O-O distances, R_{O-O} = 3.0, 2.8 and 2.6 $\overset{\circ}{A}$, using the relatively economical CNDO method. These calcula-tions also allow us to see whether the scaling procedure which we have used for the dimer APT's can override some of the shortcomings of the approximate CNDO method.

Figure 3-4 shows the calculated spectra obtained using unscaled APT's from the CNDO calculation. The intensities predicted for the stretches are very small compared to the values calculated for the bends, with the exception of A_1(EA). These results are similar to those obtained with the *ab initio* 4-31G calculated APT's [spectrum (B) in Fig. 3-3]. However, the situation is more exaggerated with the CNDO calculation, and A_1(EA) is predicted to be significant only for the

Fig. 3-4. Comparison of spectra of the water dimer calculated from
unscaled CNDO polar tensors at different O-O distances.
Spectrum (A) corresponds to $R_{O-O} = 3.0$ Å; spectrum (B)
to $R_{O-O} = 2.8$ Å; and spectrum (C) to $R_{O-O} = 2.6$ Å. The
intensity of ν_2 (EA) and the frequencies and bandwidths
have been fitted to the experimental spectrum of water
dimer in the N_2 matrix. Band assignments are indicated
at the bottom of spectrum (C).
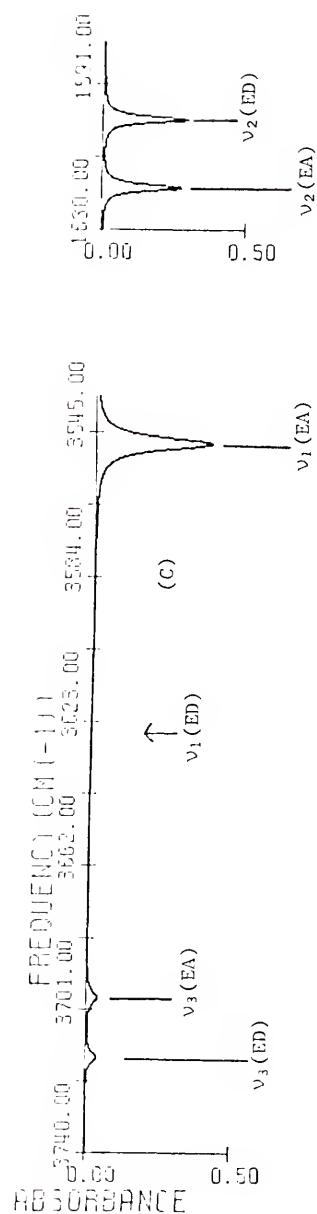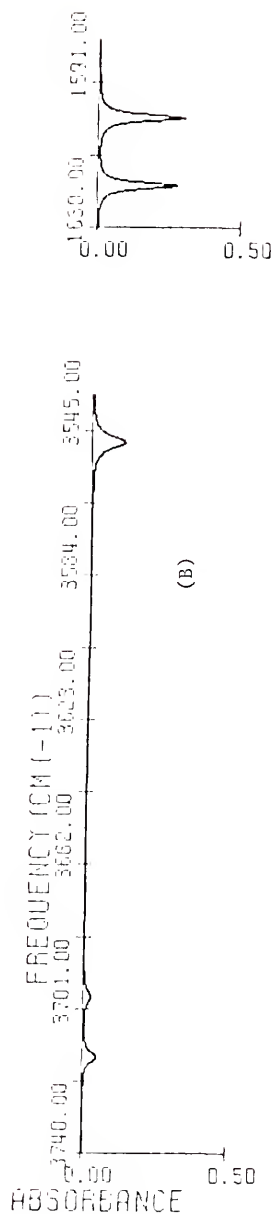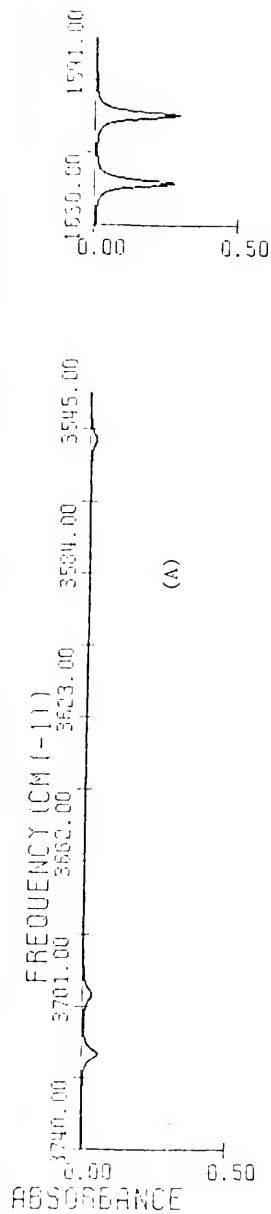
strongest H-bonded water dimer, that with R_{O-O} = 2.6 Å. Table 3-6 shows the corresponding values predicted for the intensities; they are indeed unreasonable.

Figure 3-5 shows the calculated spectra obtained using *scaled* APT's from the CNDO calculation. First we note that the relative intensities are a great deal better, thus indicating the value of scaling the APT's for obtaining quantitative intensity estimates from approximate calculations. Secondly, Fig. 3-5 shows that the intensity predicted for ν_1(EA) is indeed a very sensitive function of the O-O distance, and in fact doubles for every 0.2 Å decrease in R_{O-O}.

These results confirm that the intensity of this H-bond band [relative to A_2(EA)] is amazingly sensitive to R_{O-O} and, hence, the strength of the H-bond. Although we have not quantitatively investigated the effect of basis set superposition error on the 4-31G calculated intensity of this band, we can infer qualitatively from these results that the effect would be large. Accordingly, the intensity of the H-bond band in the experimental spectrum obtained by Tursi and Nixon [see fitted spectrum (A) in Fig. 3-3] is not inconsistent with the value that might be predicted for the linear dimer from a large basis set calculation.

The numerical values of the intensities corresponding to the calculated spectra in Fig. 3-5 are given in Table 3-7. In addition to the dramatic change for the intensity of the H-bond band, ν_1(EA), the intensity of ν_3(EA) is also predicted to increase substantially as R_{O-O} decreases. The increase in A_3(EA) can be noticed in the calculated spectra shown in Fig. 3-5, particularly for R_{O-O} = 2.6 Å. The sensitivity of the ν_3(EA) vibration to the H-bond strength probably results from the

Table 3-6. Dimer intensities calculated from *unscaled* CNDO APT's at different O-O distances. Units are km/mole.

R_{O-O} Å	$[A_3(ED)]$	$[A_3(EA)]$	$[A_1(ED)]$	$[A_1(EA)]$	$[A_2(EA)]$	$[A_2(ED)]$
3.0	10.9	7.41	0.328	4.96	32.0	33.9
2.8	9.49	6.01	0.208	26.2	32.0	34.8
2.6	7.43	8.68	0.089	97.8	33.4	35.9

Table 3-7. Dimer intensities calculated from *scaled* CNDO APT's at different O-O distances. Units are km/mole.

R_{O-O} Å	$[A_1(ED)]$	$[A_1(EA)]$	$[A_1(ED)]$	$[A_1(EA)]$	$[A_2(EA)]$	$[A_2(ED)]$
3.0	51.3	52.6	11.7	58.3	45.7	49.4
2.8	54.6	65.6	12.5	109.7	45.6	50.4
2.6	60.0	91.5	13.7	231.1	46.9	51.7

Fig. 3-5. Comparison of spectra of the water dimer calculated from *scaled* CNDO polar tensors at different O-O distances. Spectrum (A) corresponds to R_{0-0} = 3.0 Å; spectrum (B) to R_{0-0} = 2.8 Å; and spectrum (C), to R_{0-0} = 2.6 Å. The intensity of ν_2 (EA) and the frequencies and bandwidths have been fitted to the experimental spectrum of water dimer in the N_2 matrix. Band assignments are indicated at the bottom of spectrum (C).
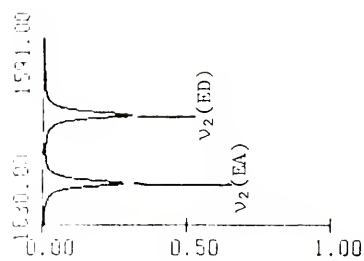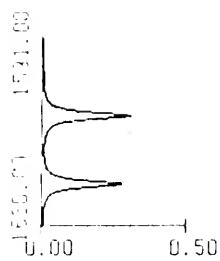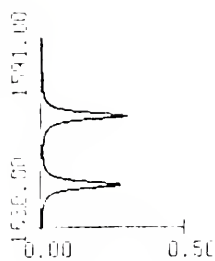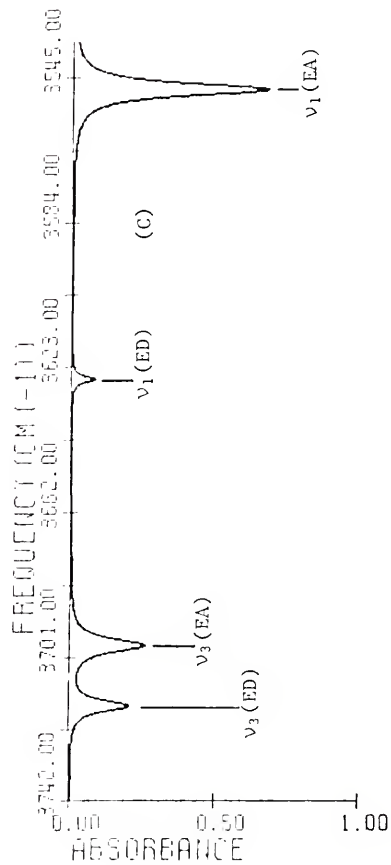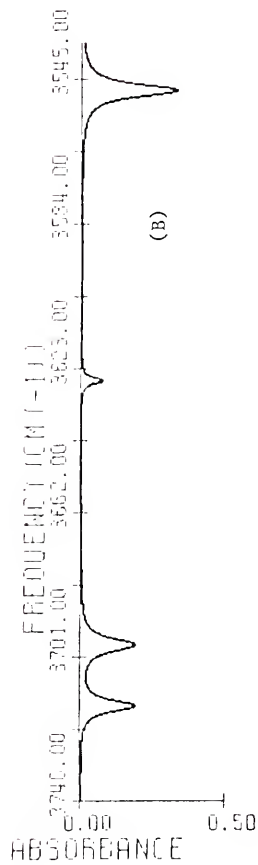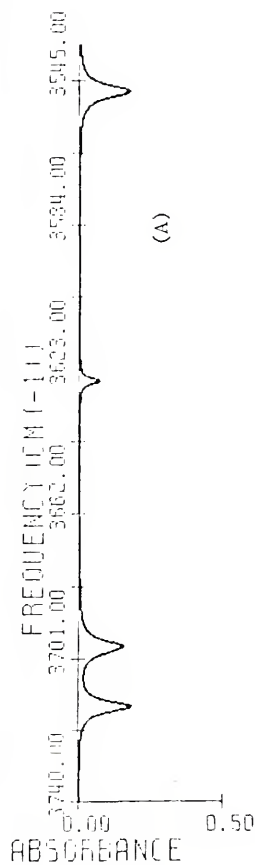
intramolecular coupling discussed in section 1.2. Basically this coupling

is described by the $\underline{L}$ matrix which, in addition to the $\underline{P}_X$ matrix (composed

of the APT's) determines the $\underline{P}_Q$ matrix and, hence, the intensities (see

Eqs. 16 and 17).

Accordingly, we wish to consider the extent to which an alternate

choice for the $\underline{L}$ matrix can affect the calculated intensities. One such

alternate $\underline{L}$ matrix is that determined from the scaled 4-31G $\underline{F}$ matrix.

This $\underline{F}$ matrix was obtained from the *ab initio* 4-31G force fields calcu-

lated by Curtiss and Pople for the water monomer and linear dimer, using

the scaling procedure discussed in section 1.4.1 (see Appendix). Both

the scaled $\underline{F}$ matrix and the resulting $\underline{L}$ matrix have been given in

Table 2-10.

Table 3-8 shows the intensities calculated using the scaled 4-31G

$\underline{L}$ matrix. These intensities are compared in the table with those

obtained using the experimental $\underline{L}$ matrix which was derived from the $\underline{F}$

matrix given by Tursi and Nixon for the water dimer in the N_2 matrix.

The latter $\underline{L}$ matrix has been used for all the intensity calculations

presented thus far and has been given in Table 2-9.

Table 3-8. Dimer intensities calculated from scaled 4-31G APT's using
two different $\underline{L}$ matrices. Units are km/mole.

	$[A_3(ED)]$	$[A_3(EA)]$	$[A_1(ED)]$	$[A_1(EA)]$	$[A_2(EA)]$	$[A_2(ED)]$
Scaled $\underline{L}$	79.2	86.4	12.8	162.5	67.4	63.3
Exptl. $\underline{L}$	79.2	74.6	26.0	182.2	49.9	50.9

Table 3-8 shows that a minor reduction is calculated for $A_1(EA)$ and

a minor increase for $A_3(EA)$ when the scaled 4-31G $\underline{L}$ matrix is used,

relative to the intensities calculated with the experimental $\underline{L}$.
However, the major effect of the alternate $\underline{L}$ matrix on the intensities
in Table 3-8 is found in the intensities of the bending vibrations,
ν_2(EA) and ν_2(ED), and of the symmetric stretch of the electron donor
molecule, ν_1(ED).

As discussed in section 2.4, the major differences between the two
force fields are the neglect of intramolecular stretch-bend coupling
constants in the scaled 4-31G force field and the neglect of intermolec-
ular coupling constants in the experimental force field. Comparison of
Tables 2-9 and 2-10 shows that the $\underline{L}$ matrix elements for stretch-bend
interaction included in the experimental force field are larger than
those for intermolecular interaction included in the scaled 4-31G force
field. This is also what we intuitively expect based on the relative
importance of intra- and intermolecular forces. We can infer from the
results in Table 3-8 that the effect of neglecting stretch-bend inter-
action in the force field results in an increase in the bending inten-
sities of the dimer and a decrease in the intensity A_1(EA).

In summary, it has been shown that the theoretical intensities
predicted for the water dimer are sensitive both to the H-bond strength
and the force field used in the calculation. Within these limitations,
we feel that the intensities calculated using scaled APT's from the
4-31G calculation [corresponding to spectrum (C) in Fig. 3-3] agree well
enough with the fitted experimental spectrum [spectrum (A) in Fig. 3-3]
to be worthy of some consideration in the interpretation of the experimental
dimer spectrum.

Various interpretations of the spectrum have been discussed in
section 1.3.2. We mentioned that the band assigned to ν_1(ED) by Tursi
and Nixon [30] was regarded by Barletta [33] as an overtone or

combination band on the basis that it was too weak to be a fundamental vibration. However, our calculated intensity for the ν_1(ED) fundamental shows that it *should* be weak. It was also mentioned that Luck [36] assigned the band at 3698 cm^{-1} to the trimer. However, the relative intensity we have predicted for ν_3(EA), to which this band was assigned by Tursi and Nixon, agrees quite well with that in the fitted experimental spectrum. Moreover, Luck reassigned the bands, assigned to ν_3(ED), ν_1(ED), and ν_2(ED) by Tursi and Nixon, to the cyclic dimer. We feel that the agreement of our intensity predictions for these three bands with the fitted experimental spectrum is more than fortuitous.

Finally, according to the interpretation by Ayers and Pullin [40] of the profuse spectrum of water in Ar, an assignment was made in which all bands in the frequency region corresponding to ν_3(ED) were attributed to vibration-rotation transitions of the monomer. Yet the intensity of this vibration is predicted to be larger than that of any other vibration with the exception of the H-bond band, ν_1(EA).

Taking into account all the considerations discussed in this section, the predicted intensity pattern assuming the linear dimer structure agrees satisfactorily with the fitted experimental spectrum. These predictions thus lend support to the assignment made by Tursi and Nixon.

CHAPTER 4

POLAR TENSOR ANALYSIS

4.1. Total Polar Tensors

The dipole derivatives used to calculate the intensities give us information about the dynamics of the electronic charge distributions as the molecule vibrates. The APT's are particularly useful, since they describe the redistribution of charge in the molecule as each *atom* in the molecule moves. The elements of the APT's are also independent of the atomic masses [1]. Thus, we are interested in investigating the changes in the APT's that are predicted to occur upon going from water monomer to dimer, according to the 4-31G calculations. As discussed in section 2.6 in connection with scaling the APT's, the monomer and dimer APT's must be evaluated in the same coordinate system in order for any comparison to be meaningful.

We have used the bond system described in section 2.6 for comparing the H atom APT's (see Fig. 2-3). This axis system is uniquely suited for examining the APT's and how they are affected by dimer formation, in terms of the bonding characteristics of the molecule. The 4-31G calculated APT's in the bond system for the three nonequivalent H atoms of the dimer (H_1, H_4 and H_6 in Fig. 1-2) are compared in Table 4-1 with that for the monomer H atom. As discussed in section 2.4, the dimer APT's in the bond system are the same for H_1 and H_2, and both bond system APT's for the H atoms in the monomer are also the same. The 4-31G calculated APT for

93

Table 4-1. *Ab initio* 4-31G polar tensors for H atoms of the water monomer (M) and dimer (D), in the bond system. Units are e, where 1e = 1.602×10^{-19} coulombs.

$P^H(M)$			$P^{H_1}(D)$		
0.47	0.0	0.0	0.47	0.0	-0.01
0.0	0.09	-0.10	0.01	0.15	-0.10
0.0	-0.02	0.34	0.0	-0.02	0.34

$P^H(M)$			$P^{H_4}(D)$		
0.47	0.0	0.0	0.47	0.0	0.0
0.0	0.09	-0.10	0.0	0.41	-0.08
0.0	-0.02	0.34	0.0	-0.06	0.36

$P^H(M)$			$P^{H_6}(D)$		
0.47	0.0	0.0	0.45	0.0	0.0
0.0	0.09	-0.10	0.0	0.05	-0.11
0.0	-0.02	0.34	0.0	-0.01	0.35

the monomer H atom in Table 4-1 can be compared with the corresponding experimental APT in Table 2-13.

Table 4-1 shows that the values calculated for most of the APT elements of the dimer do not change significantly from their corresponding values in the monomer. The major changes are predicted to occur in the P_{yy} elements (second row, second column) for each H atom in the dimer. This element is the derivative of the dipole moment component along the OH bond with respect to displacement along that bond. The fact that changes from monomer to dimer in these APT's are restricted to the P_{yy} elements shows that the effect of the H-bond interaction on the H atom APT is really quite simple and acts directly through each bond. The 4-31G calculation indicates an increase of 0.06 electrons (e) for the P_{yy} element of the electron donor atom, H_1, from the corresponding value in the monomer. For the free atom, H_6, of the electron acceptor molecule, a decrease in the P_{yy} element of 0.04 e is predicted to occur upon complex formation. The magnitude of these changes is dependent to some extent on the 4-31G basis set. However, the increase predicted in the P_{yy} element for H_1 and the decrease in this element for H_6 are probably significant.

The most dramatic change in the APT's calculated for the dimer H atoms occurs in the P_{yy} element of the APT on H_4, the H bonded H atom. This element is rather small in the monomer, but shows an amazing increase of 0.32 e upon H-bond formation. Again, the exact magnitude of the change predicted for this element would depend on the basis set used in the calculation, but the fact that it is large and positive probably has general validity.

The change predicted for the P_{zy} element (third row, second column) of the H_4 atom APT should also be mentioned. In the monomer this element--the derivative of the dipole moment component perpendicular to the bond (in-plane) with respect to displacement along the bond--is calculated to be a very small negative number. It decreases by 0.04 e in the dimer thus becoming substantial, but this change is overshadowed by the large change predicted for P_{yy}. Thus, the derivative of the dipole moment vector with respect to displacement of H_4 along the OH bond is essentially directed along that bond.

Similar systematic changes might be expected for the O atom APT's upon going from monomer to dimer. However, these changes depend on the coordinate system in which the APT's are evaluated. When we applied the scaling procedure, we transformed the APT's for the dimer O atoms from the molecular coordinate system of the dimer (MSD) to that of the monomer (MSM), as discussed in section 2.6. However, in this system (MSM) no systematic changes could be observed in the monomer and dimer APT's. Accordingly, we investigated these APT's in the MSD.

In order to do this we had to transform the monomer O atom APT's from the MSM to the MSD. The MSD is shown in Fig. 2-4 and is oriented differently with respect to each H_2O moiety in the dimer. Thus the transformation from the MSM to the MSD for O_3 is not the same as the corresponding transformation for O_5. We therefore obtained two transformed monomer APT's, one corresponding to each dimer O atom. Each transformed monomer APT, $\underline{P}^{O_i}(MSD)$, was obtained from the monomer APT in the MSM, $\underline{P}^{O}(MSM)$, according to:

$$\underline{P}^{O_i}(MSD) = (\underline{R}^{O_i})\dagger\underline{P}^{O}(MSM)\ R^{O_i} \qquad\qquad i = 3,5.$$

Table 4-2. *Ab initio* 4-31G polar tensors for O atoms of the water monomer (M) and dimer(D), in the molecular system of the dimer. Units are e, where $1e = 1.602 \times 10^{-19}$ coulombs.

$P^{O_3}(M)$			$P^{O_3}(D)$		
-0.48	0.0	0.0	-0.52	0.0	0.0
0.0	-0.60	-0.28	0.0	-0.75	-0.27
0.0	-0.28	-0.70	0.0	-0.22	-0.71

$P^{O_5}(M)$			$P^{O_5}(D)$		
-0.94	0.0	0.0	-0.96	0.0	0.0
0.0	-0.44	0.06	0.0	-0.65	0.01
0.0	0.06	-0.41	0.0	0.06	-0.42

The transformation matrices, $\underline{R}^0 i$ have been given in Table 2-15. The transformed APT's for the monomer O atom are compared in Table 4-2 with the corresponding dimer APT's, both calculated using the 4-31G basis set. Table 4-2 shows that the APT's calculated for both atoms are almost exactly the same in the monomer and dimer, except for the P_{yy} element.

In the MSD this element is the derivative of the dipole component along the linear H-bond with respect to displacement along the H-bond. In the unperturbed monomer, the corresponding element is predicted to be large and negative. In the H-bonded complex P_{yy} is even more negative, decreasing by 0.15 e for O_3 of the electron donor and by 0.21 e for O_5 of the electron acceptor. Again, the exact magnitudes of these changes depend on the basis set used for the calculation, but the large decrease in the P_{yy} element upon going from water monomer to dimer is significant. The fact that the remaining elements are almost exactly the same in the monomer and dimer is probably also significant.

It is evident that the predicted changes in the APT's resulting from the H-bond interaction in the water dimer are orientationally well-defined. The largest effects are in the diagonal terms along the appropriate bond for each atom. For the H atoms the appropriate bond is the OH bond to which each H atom belongs. For the O atoms it is the linear H-bond of the dimer molecule. By far the dominant changes are predicted for the atoms involved in the H-bond: O_3, H_4 and O_5.

As mentioned previously, we are particularly interested in the intensity of the H-bond band. Only the changes in the APT's for H_4 and O_5 affect this intensity. The relative contribution to the intensity from each APT element is related to the appropriate $\underline{A}\underline{L}$ matrix element (Eqs. 16 and 17). The $\underline{A}\underline{L}$ matrix elements for the H-bond band, corresponding to

the P_{yy} elements of H_4 and O_5, have opposite sign. Thus the large
changes from monomer to dimer, shown in Tables 4-1 and 4-2 for these two
P_{yy} elements, reinforce each other in their effect upon the intensity
of the H-bond band--since they also have opposite sign.

However, the magnitude of the $\underline{AL}$ matrix element for H_4 is much lar-
ger than that for O_5, because the $\underline{A}$ matrix element is inversely pro-
portional to the mass of the atom (see Eq. 19). Therefore the H-bond
band intensity is dominated by the large change in the P_{yy} element of H_4.

The prediction of strong orientational effects in the total APT's
indicates that the influence of the H-bond on these quantities is local-
ized in certain atomic displacements. This can be understood in terms
of the linear arrangement of atoms in the H-bond. But the chemical
basis for the large *magnitude* of these effects is not obvious. We
investigate this problem below by examining the chemical and physical
factors that contribute to each APT element.

4.2. Quantum Mechanical Analysis

4.2.1. Discussion of Model

We have analyzed the water monomer and dimer APT's according to
the charge, charge flux, overlap (CCFO) model. The term "charge flux"
comes from Decius who developed the equilibrium charge-charge flux
(ECCF) model for analyzing the physical factors that determine the in-
tensities [11]. Decius and Mast applied this model to the intensities
of a number of molecules [12], however it differs quite basically from
the CCFO model used here.

The latter model is essentially the same as that presented by King
and Mast and applied to CH_3F and CF_4 [9,10]. The terminology and

interpretation used by King and Mast are somewhat different from ours, and these discrepancies, as well as the more substantial ones between the CCFO and ECCF models, are discussed below.

The CCFO model uses the exact quantum mechanical definition of the dipole moment within the LCAO-MO method, given by Eq. 38. That equation can be rewritten as

$$(43) \qquad \vec{p} = \sum_{A} Q_{A}\vec{R}_{A} + \sum_{A,B} \vec{F}(A,B) \ ,$$

where

$$(44) \qquad \vec{F}(A,B) = - \sum_{\mu_{A},\nu_{B}} D_{\mu_{A}\nu_{B}} \int \phi_{\mu_{A}}(1)\vec{r}_{A}\phi_{\nu_{B}}(1)d\tau_{1} \qquad .$$

The first term in Eq. 43 gives the contribution from the scalar charges, Q_{A}, that can be assigned to a single atom. These are the Mulliken gross atomic charges defined in Eqs. 36 and 37. The second term in Eq. 43 gives the contribution that is intrinsically associated with a pair of atoms. Such a contribution arises from the vector properties of the dipole moment. In the ECCF model, on the other hand, a set of effective charges, ζ_{A}, is defined such that

$$(45) \qquad \vec{p} = \sum_{A} \zeta_{A}\vec{R}_{A} \qquad .$$

Thus the effective charge, ζ_{A}, contains a contribution from the Q_{A} in Eq. 43 and a contribution that is related to the $\vec{F}(A,B)$ in that equation.

Now, the APT on atom C, $\underline{p}^{C}$, is given by the transpose of the gradient of the dipole moment vector with respect to the displacement of

atom C,

$$(46) \qquad \underline{p}^C = (\hat{\nabla}_c \vec{p})^{\dagger} \quad .$$

Thus, application of Eq. 46 to Eq. 43 gives

$$(47a) \qquad \underline{p}^C = \sum_A [\hat{\nabla}_C (Q_A R_A)]^{\dagger} - \sum_{A,B} [\hat{\nabla}_C F(A,B)]^{\dagger}$$

$$(47b) \qquad \underline{p}^C = Q_C \underline{E} + \sum_A \vec{R}_A (\hat{\nabla}_C Q_A)^{\dagger} - \sum_{A,B} [\hat{\nabla}_C \vec{F}(A,B)]^{\dagger}$$

$$(47c) \qquad \underline{p}^C = \underline{p}^C(\text{charge}) + \underline{p}^C(\text{charge flux}) + \underline{p}^C(\text{overlap}) \quad .$$

Similarly, application of Eq. 46 to Eq. 45 gives

$$(48a) \qquad \underline{p}^C = \sum_A [\hat{\nabla}_C (\zeta_A R_A)]^{\dagger}$$

$$(48b) \qquad \underline{p}^C = \zeta_C \underline{E} + \sum_A \vec{R}_A (\hat{\nabla}_C \zeta_A)^{\dagger}$$

$$(48c) \qquad \underline{p}^C = \underline{p}^C(\text{charge})' + \underline{p}^C(\text{charge flux})'$$

In Eq. 47b and 48b, $\underline{E}$ is the identity tensor and we have used the fact that $\hat{\nabla}(xy) = x\hat{\nabla}y + y\hat{\nabla}x$.* Equation 47 gives the CCFO model for the APT's,

* See note p. 103.

while the ECCF model is given by Eq. 48.* It should be pointed out that the overlap tensor, given by the third term in Eq. 47b is not *neglected* in Eq. 48. The latter equation is entirely equivalent to Eq. 47 for the total APT. However, the $\underline{P}^C(\text{charge})'$ and $\underline{P}^C(\text{charge flux})'$ in Eq. 48c for the ECCF model are not the same as the corresponding unprimed quantities in Eq. 47c for the CCFO model. Rather both terms in the ECCF model contain a contribution from $\underline{P}^C(\text{overlap})$ in Eq. 47c. This is because of the fundamental difference in the definition of the charges, Q_A and ζ_A. The Q_A can be assigned to a single atom, according to the quantum mechanical expression for the APT (and the dipole moment), while the ζ_A cannot.

Comparing the two models, we see that there are only two terms for each APT in the ECCF model as compared to three for the CCFO model. As a result the parameters in the ECCF model can be determined directly from experiment for many molecules (though not for the water dimer). These parameters can also be obtained from theoretically calculated APT's. The CCFO parameters can be calculated directly from the quantum mechanical wavefunction. They cannot be obtained from experimental intensities.

The smaller number of parameters in the ECCF model suggests that the numerical values obtained for each parameter may be more reliable. However, numerical significance was not a problem in our application of the CCFO model to the changes that take place from water monomer to dimer.

---

* The ECCF model was actually presented by Decius for the dipole derivatives in the symmetry coordinate representation [11]. Decius and Mast have shown how the constraints of charge conservation, rotational invariance, and symmetry are applied for various types of molecules [12]. Using these equations, the relationship between the symmetry coordinate ECCF model and its APT analog, described here, is straightforward.

We have found that certain terms change by a large amount, while in all other terms the changes are very small. Moreover, the separation of the APT into the three terms of the CCFO model is quantum mechanically exact. Thus the physical significance of the three terms is well-defined. The general significance of the three terms has been discussed by King and Mast [9,10]. We wish to elaborate on this discussion by pointing out what the three terms have in common and the distinguishing characteristics of each term. The third term is also treated different-ly by King and Mast, with a resulting difference in interpretation.

Each term in Eq. 47b depends on an "electrical" quantity involving charge and a "mechanical" quantity involving distance. In the charge tensor, given by the first term of Eq. 47b, the mechanical quantity is implicitly contained in the $\underline{E}$ tensor.* In both the charge and charge flux tensors, the electrical and mechanical quantities are separable into independent factors. However, in the overlap tensor, given by the third term of Eq. 47b, the electrical quantity involves the $D_{\mu_A \nu_B}$, Φ_{μ_A}, and Φ_{ν_B} in Eq. 44. According to the latter equation, the electrical and mechanical quantities in this tensor are not separable.

This distinction between the charge and charge flux tensors, on the one hand, and the overlap tensor on the other, can be stated more specifically as follows. The charge and charge flux tensors depend on the electron density determined from the electronic wavefunction. But the dependence of the overlap tensor on the electronic wavefunction *cannot* be expressed in terms of the electron density function.

---

* The $\underline{E}$ tensor arises from the fact that $\hat{\nabla}_C R_A = \underline{E} \, \delta_{AC}$ where δ_{AC} is the Kronecker delta.

Each term in Eq. 47b also involves the gradient, and this is a reflection of dynamic effects in the APT. The charge tensor involves dynamic effects in an implicit manner only.* This tensor depends explicitly on just the static electrical factor. In the charge flux tensor the dynamic factor is electrical, while the static factor is mechanical. Both the electrical and mechanical factors are dynamic in the overlap tensor. The important distinction is that the charge flux and overlap tensors involve dynamic electrical effects, while the charge tensor does not.

Finally, the first, second and third terms in Eq. 47b for the CCFO model represent progressively higher orders of interatomic interaction. The contribution of the charge tensor to the total APT on atom C, given by the first term in Eq. 47b, depends *only* on that atom. The charge flux tensor on atom C, given by the second term in Eq. 47b, includes interactions among all the atoms of the molecule, because it involves a sum of contributions from these atoms. Each term in this sum depends in general on a pair of atoms, A and C. The terms in this sum are thus independent *diatomic* contributions to the total APT.

The overlap tensor, given by the third term in Eq. 47b, involves the highest order of interatomic interactions. This tensor is a double sum over pairs of atoms, each term in the sum depending in general on 3 atoms, A, B and C. When A = B in Eq. 44, $\vec{F}(A,B)$ represents the contribution of the sp (or spd) hybridization effects to the dipole moment. Thus $\vec{F}(A,A)$ represents diatomic effects, even though it depends on a single atom, because these hybridization effects are determined by the

---

* See note p. 103.

atom(s) bonded to atom A. When $A \neq B$, $\vec{F}(A,B)$ represents the dipole moment overlap effects that cannot be expressed in terms of the electron density, and is also diatomic. The general contribution to the overlap tensor, $\hat{\nabla}_C \vec{F}(A,B)$, is therefore a *triatomic* contribution to the total APT.

The explicit triatomic dependence of the overlap tensor was eliminated in the model of King and Mast. They approximated the atomic orbitals on atom A by expanding them in terms of the orbitals on atom B. Actually this approximation was applied to Eq. 43 for the dipole moment. However, only the second term in that equation is intrinsically diatomic.

Thus when the gradient operator is applied to Eq. 43, the charge and charge flux tensors, resulting from the first term in that equation, are exactly the same as those obtained by King and Mast. They obtained a different functional form for the third term in Eq. 47b--our overlap tensor. They interpreted their third term as an effect due to "interference phenomena resulting from the superposition of wavefunctions" [10, p. 9].

However, our calculation of the three terms in the CCFO model, for the water and water dimer APT's, is numerically equivalent to the three terms calculated by King for CH_3F and CF_4 [10]. This is because the third term in both models can be obtained by subtraction of the charge and charge flux tensors from the total APT on the left side of Eq. 47c. We have also calculated our overlap tensor directly, using the functional form of $\vec{F}(A,B)$ given in Eq. 44 and the output from the dipole moment overlap population analysis option of program POPULAN. This $\underline{P}^C$(overlap) agrees, to at least two decimal places, with that obtained by difference from the total $\underline{P}^C$, for all the atoms of the water monomer and dimer.

In summary, the three tensors in the CCFO model have distinguishing physical characteristics. These distinctive properties do not apply to the $\underline{p}^C$(charge)´ and $\underline{p}^C$(charge flux)´ tensors in the ECCF model of Decius. This is because each of the tensors in the ECCF model contains a contribution from $\underline{p}^C$(overlap) in the CCFO model, according to the discussion following Eq. 48. Accordingly, $\underline{p}^C$(charge)´ in the ECCF model has the properties of $\underline{p}^C$(overlap), as well as those of $\underline{p}^C$(charge) in the CCFO model. Similarly, $\underline{p}^C$(charge flux)´ also has the properties of $\underline{p}^C$(overlap). Thus no general distinctions can be made in the physical significance of the two ECCF tensors.

4.2.2. Results and Implications for the Intensity Enhancement of the H-bond Band

The charge, charge flux and overlap tensors calculated with the 4-31G basis set, for each of the independent H atoms of the water dimer are compared with those for water monomer in Table 4-3. These tensors refer to the bond system for each H atom, as discussed in section 4.1.

These data are really quite remarkable in that, among all the tensor elements presented, there is only *one* which shows a significant change from water monomer to dimer. This element is P_{yy}(charge flux) of H_4, the H-bonded H atom, which shows a large increase of 0.27 e.

A similar situation is encountered in the CCFO analysis for the O atoms. The dimer tensors on O_3 and O_5, in the molecular coordinate system of the dimer (MSD), are compared in Table 4-4 with the corresponding transformations of the monomer tensors (see discussion in section 4.1.). Both O atoms show a significant change, but again, only for the P_{yy}(charge flux) element. This element decreases by 0.14 e for O_3 and by 0.12 e for O_5.

Table 4-3. Charge, charge flux, and overlap contributions to ab $initio$ 4-31G APT's for H atoms of the water monomer (N) and dimer (D) in the bond system. Units are e, where 1e = 1.602×10^{-19} coulombs.

	$P^H(M)$			$P^{H}{}_{1}(D)$		
Charge	0.41 E~			0.42 E~		
Charge Flux	0.0	0.0	0.0	−0.01	0.0	−0.01
	0.0	−0.04	−0.06	0.0	0.0	−0.06
	0.0	0.02	−0.08	0.0	0.02	−0.09
Overlap	0.06	0.0	0.0	0.06	0.0	0.0
	0.0	−0.28	−0.04	0.0	−0.28	−0.03
	0.0	−0.05	0.01	0.0	−0.04	0.01

	$P^H(M)$			$P^{H}{}_{4}(D)$		
Charge	0.41 E~			0.46 E~		
Charge Flux	0.0	0.0	0.0	−0.02	0.0	0.0
	0.0	−0.04	−0.06	0.0	0.23	−0.04
	0.0	0.02	−0.08	0.0	−0.03	−0.09
Overlap	0.06	0.0	0.0	0.04	0.0	0.0
	0.0	−0.28	−0.04	0.0	−0.28	−0.05
	0.0	−0.05	0.01	0.0	−0.04	−0.01

	$P^H(M)$			$P^{H}{}_{6}(D)$		
Charge	0.41 E~			0.39 E~		
Charge Flux	0.0	0.0	0.0	−0.01	0.0	0.0
	0.0	−0.04	−0.06	0.0	−0.07	−0.06
	0.0	0.02	−0.08	0.0	0.03	−0.07
Overlap	0.06	0.0	0.0	0.07	0.0	0.0
	0.0	−0.28	−0.04	0.0	−0.28	−0.05
	0.0	−0.05	0.01	0.0	−0.05	0.02

Table 4-4. Charge, charge flux, and overlap contributions to *ab initio* 4-31G APT's for O atoms of the water monomer (M) and dimer (D) in the molecular system of the dimer. Units are e, where $1e = 1.602 \times 10^{-19}$ coulombs.

	$P^{O_3}(M)$			$P^{O_3}(D)$		
Charge	-0.81 $\underset{\sim}{E}$			-0.83 $\underset{\sim}{E}$		
Charge Flux	0.08	0.0	0.0	0.04	0.0	0.0
	0.0	0.10	-0.08	0.0	-0.04	-0.08
	0.0	-0.08	0.07	0.0	-0.02	0.07
Overlap	0.26	0.0	0.0	0.27	0.0	0.0
	0.0	0.11	-0.20	0.0	0.12	-0.19
	0.0	-0.20	0.04	0.0	-0.20	0.05

	$P^{O_5}(M)$			$P^{O_5}(D)$		
Charge	-0.81 $\underset{\sim}{E}$			-0.87 $\underset{\sim}{E}$		
Charge Flux	0.0	0.0	0.0	0.02	0.0	0.0
	0.0	0.11	0.04	0.0	-0.01	0.0
	0.0	0.04	0.13	0.0	0.05	0.17
Overlap	-0.13	0.0	0.0	-0.11	0.0	0.0
	0.0	0.26	0.01	0.0	0.23	0.01
	0.0	0.01	0.27	0.0	0.02	0.29

It was established in section 4.1, that the dominant changes from water monomer to dimer in the total polar tensors occur in the P_{yy} element on the O_3, H_4 and O_5 atoms. We now see that in each case the changes are sharply limited to the charge flux tensor in the CCFO analysis. The charge flux accounts for 93% of the change in the total P_{yy} element for O_3, 84% for H_4, and 58% for O_5.

Table 4-4 shows that the gross atomic charge on O_5 decreases by 0.06 e upon dimer formation. This change therefore accounts for 29% of the total P_{yy} change for O_5. However, it is also evident that the charge on this atom is very large in both the monomer and dimer, and it changes by only 7% of the monomer value upon dimer formation. This change is not significant. Thus the major changes in the dimer APT's can be attributed unequivocably to the charge flux tensor.

This result is of great consequence for understanding the character-istic intensity enhancement of the H-bond band. This enhancement has been discussed frequently in the literature. However, attention has been focused on the general nature of the H-bond interaction. The in-tensity enhancement has been regarded only as an additional property to be investigated and correlated with other characteristic properties of H-bonded complexes.

The traditional controversy associated with the intensity enhance-ment therefore involves the relative importance of charge transfer and polarization effects [23, and references cited therein]. These two effects contribute to the second order energy of molecular complexes, obtained by the method of perturbation theory [91]. Formalisms have been developed [92] for resolving these contributions in whole complex MO calculations, such as that presented here. However, there are

discrepancies in the definition of the two energy contributions, between the MO formalisms and perturbation theory [92]. In both methods, the distinction between charge-transfer and polarization effects cannot be made unambiguously, except at large intermolecular distances [19, p.45].

Investigation of the intensity enhancement in terms of these effects has been limited primarily to empirical methods [93-100]. Accordingly efforts to account for the magnitude of the intensity enhancement, and the various contributions to it, have met with only qualitative success [23, and references cited therein].

Our approach to this problem differs significantly from previous approaches. We regard the intensity enhancement as an unusual pheno-menon in the general theory of infrared intensities. Thus we have applied a model for investigation of intensities to an H-bonded complex. We have found that the magnitude of the enhancement in the water dimer can be quantitatively attributed to the increase in the charge flux tensor on H_4, from that in the monomer.

We interpret this result in terms of the distinguishing character-istics of the charge, charge flux and overlap tensors, discussed in the previous section. In doing this, we would like to address the possible implications of this result for other H-bonded complexes besides the water dimer. We restrict our attention in this regard, to the relative-ly weak interaction involved in non-ionic binary complexes.

First we consider the fact that there is a negligible change in $\underline{p}^C$(charge) on each atom in the water dimer from that in the monomer. There is evidence that the charge tensors remain largely unaffected by the H-bond interaction, for H-bonded complexes in general. Del Bene has calculated the Mulliken gross atomic charges--and therefore the charge

tensors--with the STO-3G basis set for 41 H-bonded dimer complexes [101-103]. On the whole, these charges are nearly the same as the corresponding charges in the isolated electron acceptor molecules (monomers), which were also calculated. As discussed in section 4.1, the H-bond band intensity is dominated by $P_{yy}{}^{H_b}$, where H_b is the H-bonded H atom (H_4 in the water dimer). Thus, we have calculated the difference between the monomer and dimer charges on H_b, for the complexes reported by Del Bene. For all 41 complexes the charge differences are less than 0.05 e.

Moreover the relative charge differences, ΔQ_{H_b} (rel.)--that is, the ratio of the charge difference to the monomer charge--is 27% or less for the 41 complexes. This change is insignificant, especially considering that ΔQ_{H_b} (rel.) decreases with increasing basis set size.* For the water dimer, for example, ΔQ_{H_b} (rel.) is 19% with the STO-3G basis set [101], as compared to 13% with 4-31G and 5% with the large basis set used by Hankins, Moscowitz and Stillinger [53].

The ΔQ_{H_b} (rel.) obtained from the studies of Del Bene can be used to estimate the contribution of the charge tensor to the intensity enhancement for the general H-bonded complex. Assuming that the H-bond band intensity is completely determined by $P_{yy}{}^{H_b}$,** the relative increase in $P_{yy}{}^{H_b}$(charge) could only enhance the intensity by a maximum factor of 1.6. Since the intensity of the H-bond band in the dimer is generally larger

---

* The absolute charge differences are not sensitive to the basis set. See references [104, p. 4994] and [19, p. 73]. Compare also the 6-31G* charge differences calculated by Dill, Allen, Topp and Pople [105] with those calculated by Kollman and Allen [104,106] and by Del Bene [102]. However, the monomer charges increase with basis set size so that ΔQ_{H_b} (rel.) decreases.

** Actually $P_{yy}{}^{H_b}$ accounts for 87% of the intensity in our water dimer calculation. The remaining intensity is due to a sum of several small terms from other contributions.

by a factor of 10 or 20 than the corresponding monomer band, the contribution from the charge tensor is not significant.

Nevertheless the characteristics of the charge tensor are useful in interpreting the intensity enhancement, because they tell us what is *not* involved in this phenomenon. As discussed in the previous section, one characteristic of the charge tensor on H_b is that it depends only on the H_b atom. It is generally recognized that the intensity enhancement cannot be accounted for by the effects due only to H_b. The charge tensor is also characterized by a static electrical factor. Both the dynamic and mechanical effects are only implicitly involved in the charge tensor.

The importance of the dynamic electrical effect for the intensity enhancement, and its explicit dependence on the vibrational coordinate, has been emphasized by Pimentel and McClellan [24], Mulliken and Person [25], Zgierski [26] and Witkowski [27].

Pimentel and McClellan presented a pictorial model for the intensification which showed a polarization of charge induced by the displacement of H_b. Mulliken and Person explained the enhancement in terms of vibronic coupling between the "dative" and "no-bond" electronic wavefunctions. The dative, or charge-transfer wavefunction represents an excited electronic state, in which charge is donated from the nonbonding orbital on the electron donor molecule to an antibonding orbital on the electron acceptor molecule. The two states are vibronically coupled, in that their mixing coefficients in the total wavefunction are a function of the vibrational coordinate. Zgierski and Witkowski have also attributed the intensity enhancement to vibronic coupling. However, they considered an excited electronic state involving the nonbonding orbitals on both the electron donor and acceptor molecules.

These three models may differ with regard to the nature of the H-bond, but they agree in their treatment of the intensity enhancement. According to these models the important factor in this enhancement is the variation of the electronic wavefunction at a frequency corresponding to that of the H-bond band. In other words, the intensification arises from the increase in the dynamic electrical effect associated with the charge flux tensor, as described in the previous section.

However, the overlap tensor also involves a dynamic electrical effect. If the dominant change from monomer to dimer had been found in $P_{yy}^{H_b}$(overlap)--or if both the charge flux and overlap tensors had shown substantial changes--this would also be consistent with the models described above. But $P_{yy}^{H_b}$(overlap) is the same as the corresponding monomer value, while $P_{yy}^{H_b}$(charge flux) increases by a large amount. This result pinpoints the origin of the intensity enhancement more precisely, according to the distinctions between the charge flux and overlap tensors made in section 4.2.1.

This enhancement is due to the variation of the electron density, which can be resolved into independent diatomic contributions. That part of the variation of the dipole moment, which cannot be expressed in terms of electron density, and which depends on hybridization and other triatomic effects, does not change from water monomer to dimer. Therefore it does not contribute to the intensity enhancement. The explicit dependence of the intensity enhancement on the electron density, as such, appears to be contained in the polarization model of Pimentel and McClellan. However, this explicit dependence should be emphasized. Moreover, the determining role played by the charge flux as opposed to the overlap tensor in the intensity enhancement allows us to understand the effect of interatomic interactions on this enhancement.

In considering interatomic interactions in H-bonded complexes, we can distinguish between intramolecular and intermolecular effects. Intramolecular interactions involve atoms in the same water molecule in the water dimer complex, for example, while intermolecular interactions involve one atom in the electron donor molecule and one in the electron acceptor molecule.

In the atomic polar tensors of H-bonded complexes, interatomic interactions are dominated by intramolecular effects. These effects in the isolated monomers are *perturbed* by the intermolecular interactions due to complex formation. The overlap tensor involves the contribution of higher order interatomic effects to the total polar tensor, as discussed in section 4.2.1. Thus the overlap tensor might be expected to contain only those intramolecular effects on the intensities that are not affected by the H-bond interaction.

Accordingly, it might be assumed that the overlap tensor does not contribute to the intensity enhancement, in the general H-bonded complex. This assumption should be tested by calculating charge, charge flux and overlap tensors for other H-bonded complexes and their corresponding monomers.

This calculation for the water monomer and dimer has shown that the interatomic interactions, which are perturbed by the effect of the H-bond, are isolated in the charge flux tensor. We can gain some insight into the nature of these interatomic interactions by investigating the individual contributions to this tensor. Another reason for considering these contributions is that the polarization model of Pimentel and McClellan was more specific than we have stated thus far. They actually attributed the intensity enhancement to a polarization of the *base* (electron donor molecule), induced by the displacement of H_b.

We examine only the contributions to the yy element on H_b, since the intensity of the H-bond band is determined primarily by this element. The corresponding charge flux contribution from atom A is given by $y_A (\partial Q_A / \partial y_{H_b})$, according to Eq. 47b. We note that y_A, the equilibrium y coordinate of atom A, depends on the origin of the coordinate system. We have used the center of mass as the only unique origin of the molecule.

The contributions to $P_{yy}^{H_b}$ (charge flux) are given in Table 4-5 for water monomer and dimer. We have also included the corresponding contributions for the HCN-HF dimer for comparison. Curtiss and Pople reported the $(\partial Q_A / \partial y_{H_b})$ values obtained from their 4-31G calculation for this dimer and for the HF monomer [107]. We have used their equilibrium geometrical parameters to determine the y_A values and obtain the contributions in Table 4-5.

As indicated in the table, the contributions from electron donor (ED) atoms in the dimer should be compared with zero in the monomer. That is, the charges in the isolated ED molecule will not change when H_b in the electron acceptor (EA) is displaced. The contribution from H_b is compared with the corresponding contribution from the H atom in the monomer which is displaced. It is interesting that the change in this monatomic contribution, for both complexes, actually detracts from the increase from monomer to dimer which is found for the total charge flux element--and which enhances the intensity in the dimer.

The contributions from the remaining atoms in Table 4-5 give the charge flux on one atom with respect to displacement of another. In this sense, these contributions represent interatomic effects in the total atomic polar tensor. The contributions from O_3 and N of the ED molecules

Table 4-5. Individual contributions to $P_{yy}^{H_b}$ (charge flux), in the bond system of H_b, for $(H_2O)_2$ and HCN-HF. Partial sums over the atoms of the ED and EA molecules are given. Units are e.

$y_A(\partial Q_A/\partial y_{H_b})$ for $(H_2O)_2$				$y_A(\partial Q_A/\partial y_{H_b})$ for HCN-HF[a]			
Atom	Monomer	Dimer	Difference[b]	Atom	Monomer	Dimer	Difference[b]
H_1(ED)	0.0	0.061	0.061	H´(ED)	0.0	0.121	0.121
H_2(ED)	0.0	0.061	0.061	C(ED)	0.0	0.199	0.199
O_3(ED)	0.0	−0.030	−0.030	N(ED)	0.0	−0.051	−0.051
Total ED	0.0	0.091	0.091	Total ED	0.0	0.269	0.269
H_b(EA)	−0.020	−0.046	−0.026	H_b(EA)	0.105	−0.211	−0.316
O_5(EA)	−0.014	0.184	0.198	F(EA)	0.006	0.556	0.550
H_6(EA)	−0.006	0.002	0.008				
Total EA	−0.039	0.140	0.179	Total EA	0.111	0.345	0.234

[a] Curtiss and Pople [107].

[b] Dimer minus monomer.

also detract from the total increase in the charge flux element from monomer to dimer.

The major increase occurs on O_5 and F of the EA molecules. This increase gives the perturbation of the intramolecular interaction of O_5 and F with H_b, due to the intermolecular effect of complex formation. Smaller but substantial contributions come from the ED atoms not involved in the H-bond: H_1 and H_2 of the water dimer, and H´ and C of the HCN-HF dimer. These contributions represent purely intermolecular interactions.

The individual contributions in Table 4-5 are subject to limited numerical accuracy. However, the sums over the atoms of the ED molecule and over those of the EA molecule are probably reliable, at least qualitatively. Table 4-5 shows that for the water dimer the total contribution to $P_{yy}^{H_b}$ (charge flux) from the EA is larger than that from the ED, but both are substantial. For the HCN-HF dimer, on the other hand, the total contribution from the EA is slightly smaller than that from the ED. But again, both are substantial.

The 4-31G calculations for these two dimers thus indicate that the polarization of charge, which is responsible for the intensity enhancement, cannot be localized on the ED molecule. Rather, the perturbation of the intramolecular polarization effects by the formation of the H-bond must be considered in addition to the intermolecular effects.

In all our discussion of the charge, charge flux, and overlap tensors, we have restricted our attention to those on H_b. The atomic polar tensor on this atom plays a determining role in the intensity enhancement, and this is our main interest. However, Table 4-4 shows that similar changes take place in the contributions to the O atom polar

tensors. That is, the charge and overlap tensors do not change significantly from monomer to dimer; but the charge flux tensors change by a large amount. We have also calculated the individual contributions to the charge flux tensor on O_5. These results parallel those in Table 4-5 for the charge flux tensor on H_b.

In other words, the results of the CCFO analysis for the O atoms are similar in *detail* to those for H_b. Therefore, the important factors in the intensity enhancement also determine the effect of the H-bond on the overall vibrational redistribution of charge in the water dimer.

These important factors include the dynamic electrical effect, which can be expressed in terms of the electron density function. With regard to interatomic interactions, diatomic effects are more important than monatomic or triatomic effects. And finally, both intermolecular effects and the perturbation of intramolecular effects are important for the diatomic interactions. It is hoped that these results provide some insight into the nature of the H-bond.

APPENDIX

We have determined a set of scaled force fields for the linear water dimer in order to obtain frequencies for comparison with experiment. As discussed in section 1.4.1, the scaling procedure we have used depends on theoretically calculated force constants for the water monomer and linear dimer. We have applied this scaling procedure to the 4-31G force fields calculated by Curtiss and Pople [47], as well as force fields we have calculated by the method of CNDO, for these two molecules. Curtiss and Pople obtained the linear dimer force field with respect to the theoretical 4-31G equilibrium geometry, for which R_{O-O} = 2.832 $\overset{\circ}{A}$. The CNDO force fields were calculated with respect to three different equilibrium geometries with R_{O-O} = 3.0 $\overset{\circ}{A}$, 2.8 $\overset{\circ}{A}$ and 2.6 $\overset{\circ}{A}$.

The theoretical monomer and dimer force constants from the 4-31G calculation of Curtiss and Pople are given in Table A-1, while those from the CNDO calculations appear in Table A-2. The dimer force constants are given in terms of the symmetry coordinates defined in Table 2-5. These dimer symmetry coordinates correspond to differently numbered symmetry coordinates in the monomer or to monomer internal coordinates, both of which were defined in Table 2-2. Each monomer internal (F_{ij}) or symmetry (F_{ij}) force constant is written on the same line in Tables A-1 and A-2 as the dimer force constant to which it corresponds. The corresponding monomer and dimer theoretical force constants were subtracted to give the change

119

Table A-1. *Ab initio* 4-31G force constants for water monomer and linear dimer calculated by Curtiss and Pople [47].

Units	f_k(theor.,monomer)		f_k(theor.,dimer)	
md Å^{-1}	F_{11}	8.934	F_{22}	9.027
md Å rad^{-2}	F_{22}	0.7843	F_{55}	0.7861
md Å^{-1}	F_{33}	9.166	F_{66}	9.273
md Å^{-1}		0.0	F_{12}	-0.0170
md Å^{-1}		0.0	F_{23}	-0.0070
md Å rad^{-2}		0.0	F_{45}	0.0027
md Å^{-1}	F_{11}	9.05	F_{11}	9.15
md Å^{-1}	F_{12}	-0.116	F_{13}	-0.117
md Å^{-1}	F_{11}	9.05	F_{33}	8.66
md Å rad^{-2}	F_{22}	0.7843	F_{44}	0.8228

Table A-2. Force constants for water monomer and linear dimer calculated by the CNDO method.

Units	CNDO f_k(theor.,monomer)		CNDO f_k(theor.,dimer)			
				$R = 3.0$ Å	$R = 2.8$ Å	$R = 2.6$
md Å^{-1}	F_{11}	25.20	F_{22}	25.21	25.21	25.22
md rad^{-1}	F_{12}	0.5637	F_{25}	0.5600	0.5573	0.5521
md Å rad^{-2}	F_{22}	0.9106	F_{55}	0.9059	0.9038	0.9008
md Å^{-1}	F_{33}	24.44	F_{66}	24.45	24.45	24.46
md Å^{-1}	F_{11}	24.82	F_{11}	24.82	24.81	24.81
md Å^{-1}	F_{12}	0.3805	F_{13}	0.3798	0.3781	0.3726
md rad^{-1}	F_{13}	0.3986	F_{14}	0.3999	0.4007	0.4022
md Å^{-1}	F_{11}	24.82	F_{33}	24.51	24.32	24.23
md rad^{-1}	F_{13}	0.3986	F_{34}	0.3950	0.3889	0.3799
md Å rad^{-2}	F_{22}	0.9106	F_{44}	0.9260	0.9336	0.9298

in each theoretical force constant, $\Delta f_k(th.)$:

(A-1) $\Delta f_k(th.) = f_k(th., dimer) - f_k(th., monomer)$.

The $\Delta f_k(th.)$ were then added to the experimental force constant, $f_k(exptl., monomer)$, with respect to the same monomer internal or symmetry coordinates to give the scaled dimer force constant, $f_k(scaled, dimer)$:

(A-2) $f_k(scaled, dimer) = f_k(exptl., monomer) + \Delta f_k(th.)$.

We are mainly interested in obtaining frequencies for comparison with the experimental spectrum of the water dimer obtained by Tursi and Nixon in the N_2 matrix [30]. Accordingly we have used the $f_k(exptl., monomer)$ which they determined by fitting the observed monomer frequencies in the N_2 matrix. These force constants have been given in Table 2-8, with respect to the monomer symmetry coordinates. The relevant experimental force constants with respect to the monomer internal coordinates are $F_{11} = 7.516$ md $\overset{o}{A}^{-1}$, $F_{12} = -0.181$ md $\overset{o}{A}^{-1}$, and $F_{13} = -0.2986$ md rad^{-1}.

The scaled $\underline{F}$ matrix derived from the 4-31G force fields in Table A-1, according to equations (A-1) and (A-2), has been given in Table 2-10. Table A-3 shows the scaled F matrices derived from the CNDO force fields in Table A-2. Each of these scaled $\underline{F}$ matrices was used (together with the linear dimer G matrix determined from the B matrix in Table 2-6) to set up the eigenvalue problem, Eq. 14. The equation was solved for the eigenvector matrix, $\underline{L}$, and the diagonal frequency parameter matrix, $\underline{\Lambda}$. The $\underline{L}$ matrix for the scaled 4-31G force field was used to obtain a set of dimer intensities from the scaled 4-31G calculated APT's, as discussed in section 3.3. This $\underline{L}$ matrix has been given in Table 2-10.

Table A-3. Scaled CNDO force constants for water monomer and linear dimer.

		$R = 3.0\ \overset{\circ}{A}$	$R = 2.8\ \overset{\circ}{A}$	$R = 2.6\ \overset{\circ}{A}$
F_{22}	md $\overset{\circ}{A}{}^{-1}$	7.339	7.343	7.350
F_{25}	md rad^{-1}	−0.4260	−0.4287	−0.4339
F_{55}	md $\overset{\circ}{A}$ rad^{-2}	0.6898	0.6876	0.6847
F_{66}	md $\overset{\circ}{A}{}^{-1}$	7.701	7.704	7.711
F_{11}	md $\overset{\circ}{A}{}^{-1}$	7.511	7.508	7.501
F_{13}	md $\overset{\circ}{A}{}^{-1}$	−0.1818	−0.1834	−0.1890
F_{14}	md rad^{-1}	−0.2973	−0.2965	−0.2951
F_{33}	md $\overset{\circ}{A}{}^{-1}$	7.202	7.018	6.926
F_{34}	md rad^{-1}	−0.3022	−0.3083	−0.3174
F_{44}	md $\overset{\circ}{A}$ rad^{-2}	0.7098	0.7175	0.7137

Here we present the results for the $\underline{\Lambda}$ matrices. The fundamental absorption frequencies, ω_i in cm^{-1}, are related to the $\underline{\Lambda}$ matrix elements by

$$\Lambda_{ii} = (4\pi^2 c^2 \omega_i{}^2/N_A) \times 10^{-5}$$

for the units we have used, where c and N_A have been defined in connection with Eq. 15. The predicted frequencies from the scaled forced fields are compared in Table A-4 with a number of experimentally observed values. The ω_i in the table correspond to the dimer normal coordinate numbering, while the ν_i in brackets give the analogous monomer normal coordinate numbers for the vibrations of the electron acceptor (EA) and the electron donor (ED) molecules of the dimer (see Fig. 1-2).

The errors for each predicted frequency are given in parentheses with respect to the frequencies observed by Tursi and Nixon. For the 4-31G calculation the errors in the bending vibrations, $\nu_2(ED)$ and $\nu_2(EA)$, are quite large. However, this is primarily due to the neglect of stretch-bend interaction (see discussion in sections 2.4 and 3.3), rather than to the errors in the calculated force constants. The remaining frequencies agree quite well considering that the force field is harmonic while the observed frequencies are not. Some indication of the effect of this discrepancy is given by the "best fit" to the observed frequencies of Tursi and Nixon, shown in parentheses in Table A-4.

For the CNDO calculations it can be seen that the frequencies most sensitive to the O-O distance, R_{O-O}, are the electron acceptor stretches, $\nu_1(EA)$ and $\nu_3(EA)$. The intensities of these bands were also found to be most sensitive to R_{O-O}, as discussed in section 3.3.

Table A-4. Comparison of predicted frequencies for the linear water dimer in the N_2 matrix with experimental frequencies. Units are cm^{-1}.

Predicted Frequencies	ω_1 [$\nu_3(EA)$]	ω_2 [$\nu_1(ED)$]	ω_3 [$\nu_1(EA)$]	ω_4 [$\nu_2(EA)$]	ω_5 [$\nu_2(ED)$]	ω_6 [$\nu_3(ED)$]
4.31G (R = 2.832 Å)	3726.4	3619.9	3538.5	1705.4	1661.8	3765.9
(% error[a])	(0.8)	(-0.1)	(-0.3)	(5.1)	(3.7)	(1.4)
CNDO (R = 3.0 Å)	3713.3	3638.9	3587.0	1626.2	1603.4	3740.9
(% error[a])	(0.4)	(0.4)	(1.1)	(0.5)	(0.2)	(0.7)
CNDO (R = 2.8 Å)	3705.4	3640.0	3549.2	1633.5	1600.3	3741.7
(% error[a])	(0.2)	(0.4)	(0.0)	(0.9)	(0.0)	(0.7)
CNDO (R = 2.6 Å)	3702.2	3642.2	3528.8	1627.2	1595.8	3743.3
(% error[a])	(0.1)	(0.5)	(-0.5)	(0.6)	(-0.3)	(0.8)
Observed frequencies in the N_2 Matrix[b]	3697.7	3625.6	3547.5	1618.1	1600.3	3714.4
(Best fit[c,b])	(3711.6)	(3631.1)	(3552.0)	(1628.2)	(1609.7)	(3731.0)

[a] $[\omega(calc.) - \omega(obs.)]/\omega(obs.)$.

[b] Tursi and Nixon [30].

[c] Least-squares fit to observed frequencies of $(H_2O)_2$, $(D_2O)_2$ and $(HDO)_2$. See section 1.3.2.

Although these frequency calculations are approximate, they lend support to the assignment of the matrix-isolated spectra in terms of the linear water dimer. In particular, the frequency of the H-bond band, $\nu_1(EA)$, is not at variance with the predicted frequencies.

REFERENCES

1. W. B. Person and J. H. Newton, J. Chem. Phys. 61, 1040 (1974).

2. J. H. Newton and W. B. Person, J. Chem. Phys. 64, 3036 (1976).

3. J. H. Newton, Ph.D. Dissertation, University of Florida (1974).

4. W. B. Person and J. D. Rogers, European Congress on Molecular Spectroscopy, Frankfurt, West Germany (September, 1979). J. D. Rogers and W. B. Person, Symposium on Molecular Spectroscopy, Columbus, Ohio (June, 1979); American Chemical Society National Meeting, Washington, D.C. (September, 1979).

5. J. H. Newton and W. B. Person, J. Chem. Phys. 68, 2799 (1978); J. Phys. Chem. 82, 226 (1978). J. H. Newton, R. A. Levine and W. B. Person, J. Chem. Phys. 67, 3282 (1977). B. J. Krohn, W. B. Person and J. Overend, J. Chem. Phys. 65, 969 (1976); 67, 5091 (1977). W. B. Person and J. Overend, J. Chem. Phys. 66, 1442 (1977).

6. J. F. Biarge, J. Herranz and J. Morcillo, An. R. Soc. Esp. Fis. Quim. A57, 81 (1961).

7. J. Morcillo, L. J. Zamorano and J. M. V. Heredia, Spectrochim. Acta 22, 1969 (1966). M. De la Lastra, A. Medina and J. Morcillo, An. R. Soc. Esp. Fis. Quim. B63, 1079 (1967). J. Morcillo, J. F. Biarge, J. M. V. Heredia and A. Medina, J. Mol. Struct. 3, 77 (1969).

8. W. T. King, G. B. Mast and P. P. Blanchette, J. Chem. Phys. 56, 4440 (1972). G. B. Mast and W. T. King, J. Phys. Chem. 80, 2004 (1976).

9. W. T. King and G. B. Mast, J. Phys. Chem. 80, 2521 (1976).

10. W. T. King in "Vibrational Intensities," W. B. Person and G. Zerbi, Eds. (Elsevier, Amsterdam, to be published, 1980), chap. 6.

11. J. C. Decius, J. Mol. Spectrosc. 57, 348 (1975).

12. J. C. Decius and G. B. Mast, J. Mol. Spectrosc. 70, 294 (1978). G. B. Mast and J. C. Decius, J. Mol. Spectrosc. 79, 158 (1980).

13. M. Gussoni and S. Abbate, J. Chem. Phys. 65, 3439 (1976); J. Mol. Spectrosc. 62, 53 (1976).
    S. Abbate and M. Gussoni, J. Mol. Spectrosc. 66, 1 (1977).
    S. Abbate, M. Gussoni G. Masetti and G. Zerbi, J. Chem. Phys. 67, 1519 (1977).

14. A. J. van Straten and W. M. A. Smit, J. Mol. Spectrosc. 56, 484 (1975); 62, 297 (1976); 65, 202 (1977).

15. L. S. Mayants and B. S. Averbukh, J. Mol. Spectrosc. 22, 197 (1967).

16. S. K. Samvelyan, V. T. Aleksenyan and B. V. Lokshin, J. Mol. Spectrosc. 48, 47 (1973).

17. L. M. Sverdlov, Opt. Spek. 39, 268 (1975).
    L. M. Sverdlov, M. A. Kovner and E. P. Krainov, "Vibrational Spectra of Polyatomic Molecules" (Wiley, New York, 1974).

18. K. Morokuma and L. Pederson, J. Chem. Phys. 48, 3275 (1968).

19. P. Schuster in "The Hydrogen Bond," P. Schuster, G. Zundel and C. Sandorfy, Eds. (North-Holland Publishing, New York, 1976), Vol. 1, chap. 2.

20. G. C. Pimentel and A. L. McClellan, "The Hydrogen Bond" (Freeman, San Francisco, 1960). Many books have been published on the subject of H-bonding. This one covers the earlier work quite thoroughly, and the following reference covers the more recent work.

21. P. Schuster, G. Zundel and C. Sandorfy, Eds., "The Hydrogen Bond," 3 Vols. (North-Holland Publishing, New York, 1976).

22. D. Hadzi and S. Bratos, *ibid.*, Vol. 2, chap. 12.

23. H. Ratajczak, W. J. Orville-Thomas and C. N. R. Rao, Chem. Phys. 17, 197 (1976).

24. G. C. Pimentel and A. L. McClellan in "The Hydrogen Bond" (Freeman, San Francisco, 1960), p. 248.

25. R. S. Mulliken and W. B. Person, Ann. Rev. Phys. Chem. 13, 107 (1962).
    R. S. Mulliken and W. B. Person, "Molecular Complexes" (Wiley, New York, 1969).

26. M. Z. Zgierski, Acta Phys. Polon. A51, 877 (1977).

27. A. Witkowski, Mol. Phys. 29, 1441 (1975).

28. H. E. Hallam in "The Hydrogen Bond," P. Schuster, G. Zundel and C. Sandorfy, Eds. (North-Holland Publishing, New York, 1976), Vol. 3, chap. 22.
    H. E. Hallam, Ed. "Vibrational Spectroscopy of Trapped Species" (Wiley, New York, 1973).

29. M. Van Thiel, E. D. Becker and G. C. Pimentel, J. Chem. Phys. 27, 486 (1957).

30. A. J. Tursi and E. R. Nixon, J. Chem. Phys. 52, 1521 (1970).

31. A. J. Tursi, Ph.D. Dissertation, University of Pennsylvania (1970).

32. L. Fredin, B. Nelander and G. Ribbegard, J. Chem. Phys. 66, 4065, 4073 (1977).

33. R. E. Barletta, Ph.D. Dissertation, Brown University (1977).

34. P. V. Huong and J.-C. Cornut, J. Chim. Phys. 72, 534 (1975).

35. B. Mann, T. Neikes, E. Schmidt and W. A. P. Luck, Ber. Bunsenges. Phys. Chem. 78, 1236 (1974).

36. W. A. P. Luck in "The Hydrogen Bond," P. Schuster, G. Zundel and C. Sandorfy, Eds. (North-Holland Publishing, New York, 1976), Vol. 2, chap. 11.

37. R. L. Redington and D. E. Milligan, J. Chem. Phys. 37, 2162 (1962); 39, 1276 (1963).

38. H. P. Hopkins, R. F. Curl, Jr. and K. S. Pitzer, J. Chem. Phys. 48, 2959 (1968).

39. G. P. Ayers and A. D. E. Pullin, Chem. Phys. Lett. 29, 609 (1974); Ber. Bunsenges. Phys. Chem. 82, 62 (1978).

40. G. P. Ayers and A. D. E. Pullin, Spectrochim. Acta 32A, 1629, 1641, 1689, 1695 (1976).

41. R. C. Kerns and L. C. Allen, J. Am. Chem. Soc. 100, 6587 (1978).

42. E. Whalley in "The Hydrogen Bond," P. Schuster, G. Zundel and C. Sandorfy, Eds. (North-Holland Publishing, New York, 1976), Vol. 3, chap. 29 (see section 29.3).

43. O. Matsuoka, E. Clementi and M. Yoshimine, J. Chem. Phys. 64, 1351 (1976).

44. H. A. Gebbie, W. J. Burroughs, J. Chamberlin, J. E. Harris and H. G. Jones, Nature 221, 143 (1969).

45. R. W. Bolander, J. L. Kassner and J. T. Zung, J. Chem. Phys. 50, 4402 (1969).

46. D. Maillard, A. Schriver, J. P. Perchard, C. Girardet and D. Robert, J. Chem. Phys. 67, 3917 (1977).

47. L. A. Curtiss and J. A. Pople, J. Mol. Spectrosc. 55, 1 (1975).

48. R. Janoschek in "The Hydrogen Bond," P. Scuster, G. Zundel and C. Sandorfy, Eds. (North-Holland Publishing, New York, 1976), Vol. 1, chap. 3.

49. E. B. Wilson, Jr., J. C. Decius and P. C. Cross, "Molecular Vibrations" (McGraw-Hill, New York, 1955).

50. J. Overend in "Infrared Spectroscopy and Molecular Structure," M. Davies, Ed. (Elsevier, Amsterdam, 1963), chap. 10.

51. R. L. Cook, F. C. De Lucia and P. Helminger, J. Mol. Spectrosc. 53, 62 (1974).

52. W. S. Benedict, N. Gailar and E. K. Plyler, J. Chem. Phys. 24, 1139 (1956).

53. D. Hankins, J. W. Moscowitz and F. H. Stillinger, J. Chem. Phys. 53, 4544 (1970).

54. G. H. F. Diercksen, Theor. Chim. Acta 21, 335 (1971).

55. J. Overend, "Program Manual of the Molecular Spectroscopy Laboratory," University of Minnesota, Vol. 2 (August, 1966). We are grateful to J. Overend of the University of Minnesota for making these programs available to us.

56. G. E. Sanchez, Ph.D. Dissertation, University of Florida (1971).

57. S. A. Clough, Y. Beers, G. P. Klein and L. S. Rothman, J. Chem. Phys. 59, 2254 (1973).

58. R. A. McClatchey, W. S. Benedict, S.A. Clough, D. E. Burch, R. F. Calfee, K. Fox, L. S. Rothman and J. S. Garing, Air Force Cambridge Research Laboratories Report TR-73-0096 (January, 1973). J. S. Garing and R. A. McClatchey, Appl. Opt. 12, 2545 (1973).

59. G. Herzberg, "Infrared and Raman Spectra of Polyatomic Molecules" (Van Nostrand Reinhold, New York, 1945), p. 377.

60. T. R. Dyke, K. M. Mack and J. S. Muenter, J. Chem. Phys. 66, 498 (1977).

61. H.Popkie, H.Kistenmacher and E.Clementi, J. Chem. Phys. 59, 1325 (1973).

62. J. A. Pople and D. L. Beveridge, "Approximate Molecular Orbital Theory" (McGraw-Hill, New York, 1970).

63. P. A. Dobosh, Program QCPE 141, from Quantum Chemistry Program Exchange, Indiana University, Bloomington, Indiana.

64. E. Clementi and J. W. Mehl, IBM Research Laboratory Reports RJ 853 (May, 1971) RJ 883 (June, 1971) and RJ 889 (July,1971). We are grateful to J. R. Sabin of the University of Florida Quantum Theory Project for making this program available to us.

65. R. Ditchfield, W. J. Hehre and J. A. Pople, J. Chem. Phys. 54, 724 (1971).

66. R. N. Kortzeborn, IBM Research Laboratory Report RJ 577 (June,1969). We are grateful to J. R. Sabin of the University of Florida Quantum Theory Project for making this program available to us.

67. R. S. Mulliken, J. Chem. Phys. 23, 1833, 1841, 2338, 2343 (1955); 36, 326 (1962).

68. J. A. Pople and G. A. Segal, J. Chem. Phys. 43, S136 (1965).

69. P. Pulay, Mol. Phys. 18, 473 (1970).

70. J. A. Smith, P.Jorgensen and Y. Ohrn, J. Chem. Phys. 62, 1285(1975).

71. B. J. Krohn and C. W. Kern, J. Chem. Phys. 69, 5310 (1978).

72. C. E. Blom and C. Altona, Mol. Phys. 34, 177 (1977). C. E. Blom, C. Altona and A. Oksam, Mol. Phys. 34, 557 (1977).

73. P. Pulay, C. Fogarasi, F. Pang and J. E. Boggs, J. Am. Chem. Soc. 101, 2550 (1979).

74. J. Smith, M.S. Thesis, University of Florida (1973).

75. R. A. Toth, J. Quant. Spectrosc. Radiat. Transfer 13, 1127 (1973).

76. R. Goldstein, J. Quant. Spectrosc. Radiat. Transfer 4, 343 (1964).

77. G. J. Maclay, J. Chem. Phys. 43, 185 (1965).

78. J. M. Flaud and C. Camy-Peyret, J. Mol. Spectrosc. 55, 278 (1975).

79. C. B. Ludwig, C. C. Ferriso and C. N. Abeyta, J. Quant. Spectrosc. Radiat. Transfer 5, 281 (1965).

80. A. Goldman and U. P. Oppenheim, Appl. Opt. 5, 1073 (1966).

81. J. H. Jaffe and W. S. Benedict, J. Quant. Spectrosc. Radiat. Transfer 3, 87 (1963).

82. Y. Ben Aryeh, J. Quant. Spectrosc. Radiat. Transfer 7, 211 (1967).

83. M. A. Hirshfeld, J. H. Jaffe and G. Ross, J. Quant. Spectrosc. Radiat. Transfer 6, 311 (1966).

84. B. Krakow and A. R. Healy, J. Opt. Soc. Am. 59, 1490 (1969).

85. C. W. von Rosenberg, N. H. Pratt and K. N. C. Bray, J. Quant. Spectrosc. Radiat. Transfer, 10, 1155 (1970).

86. W. Kolos, Theor. Chim. Acta 51, 219 (1979).

87. A. Meunier, B.Levy and G. Berthier, Theor. Chim. Acta 29, 49 (1973).

88. A. Johansson, P. Kollman and S. Rothenberg, Theor. Chim. Acta 29, 167 (1973).

89. S. Iwata and K. Morokuma, J. Am. Chem. Soc. 95, 7563 (1973).

90. D. Kocjan, J. Koller and A. Azman, J. Mol. Struct. 34, 145 (1976).

91. J. N. Murrell, M. Randic and D. R. Williams, Proc. Roy. Soc. A284, 566(1965).

92. K. Morokuma, J. Chem. Phys. 55, 1236 (1971).
    K. Kitaura and K. Morokuma, Int. J. Quantum Chem. 10, 325 (1976).

93. H. Tsubomura, J. Chem. Phys. 24, 927 (1956).

94. P. C. McKinney and G. M. Barrow, J. Chem. Phys. 31, 294 (1959).

95. K. Szczepaniak and A. Tramer, J. Phys. Chem. 71, 3035 (1967).

96. S. Bratos, Adv. Quantum Chem. 3, 209 (1967).

97. M. Dreyfus and A. Pullman, Theor. Chim. Acta 18, 388 (1970).

98. P. A. Kollman and L. C. Allen, Chem. Rev. 72, 283 (1972).

99. W. B. Person in "Spectroscopy and Structure of Molecular Complexes," J. Yarwood, Ed. (Plenum, New York, 1973), chap. 1.

100. H. Ratajczak and W. J. Orville-Thomas, J. Mol. Struct. 19, 237 (1973).

101. J. E. Del Bene, J. Chem. Phys. 55, 4633 (1971).

102. J. E. Del Bene J. Am. Chem. Soc. 95, 5460 (1973).

103. J. E. Del Bene, J. Chem. Phys. 56, 4923 (1972); 57, 1899 (1972); 58, 3139 (1973); 62, 1314, 1961 (1975); 63, 4666 (1975); Chem. Phys. 15, 463 (1976).
     J. E. Del Bene and F. T. Marchese, J. Chem. Phys. 58, 926 (1973).
     J. E. Del Bene and W. L. Kochenour, J. Am. Chem. Soc. 98, 2041(1976).
     J. E. Del Bene and I. Cohen, J. Am. Chem. Soc. 100, 5285 (1978).

104. P. A. Kollman and L. C. Allen, J. Am. Chem. Soc. 93, 4991 (1971).

105. J. D. Dill, L. C. Allen, W. C. Topp and J. A. Pople, J. Am. Chem. Soc. 97, 7220 (1975).

106. P. A. Kollman and L. C. Allen, J. Chem. Phys. 52, 5085 (1970).

107. L. A. Curtiss and J. A. Pople, J. Mol. Spectrosc. 48, 413 (1973).

BIOGRAPHICAL SKETCH

Barbara Ann Zilles was born in Arcadia, Florida. She received the bachelor's degree in chemistry from Mount St. Mary's College in Los Angeles, California and the master's degree in teaching from the University of Florida. She has been with Old Dominion University in Norfolk, Virginia, as research assistant professor and with NASA Langley Research Center in Hampton, Virginia, as research contractor. She is receiving the Ph. D. degree in physical chemistry from the University of Florida.

I certify that I have read this study and that in my
opinion it conforms to acceptable standards of scholarly
presentation and is fully adequate, in scope and quality,
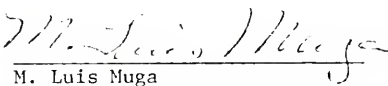as a dissertation for the degree of Doctor of Philosophy.

Willis B. Person, Chairman
Professor of Chemistry

I certify that I have read this study and that in my
opinion it conforms to acceptable standards of scholarly
presentation and is fully adequate, in scope and quality,
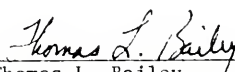as a dissertation for the degree of Doctor of Philosophy.

Martin T. Vala
Professor of Chemistry

I certify that I have read this study and that in my
opinion it conforms to acceptable standards of scholarly
presentation and is fully adequate, in scope and quality,
as a dissertation for the degree of Doctor of Philosophy.
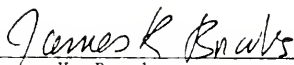
M. Luis Muga
Professor of Chemistry

I certify that I have read this study and that in my
opinion it conforms to acceptable standards of scholarly
presentation and is fully adequate, in scope and quality,
as a dissertation for the degree of Doctor of Philosophy.

Thomas L. Bailey
Professor of Physics

I certify that I have read this study and that in my opinion it conforms to acceptable standards of scholarly presentation and is fully adequate, in scope and quality, as a dissertation for the degree of Doctor of Philosophy.

James K. Brooks
Professor of Mathematics

This dissertation was submitted to the Graduate Faculty of the Department of Chemistry in the College of Liberal Arts and Sciences and to the Graduate Council, and was accepted as partial fulfillment of the requirements for the degree of Doctor of Philosophy.

June, 1980

Dean, Graduate School